Ion Binding to Polymers
and Lipid Membranes
in Aqueous Solutions

**Ionenbindung an Polymeren
und Lipidmembranen
in Wässrigen Lösungen**

Dissertation

zur Erlangung des akademischen Grades
"doctor rerum naturalium"
(Dr. rer. nat.)
in der Wissenschaftsdisziplin Physikalische Chemie

eingereicht an der
Mathematisch-Naturwissenschaftlichen Fakultät
der Universität Potsdam

von
Cornelia G. Sinn
geboren am 17. August 1976 in Kaiserslautern

Potsdam, im September 2004

Die vorliegende Arbeit wurde in der Zeit von März 2002 bis September 2004 am Max-Planck-Institut für Kolloid- und Grenzflächenforschung in Golm unter der Leitung von Prof. Dr. M. Antonietti angefertigt.

Die Disputation fand am 06.12.2004 statt.

Erstgutachter: Prof. Dr. M. Antonietti
Zweitgutachter: Prof. D. Discher, Ph.D.
Drittgutachter: PD Dr. W. Schärtl

Table of Contents

Chapter 1

Introduction

Ions are ubiquitous entities, which are crucial in any scientific and technological field. Few of them to mention are biology, chemistry and engineering. In biology, ions regulate electrostatic potentials, conductances and permeabilities of cell membranes. Ion complexation in cells plays a key role in the activities of enzymes and drugs [1], [2]. In chemistry, they play an important role in many colloidal systems such as micellar systems. They influence a large number of properties, such as ion-exchange mechanisms [3], expansions and contraction of clays [4] and rates of gelation [5]. In technology, ions are involved in desalination, the removal of ions from water, and scaling. In addition, they play a key role in complex media for bacteria used industrially in biotechnological processes for genetic drug production.

Among the various ions found in biological and chemical systems, calcium is particularly important. In living cells, for instance, calcium is needed for proper cell function and calcium binding to the lipid membrane plays a crucial role in cell fusion, endocytosis and protein signaling. In technology, deposition of $CaCO_3$ on pipes and heating elements causes incrustation, which reduces the life time of heating elements. Polymeric additives are consequently used as scale inhibitors in industrial processes to prevent unwanted $CaCO_3$ formation.

Any process involving ion binding is governed by ion-water interactions and there is a naturally high demand for understanding the underlying mechanisms. In particular, the manner in which water molceules solvate ions is relevant to chemical and physical processes such as chemical reactions at the interface. Also, the structure and

stability of large molecules and membranes depend on the distribution of ions.

A large number of phenomena involving ions are not explained by present theories and are therefore often referred to as "ion specific". Ion specific, or Hofmeister, effects in biological and biochemical systems have been known since 1888, when Hofmeister [6] defined a series of cations and anions according to the concentration of salt required to precipitate proteins from whole egg white. The various ions in the Hofmeister series, or lyotropic series, have been classified as chaotropes (structure breakers) or kosmotropes (structure makers) according to their relative abilities to induce the structuring of water. However, it is not yet clearly understood if the effect of the ions can be ascribed to their direct interaction with the proteins or to their influence on water structure. The series has been expanded from protein solubility to a broad range of other phenomena such as folding of proteins, gelatin melting, macromolecular conformation and phase transitions of lipid and surfactant structures [7], [8].

The first part of this work is directly related to the understanding of the interactions of ions with their local environment, and is aimed on evaluating the role of different ions on the structure of water. As a tool for this research, we use Isothermal Titration Calorimetry (ITC), which belongs to the most precise among the thermodynamic methods that provide information on ion-ion and ion-solvent interactions. The heat of dilution of various inorganic and polyelectrolyte salt solutions measured by ITC is consequently used as a scale of water structure making and breaking by the ions.

To learn about the competition of electrostatic and hydration forces we then investigate the interaction of Ca^{2+} with negatively charged poly(acrylic acid) (PAA) and two technical scale inhibitors, poly(sodiumaspartate) and Sokolan. We compare the binding of the ion to the one-dimensional polymer chain with binding to negatively charged phospholipid membranes which the ions perceive as two-dimensional surfaces. As negatively charged lipids we use phosphatidylserine where the functional carboxylate groups mimic the functional group of the polymer. Isothermal Titration Calorimetry (ITC) and Ion Selective Electrode (ISE) are used to measure the reaction enthalpy and binding isotherm.

Finally, we study a particular example of ion binding in biology, namely the char-

acteristic partitioning of Na$^+$ and K$^+$ in living cells. The general theory states that the potassium enrichment in cells is established through ion pumps and chanels. However, it is not yet clear whether ion partitioning in the cell is mediated by the pumps themselves or if ions are excluded from the cell due to physicochemical effects. We therefore analyze the preferential ion binding of K$^+$ versus Na$^+$ onto charged poly(acrylic acid) and microgels made of the electrically neutral poly(N-Isopropyl-acrylamide) (PNIPAAM) to test for the existance of bare physicochemical effects for the buildup of concentration gradients.

The following *chapter 2* provides the theoretical background which is neccessary to understand the chemical reactions studied in this work and to determine driving forces of the reactions. Properties of aqueous electrolyte solutions are presented along with the general theory on ion distribution close to a charged surface and standard binding models. In the *third chapter*, the experimental techniques and the materials used for our research are introduced. Emphasis is given on the two major techniques, Isothermal Titration Calorimetry and Ion Selective Electrodes. The *fourth chapter* deals with the interactions of ions and polyelectrolytes in aqueous solutions with their local environement. The heat of dilution of different (poly)ions measured by ITC is presented and discussed with regard to water structure making and breaking of the ions. In *chapter 5*, the results on calcium binding to polymers and lipid membranes are discussed, and binding to the one-dimensional chain is compared to the binding to the two-dimensional surface. Finally, the experiments on interactions of sodium and potassium with a charged polymer and with neutral microgel particles are presented in *chapter 6*. The results of the present work are summarized in *chapter 7* along with an outlook on conceivable improvements.

Chapter 2

Basic Principles and Theory

In this chapter we provide the essential theoretical background which is necessary to interpret and analyze the physicochemical reactions studied in this work. The basic thermodynamic relationships and definitions presented in chapter 2.1 are the basis to understand driving forces and to determine equilibrium constants of chemical reactions. The following chapter 2.2 deals with the characterization of aqueous solutions which is fundamental for the understanding of the specific effects of ions on the structure of water presented in chapter 4. In chapter 2.3, the formation of ion pairs in water and the Hofmeister Series are explained. The distribution of ions close to a charged surface is essential in any binding reaction and is discussed in chapter 2.4 together with different binding models. Chapter 2.5 presents the state of the art of a concrete example of specific ion effects, the Na^+/K^+ specificity.

2.1 Basic Thermodynamic Relationships Describing Chemical Reactions

The Gibbs Free Energy change of a chemical reaction at constant pressure and temperature T is given by

$$\Delta G = \Delta H(T_R) - T\Delta S(T_R) \tag{2.1}$$

where ΔH and ΔS are the change in the enthalpy and entropy, respectively, and T_R is an appropriate reference temperature. The sign of the Gibbs Free Energy change determines the spontaneity of an event. At a constant temperature and pressure, a

change can be spontaneous only if it is accompanied by a decrease in the free energy of the system. Therefore, any reaction for which ΔG is negative is spontaneous:

$$Spontaeous\ reactions : \Delta G < 0$$

Thus, chemical reactions occur spontaneously if energy is released in the form of heat ($\Delta H < 0$) and if the entropy of the system increases ($\Delta S > 0$). On the contrary, when a change is endothermic ($\Delta H > 0$) and is accompanied by a lowering of the entropy ($\Delta S < 0$) ΔG is positive and the reaction therefore non-spontaneous.

If ΔH and ΔS have the same sign, the temperature becomes the determining factor in controlling spontaneity. If ΔH and ΔS are negative, ΔG can only be smaller than zero if the term ΔH is larger in magnitude than $T\Delta S$. These reactions are therefore *enthalpy driven*. Similarly, if ΔH and ΔS are positive, ΔG will be negative (and the change spontaneous) if $T\Delta S$ is larger in magnitude than ΔH. In this case, the change is *entropy driven*. Calculations of ΔH and ΔS can therefore be used to probe the driving force behind a particular reaction.

Processes are classified as either *exothermic* ($\Delta H < 0$) or *endothermic* ($\Delta H > 0$) on the basis of whether they release or absorb heat. Processes can also be classified as *exergonic* ($\Delta G < 0$) or *endergonic* ($\Delta G > 0$) on the basis of whether the free energy of the system decreases or increases during the reaction.

The Gibbs Free Energy change of a binding reaction can be calculated from the association constant K_A using the equation:

$$\Delta G = -RT \ln K_A \tag{2.2}$$

where R is the gas constant (8.314 K^{-1} mol^{-1}) and T is the absolute temperature in Kelvin. To take the logarithm, K_A must be dimensionless, as discussed in detail in chapter 2.4.2. The association constant K_A can be measured by several techniques such as ultracentrifugation, equilibrium dialysis or Isothermal Titration Calorimetry. Using the obtained value for ΔG, the change in the entropy of the system, ΔS, can be calculated from equation 2.1 if the heat of a reaction, ΔH, is known. ΔH can directly be measured from Isothermal Titration Calorimetry or Differential Scanning Calorimetry as shown in chapters 3.3.1 and 3.3.3, respectively.

2.2   Aqueous Solutions and Solvation

Aqueous electrolyte solutions are crucial in any scientific and technological field. Their properties are determined by the ionic species present in the system. Generally, ions are classified with regard to their influence on the structure of water and there is a high demand for understanding the underlying mechanisms.

2.2.1   Water as a Special Solvent

Water, at first sight, is a very simple molecule consisting only of one oxygen atom and two hydrogen atoms. However, it is very different compared to other liquids and it has often been stated that its anomalies are essential for life on earth. For instance, liquid water expands when cooled below 4°C whereas other liquids expand only when heated. This density maximum at 4°C makes rivers, lakes and oceans freeze from the top down, thus insulating the water from further freezing. This property has offered hospitable underwater environment for many life forms to develop on this planet. The density anomaly is only one of many anomalous properties of water. However, in spite of much work on water, many anomalies are still puzzling. Enlightenment comes from an understanding that water molecules form a continuous hydrogen-bonded network with localized and structured clustering.

The water molecule is a very polar molecule with a strong dipole moment μ, as shown in Figure 2.1 A. Each hydrogen atom is covalently bound to the oxygen via a shared pair of electrons. Typically, the water molecule is described as having four, approximately tetrahedrally arranged sp^3 hybridized electron pairs, two of which are associated with the hydrogen atoms [9]. The other two electron pairs of the oxygen atom are lone pairs leading to a partial negative charge near the oxygen and a partial positive charge near the hydrogen atoms. This uneven distribution of electron density makes the water molecule polar, giving rise to the dipole moment. The weak electrostatic attraction between the partial positive and partial negative ends of the water molecules allows for the formation of hydrogen bonding (H-bonding) in liquid water, as shown in Figure 2.1 B, leading to a high degree of internal structure. The mean lifetime of a H-bond is a few picoseconds [10] and the energy of a hydrogen bond in water is around 23.3 kJ/mol [11]. Although other liquids can also form hydrogen
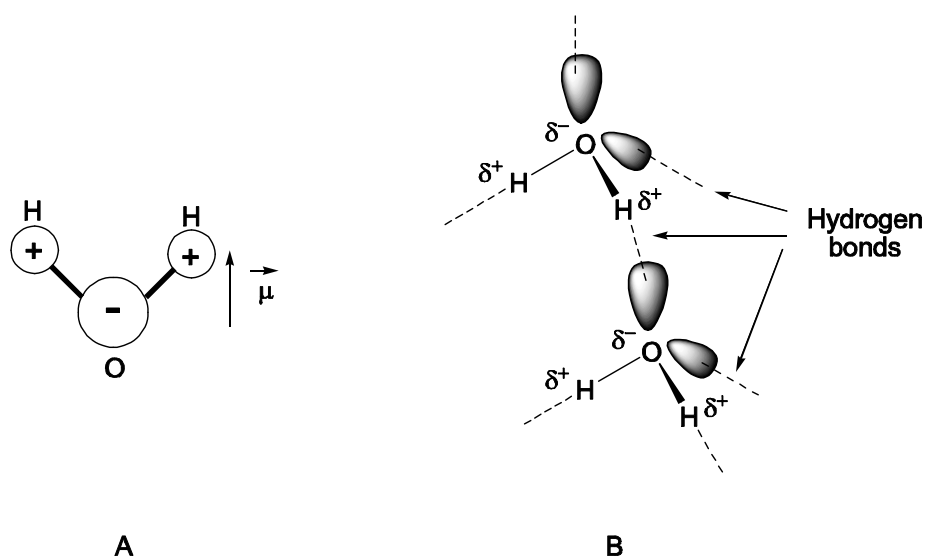
Figure 2.1: A: The water molecule, H_2O, with its dipole moment μ. B: Illustration of the H-bonding in liquid water. The gray ovals depict the lone pair orbitals (reproduced from [12]).

bonds, water, due to its tetrahedral geometry, is the only one that can expand the network in three dimensions. Hence, water's strangeness is mainly due to its ability to form highly organized intermolecular hydrogen-bond networks.

Water's chemical structure also determines its unique properties as a solvent. Due to its polarity, small size and high dielectric constant, water is an excellent solvent particularly for polar and ionic compounds. Ions change the structure of water in their vicinity. However, the extent of water structuring is still under debate. While theorists usually assume two layers of structured water [13], experimentalists report about up to 600 layers of structured water in the vicinity of charged surfaces [14].

2.2.2   Heat of Solution

The formation of an aqueous salt solution from a crystal occurs spontaneously because the interaction between the solvent and the solute is stronger than that of both solvent-solvent and solute-solute. The enthalpy exchanged between the system and its surroundings when one mole of a solute dissolves in a solvent at constant pressure to make a dilute solution is called the molar enthalpy of solution or just the *heat*

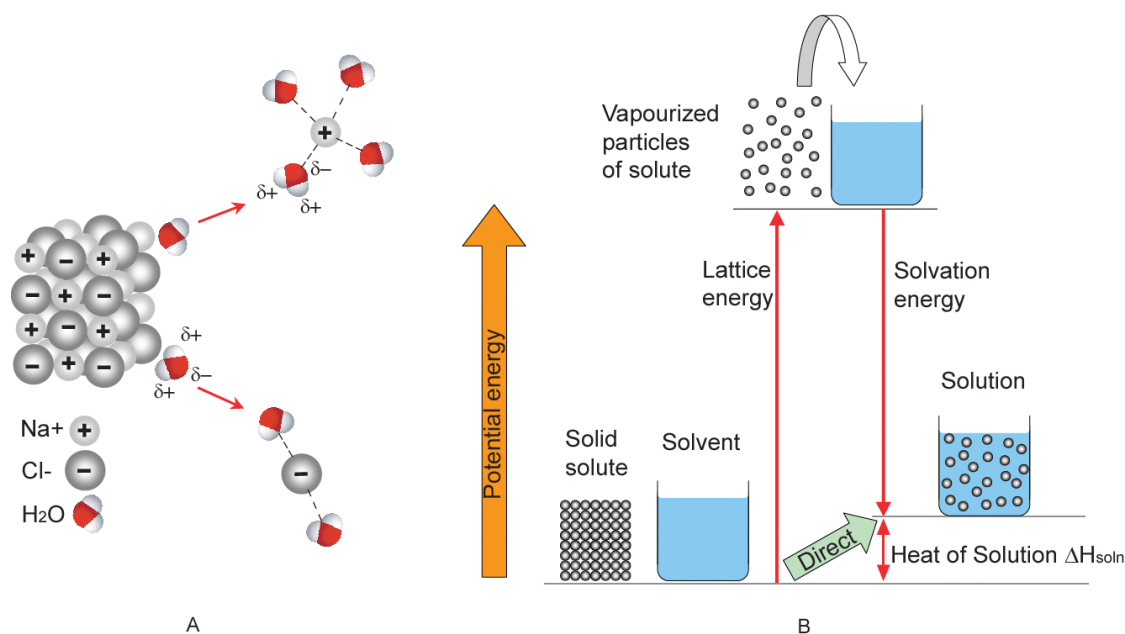**Figure 2.2:** A: Hydration of ions from a NaCl crystal as described in the text. B: Enthalpy diagram of a solid dissolving in a liquid, for the case where the formation of solution is endothermic.

of solution, ΔH_{soln}. It is composed of two steps, one dealing with the break-up of the ionic bonds of the crystal and a second step dealing with the hydration of the individual ions. An atomic picture of the hydration of ions from a crystal lattice is shown in Figure 2.2 A. When a crystal is immersed in water, the attractive forces between the ions in the crystal lattice will be considerably reduced due to the high relative permittivity of water. However, the reduction of the attractive energy in the aqueous phase would not be sufficient to dissolve NaCl. The decisive role in this process is played by the strong dipole moment of water which preferentially orients its negative pole towards a cation and its positive pole towards an anion.

An energy diagram of the solution process is shown in Figure 2.2 B. The ions in a crystal lattice are held together at an equilibrium interionic distance where strong coulombic forces and short-range repulsive forces are in balance. To break down the lattice therefore requires a large amount of energy, called the *lattice energy,* resulting in an increase in the potential energy of the system. By receiving the required lattice energy, the solid is converted into its gaseous state. In the second step, the solution is formed by solvation of the gaseous solute particles. The potential energy of the

system decreases because solute and solvent particles attract each other. Hydration reactions are therefore always exothermic and the energy released is called *solvation energy* (or *hydration energy* in the case of water as the solvent). The net energy change, the difference between the lattice and the hydration energy, is the heat of solution. If the lattice energy is larger in magnitude than the solution energy, the solution forms endothermically, i.e. cools down, and ΔH_{soln} is set to be positive. It forms exothermically, i.e. heats up, if the solution energy is larger in magnitude than the lattice energy and ΔH_{soln} is set to be negative in this case.

The absolute amount of heat Q in J which is released or absorbed when a salt is dissolved in water is proportional to the mass, m_s, of the dissolved salt (in g). It can be calculated from the molar heat of solution ΔH_{soln} in J mol^{-1}:

$$Q = \frac{m_S \Delta H_{soln}}{M_W} \tag{2.3}$$

where M_W is the molecular weight of the salt in g mol^{-1}. It can also be expressed as a function of a well defined, constant volume V ($V = m_s/C_S$):

$$Q = C_S V \Delta H_{soln} \tag{2.4}$$

where C_S is the final concentration of the salt solution in mol l^{-1}.

2.3 Ions in Water

2.3.1 Ion Pairs

When an ionic crystal XY is dissolved in an appropriate solvent, the Coulombic attractions in the solution give rise to the association of ions of opposite charge. These ion pairs are not bound by ionic bonds, but move around in the dissolved state and are held together without the formation of a covalent bond.

If the constituent ions of an ion pair are in direct contact with each other and not separated by an intervening solvent molecule the ion pair is called *contact ion pair* (or *tight* or *intimate ion pair*). A contact ion pair of X^+ and Y^- is symbolically represented as X^+Y^-. By contrast, the constituent ions can also be separated by

one or several solvent molecules. These pairs, called *loose ion pairs,* are symbolically represented as $X^+||Y^-$. If the ions are separated by a single solvent molecule, they are called *solvent shared ion pairs* whereas in *solvent separated ion pairs* more than one solvent molecule intercedes.

2.3.2   The Hofmeister Series

Many biophysical processes are ion specific, i.e. they depend on the sort of ion present in these processes. Examples of the such biophysical processes are protein stability [15], ion transport [16], the shrinkage temperature of collagen fibres [17] or the phase transitions of biomolecules [18]. The remarkable systematic effects of different neutral salts on the solubility of proteins was first documented in an organized way by Franz Hofmeister, in 1888 [6]. The ranking of anions and cations towards their ability to precipitate proteins is nowadays known as the *Hofmeister Series (HS).*

   The main characteristics of the HS summarized in a recommendable review from Cacace et al. [8] are:

1. Hofmeister effects become important at moderate to high salt concentrations in the 0.01 - 1 M range. Where higher sensitivity can be attained, the lower limit is pushed downwards.

2. They are approximately additive over all dissolved species.

3. The sign of characteristic coefficients (e.g. salting out coefficients) changes at about NaCl, which has itself a very small effect even at high concentrations.

4. They are dominated by anion effects - that is, for a given change in ionic radius, anion parameters change more than cation parameters.

	Kosmotropic (salting out)	Chaotropic (salting in)
Anions	F^- PO_4^{3-} SO_4^{2-} CH_3COO^- Cl^-	Br^- NO_3^- CO_4^- I^- CNS^-
Cations	$(CH_3)_4N^+$ $(CH_3)_2NH_2^+$ NH_4^+ Rb^+ K^+	Na^+ Cs^+ Li^+ Mg^{2+} Ca^{2+} Ba^{2+}

Table 2.1: The Hofmeister Series [8]

The series has been expanded from protein solubility to a broad range of other phenomena (given in the review from Collins & Washabaugh [7] with almost a thousand references). Different measurements of the HS typically give a similar, characteristic rank ordering, with only slight alterations. However, until today, more than 100 years later, there is still no general theory available to provide a persuasive explanation to why these effects occur. The extended series is presented in Table 2.1.

A principal reason for the ion specificity could arise from their influence on the structure of the solvent water because the ability of ions to precipitate proteins can be explained in terms of the extent of the ions binding to water. Hence, the ions within the series are distinguished by their ability to either make or break the bulk water structure. Close to the ion, primarily within the solvation shell, the water molecules are considered attached to the ions and the structure of water is enhanced relative to the bulk. At larger distance the molecules are less rigidly aligned and they may be less ordered than in bulk water. Structure-making or breaking of ions refers to the *net* effect of ions on the bulk water, which is inherently related to the system's entropy change. Ions in the series positioned to the left of Cl^- and Na^+, known as structure-makers or *kosmotropes,* exhibit stronger interactions with water molecules than water itself and are most effective in precipitating proteins ("salting-out"). Contrarily, the species to the right side, known as water structure-breakers or *chaotropes*, exhibit weaker interactions with water than water itself and are most effective in solubilizing proteins ("salting-in").

2.4   Ions and Surfaces

2.4.1   The Electrical Double Layer

To understand the process of ion binding, it is necessary to consider an atomic picture of an electrolyte close to a charged surface, since in a solution of charged colloidal particles, the distribution of ions close to the solid/liquid interface differs from the bulk phase. Far away from the phase boundary, in the bulk phase, the cations and anions of the electrolyte are evenly distributed, and the water molecules, with their large dipole moment, are more or less randomly oriented. The interactions (attractive and repulsive forces) of the individual charged species are balanced out, and the sum
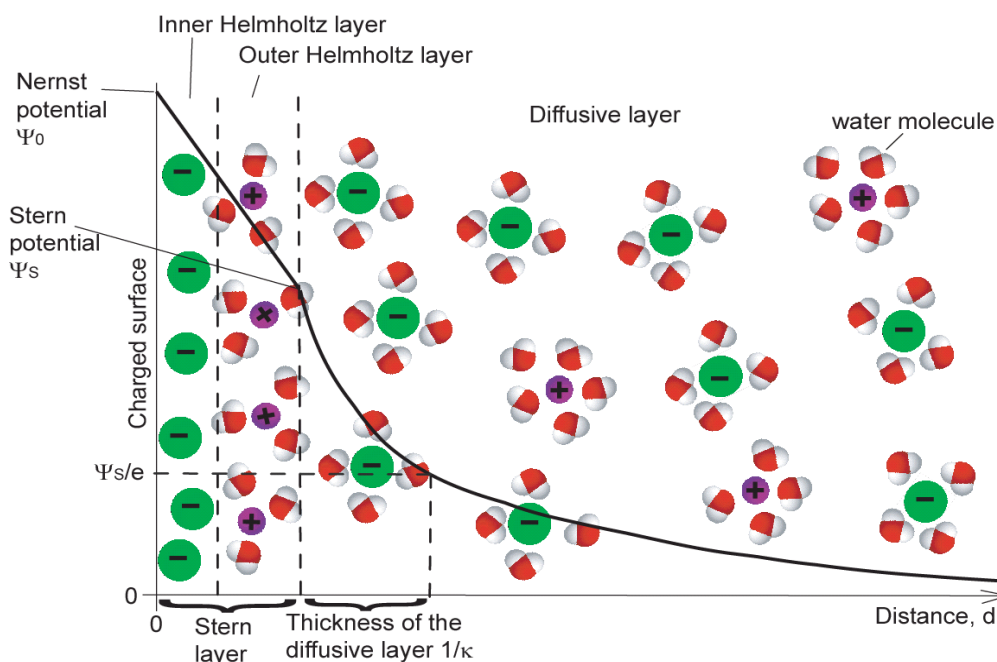
Figure 2.3: Schematic picture of the electrical double layer with the course of potential. The potential decreases linearly in the inner and outer Helmholtz layer and exponentially twoards zero in the diffusive layer.

of the forces acting on a particle over space is zero.

Close to the solid/liquid interface this balance is disturbed in a delicate way because the properties of the charged surface differ entirely from the bulk. The simplest model to describe the ion distribution close to the surface was developed by Helmholtz in 1850, who put forward the term *electrical double layer*. He assumed that in order for the interface to remain neutral, the surface charge is balanced by the redistribution of counter-ions close to the surface and ions are attracted to the surface. These ions are assumed to approach the surface and to form a fixed layer balancing the surface charge. The distance of approach is assumed to be limited to the radius of the counter-ion and a single sphere of solvation around each ion. The overall result is two layers of charge (the double layer) and a potential drop which is confined to only this region (termed the *outer Helmholtz Plane*) in solution.

If the electrolyte consists of a mixture of ions, the adsorption of ions can be specific, i.e. certain ions will adsorb while others will not. In this case, the specifically adsorbed ions will form a fixed double layer, just as the counter-ions in the Helmholtz plane, but

they will be closer to the surface than the counter-ions. In this case, the fixed layer is divided into the *inner Helmholtz layer* containing the specifically adsorbed ions and the *outer Helmholtz layer* containing the counter-ions. The two layers of charge, namely the inner and outer Helmholtz planes are called the *Stern layer*. Within this layer, the potential drops linearly from the Nernst Potential Ψ_0 at the charged surface to the Stern potential, Ψ_S.

Helmholtz's model does not represent reality, because due to diffusion or mixing in solution the double layer will not be fixed but rather statistically distributed. In fact, collisions between ions and solvent molecules induced by Brownian motion lead to a certain distribution of the ions into the bulk solution beyond the double layer. On the basis of such a picture, Gouy (1910) and Chapman (1913) built up their model of a *diffusive double layer* (the *Gouy-Chapman layer*). However, they assumed that the ions are point charges and can get infinitely close to the charged surface. Therefore, the Gouy-Chapman model predicts an unrealistically large surface concentration. The model put forward by Stern addresses this limitation by locating the centers of the first layer of ions at a mean distance from the solid surface. Beyond the first layer, the ionic distribution follows the Gouy-Chapman picture of a diffuse layer based on point charges. In this region, the concentration of excess ions decreases exponentially and approaches zero asymptotically at infinite distance. Theoretically, the double layer would therefore be infinitely thick. To avoid an infinite thickness, the electrical double layer is defined as the point where the potential reaches the value $1/e$, that is at ~43% of the Stern potential. It is given by the reciprocal of the Debye Hückel parameter κ in the electrolyte solution:

$$\frac{1}{\kappa} = [\varepsilon\varepsilon_0 RT/(F^2\sum_i C_i z_i^2)]^{1/2} \qquad (2.5)$$

where ε is the dielectric constant of the solution, ε_0 is the permittivity of free space, R is the gas constant, T is the temperature, F is the Faraday constant, and C_i is the concentration of species i and z_i is the valence of the ion i. Figure 2.3 shows the distribution of ions in the electrical double layer using the present notation.

Ion binding to phospholipid membranes is most frequently described by the Gouy-Chapman theory. Within the framework of this theory, the relation between the

concentration of a certain ion, i, close to a phospholipid membrane, $C_{i,0}$, and its concentration in the bulk, $C_{i,\infty}$, is given by the Boltzmann equation

$$C_{i,0} = C_{i,\infty} exp \left(\frac{-z e_0 \Psi_{el,0}}{kT} \right) \tag{2.6}$$

where, e_0 is the magnitude of the electronic charge, k is Boltzmann's constant and $\Psi_{el,0}$ is the electrostatic surface potential. The surface potential in the Gouy-Chapman high potential approximation [19] in MKS units is written as:

$$\Psi_{el,0} = -\frac{kT}{e_0} ln \left(\frac{\sigma^2}{2 \times 10^3 \varepsilon \varepsilon_0 k T N_A \sum_i C_i z_i^2} \right) \tag{2.7}$$

where σ is the surface charge and N_A is Avogadro's number. The factor 10^3 appears here because the concentration C_i is given in moles per liter. An approximate experimental quantification of σ can be obtained from electrophoretic measurements of the zeta potential, ζ, of the vesicles in solution [20] using the Graham equation ($\sigma = \varepsilon \varepsilon_0 \zeta / \kappa$).

2.4.2 Binding Models

When an ion interacts with a charged surface, an equilibrium between the free and bound ions will be established. This binding equilibrium is defined by the association constant, K_A, which can be described by various models differing in their assumptions. Quantitative information about the extent of ion binding can be obtained from the association constant, which can be calculated using different binding models. The relevant models used in this work will be described in the following paragraphs.

The different binding models yield association constants, K_A, usually in units of M^{-1} or M^{-2} depending on the stoichiometry of the reaction. However, to calculate the Gibbs free energy change, the association constant, K_A, must be dimensionless (because its logarithm must be taken, see equation 2.2). This can be obtained in two manners: either by normalizing the molar concentrations to the standard state concentration of 1 mol l^{-1} or by expressing K_A as (mol fraction)$^{-1}$, where 1 mol l^{-1} equals 1.8×10^{-2} mol fraction (corresponding to 1/55.56 mol H_2O per l). The choice

of the standard state is a matter of convention, but is important when comparing values of ΔG and ΔS.

It should also be noted that the association constant, K_A, of a binding equilibrium is both temperature-dependent and related to the Gibbs free energy (equation 2.2) and hence to the enthalpy change of the process (equation 2.1).

Henry-Dalton Partition Equilibrium

The simplest binding model assumes that the partition of an ion L (the ligand) bound to the surface and free in the bulk solution is nonspecific. Hence, the chemical equilibrium is given by:

$$L_F \overset{K_A}{\rightleftharpoons} L_B$$
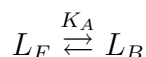
and the equilibrium constant is

$$K_A = \frac{[L_B]}{[L_F]} \tag{2.8}$$

where $[L_F]$ and $[L_B]$ denote the concentrations of free and bound ion, respectively.

Langmuir Adsorption

The Langmuir adsorption was developed by Irving Langmuir in 1916 to describe the dependence of the surface coverage of an adsorbed gas on the pressure of the gas. The main assumption of the Langmuir adsorption isotherm is that each site on the surface can accommodate only one molecule or atom. Therefore, this model is also called *1:1 binding model.* The equilibrium of an ion L binding to the binding site M of a molecule to form a complex LM can be described by

$$L + M \overset{K_A}{\rightleftharpoons} LM$$
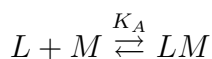
Generally, the association constant is expressed as a function of mole fraction of bound sites, Θ:

$$K_A = \frac{\Theta}{(1 - \Theta)[L_F]} \tag{2.9}$$

where Θ is the concentration of bound sites over the total concentration of binding sites.

Formation of a Ternary Complex

In the case of divalent ions, binding to a charged surface, it is reasonable to assume that a ternary complex consisting of the divalent ion L and two independent binding sites M will be formed. In this case, the chemical equilibrium can be written as

$$L + 2M \overset{K_A}{\rightleftarrows} LM_2$$

where the equilibrium constant can be exressed using the present notation as
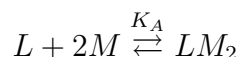
$$K_A = \frac{[L_B]}{[L_F][M_F]^2} \tag{2.10}$$

Some of these models have been used further in this work to describe the binding of Ca^{2+} to polymers and lipid membranes as presented in chapter 5.

2.5 Ions in Biology: The Na^+/K^+ Specificity

Since the early days of molecular biology, it has been known that living cells selectively retain certain ions, such as potassium and exclude others, such as sodium. In fact, the intracellular concentrations of potassium and sodium are 140 mM and 5 - 15 mM, respectively, whereas their extracellular concentrations are 5 mM and 145 mM, respectively [21]. Thus, the potassium concentration is relatively higher inside the cell and the sodium concentration is relatively higher outside. This leads to both electrical and chemical gradients across the cell membrane, which are crucial for cell function. The electrical gradient across the cell membrane is the basis for excitability in nerve and muscle cells and export of sodium from the cell provides the driving force for several facilitated transporters, which import glucose, amino acids and other nutrients into the cell.

For many years, researchers have tried to understand the characteristic partitioning of sodium and potassium in cells and tissues. Most physiologists believe that it is due to ion pumps and channels in the membrane. It is assumed that pumps transport solutes across the cell boundary against their respective concentration gradients while channels permit the solutes to flow back in the opposite direction. The pumps which

are special proteins integrated into the membrane are believed to use the cell energy to transport ions into and out of the cell. Crucial experiments and calculations have been performed that provide strong evidence for the existence of pumps. Genes coding for these proteins have been cloned and the proteins themselves have been studied in great detail.

However, it is not yet clear whether ion partitioning in the cell is mediated by the pumps themselves or if ions are excluded from the cell due to their low solubilities in cellular water. It has been shown by nuclear magnetic resonance (NMR) [22], [23], [24] that cell water is more structured than liquid water and less structured than ice. The hypothesis challenging the conventional ion pump theory is that this special structure affects the solubility of various ions in the cell and accounts for selective ion exclusions. The theory of structured water and ion binding was first established in 1962 by Gilbert Ling [25] who performed experiments on muscle cells to determine how much energy would be required for a sodium pump. He concluded that a sodium pump operating at 100% efficiency, would require at least 15-30 times as much energy as available. He concluded that ion pumps are thermodynamically not feasible.

Later, Freedman and Miller [26] reported that Lings calculations are based on a sodium transport out of the cells at least 20 times faster than the rate accepted by muscle physiologists. If these critics are correct, pumps are thermodynamically feasible. Still, many investigators, including advocates of pumps, agree that cell water is ordered differently than liquid water. But the details of the role of structured water in cell physiology remain to be determined.

Chapter 3

Experimental Methods and Materials

The following chapter contains a description of the materials and experimental methods used in this work. Since the main techniques used here are Isothermal Titration Calorimetry (ITC) and Ion Selective Electrodes (ISE), chapters 3.3.1 and 3.3.2 provide a detailed description of these methods. For details on the other techniques used in this work, the reader is referred to the literature.

The heat of dilution of salts and polyelectrolytes discussed in chapter 4 were studied by ITC. Experiments on the binding of Ca^{2+} to polymers and lipid membranes presented in chapter 5 were performed using ITC to determine binding enthalpies and a Ca^{2+} ISE to determine the amount of bound calcium. Spectrophotometry (chapter 3.3.6) was used to detect the maximal calcium loading of different polymers. Vesicles were characterized by Dynamic Light Scattering (chapter 3.3.5), electrophoresis (chapter 3.3.4) and Differential Scanning Calorimetry (chapter 3.3.3). Studies on individual vesicles were performed by phase contrast microscopy (chapter 3.3.7). The Na^+/K^+ specificity discussed in chapter 6 was investigated using ITC and a K^+ ion selective electrode.

3.1 Materials

All solutions were prepared using deionized water from Elix MilliQ Millipore system with a TOC of less than 15 ppb and a resistivity of 18 MΩcm. Figure B.1 displays

the chemical structure of the different polymers and lipids used here. The molecular weights, the degree of polymerization and the concentration ranges of the solutions used in the various experiments are summarized in Table A.1.

3.1.1 Inorganic Salts and Polyelectrolytes

Sodium iodide, NaI, lithium chloride, LiCl, sodium sulphate, Na_2SO_4, sodium acetate, CH_3COONa (NaAc), magnesium chloride, $MgCl_2$ and potassium chloride, KCl, were purchased from Aldrich (Germany). Calcium chloride, $CaCl_2$ and cesium chloride, CsCl, were purchased from Merck (Germany).

Three poly(sodium acrylates) (NaPAA) of different degrees of polymerization (DPn) were used. NaPAA1 and NaPAA2 used for the dilution measurements were purchased from Aldrich (Germany). Their weight average molecular weights, M_W, are 2.1×10^3 g/mol for NaPAA1 and 5.1×10^3 g/mol for NaPAA2 with a DPn of about 22 and 53, respectively. NaPAA3 used for the titration experiments was prepared from PAA (Aldrich, Germany, $M_W \cong 100 \times 10^3$ g/mol, DPn $\cong$ 1040) by adjusting the pH to 7 using NaOH (Merck, Germany). The poly(acrylic-co-maleic acid) (Sokalan) and poly(aspartic acid) (PAsp) with $M_W \cong 70 \times 10^3$ g/mol and $M_W \cong 20 \times 10^3$ g/mol, respectively, were purchased from BASF (Germany). The solutions of Sokalan and PAsp used for the titration experiments were adjusted to pH 7 using NaOH. PAsp at pH 7 will be further denoted as NaPAsp. Poly(sodium styrene sulphonate) (NaPSS) was a commercial standard supplied by Polymer Standard Service (Mainz, Germany) with $M_W \cong 8 \times 10^3$ g/mol, corresponding to a DPn of about 40. A ^{1}H NMR spectrum indicated a monomer purity of about 95%.

Poly(N-Isopropylacrylamide) (PNIPAAM) microgel particles were prepared by emulsion polymerization of NIPAAM monomer in the presence of methylene-bis-acrylamide (MBA) as crosslinker, potassium peroxy disulfate (KPS) as initiator and sodiumdodecylsulfate (SDS) as surfactant. The obtained PNIPAAM particles contain 1.6 wt% MBA, 1% SDS and remainder of sulfate due to the initiator KPS. The solution was adjusted to pH 7 using NaOH. The weight average particle size determined by DLS measurement is 130 nm.

3.1.2 Phospholipids

1,2- Dioleoyl- sn- Glycero- 3- Phosphocholine (DOPC) and 1,2- Dioleoyl- sn- Glycero-3- [Phospho- L- Serine] (Sodium Salt) (DOPS), 1- Stearoyl- 2- Oleoyl- sn- Glycero-3- Phosphocholine (SOPC) and 1- Stearoyl- 2- Oleoyl- sn- Glycero- 3- [Phospho- L-Serine] (Sodium Salt) (SOPS) were purchased from Avanti Polar Lipids, Inc. (Birmingham, AL) and used without further purification. The lipids were transported from the manufacturer solubilized in chloroform solution filled into amber borosilicate glass bottles. The glass bottles were stored at –20°C immediately upon arrival.

3.2 Preparational Methods

3.2.1 Preparation of Poly(calcium acrylate)

Because poly(calcium acrylate) is a by-product of the process of calcium binding, we studied the dilution of the polymer in water. However, poly(calcium acrylate) is insoluble in water. Therefore we analyzed the heat of dilution of a modified NaPAA2 salt where the sodium was partially exchanged with Ca^{2+} ions (this product will be further denoted as CaPAA). In order to determine the critical exchange limit at which CaPAA gives a homogeneous solution, we prepared solutions of different molar concentration ratios of Ca^{2+} to NaPAA2. For a fixed monomer concentration the molar ratio was increased from 0.20 in steps of 0.02 up to 0.30. The solutions were prepared by mixing an 0.4 M NaPAA2 solution with a certain amount of CaO (purchased from Aldrich, USA) giving the desired concentration ratio. The solutions were shaken to obtain good mixing of the reactants and stirred for three days to ensure complete equilibration of the reaction. The maximum ratio (or the critical exchange limit) at which CaO fully dissolved in the NaPAA2 solution was found to be about 20 mol% corresponding to a neutralization of 40% of all acrylate sites (note that the critical exchange limit depends both on the polymer concentration and the pH of the system).

3.2.2 Vesicle Preparation

Two different kinds of vesicles were used to study the binding of Ca^{2+} to lipid membranes (chapter 5.2). The phase contrast microscopy measurements were performed with giant unilamellar vesicles (GUVs). GUVs have a diameter of 1 - 100 μm and can therefore be used for the study of individual vesicles using optical microscopy. However, these vesicles can be prepared only with low bulk concentrations (μM) and they are very polydisperse. In contrast, large unilamellar vesicles (LUVs) with diameters ranging from 50 to 500 nm can be produced up to 50 mM concentrations with very narrow size distributions. LUVs were used for all the measurements except in the phase contrast microscopy measurements.

Preparation of Large Unilamellar Vesicles

Large unilamellar vesicles were prepared by extrusion using the method of Nayar et al. [27]. Lipid solubilized in chloroform was transferred to 5 ml round-bottom flasks and the chloroform was removed from solubilized lipid by rotary evaporation for 1h using a Laborota 4002-control (Heidolph instruments, Kelheim, Germany) at 400 mbar. Following this, the lipid film was placed under vacuum overnight to ensure complete removal of the solvent. It was then dissolved in an 0.01 N NaCl solution by vortexing the solution for 2 min. The LUVs were obtained by extruding this solution with a LiposoFast^{TM} pneumatic extruder (Avestin Inc., Ottawa, Canada) at a pressure of 200 kPa and lipid concentrations ranging from 0.01 to 0.04 M. The extrusion was performed in three stages: (1) 31 times through a 200- nm- diameter pore polycarbonate filter; (2) 21 times through a 100- nm- diameter pore filter and (3) 41 times through a 50- nm- diameter pore filter. Vesicles prepared in this way are generally believed to have a narrow size distribution and are known to be almost entirely unilamellar [28]. The size distribution of LUVs was measured by Dynamic Light Scattering and was found to be r = 28 - 32 $\pm$ 0.2 nm. The vesicles were used within 5 days after the extrusion.

Preparation of Giant Unilamellar Vesicles

The method used to prepare GUVs was similar to the method presented by Evans & Rawicz [29]. A small volume (23.8 μl) of a DOPS/DOPC (molar ratio 2:8) solution

in chloroform (total lipid concentration 16.7 mg/ml) was spread on the rough side of a Teflon disc. The disc was placed with the rough side facing upwards into an open 10ml flask and left to stand under vacuum overnight to ensure complete removal of the chloroform. The sample was then prehydrated by allowing it to stand at $37°C$ in a humid atmosphere for 6 h. Then, 5 ml of a filtered sucrose solution with osmolarity of 0.1 osmol/l were gently poured onto the sample and the bottle was closed and left to stand at $37°C$ for one to two days. After this time, a typical cloud of concentrated vesicles was observed. The vesicles were stored at $37°C$ until use. The vesicle cloud was then diluted by transferring it into a solution of 0.01 N NaCl and glucose. The osmolarity of this glucose solution was carefully adjusted to be the same as the solution of vesicles in sucrose in order to avoid osmotic stress. The osmolarities of the glucose and sucrose solutions were measured using a freezing point osmometer Osmomat 030 from Gonotec (Berlin, Germany).

3.3 Experimental Techniques

3.3.1 Isothermal Titration Calorimetry

In essentially all binding reactions, heat is either generated or absorbed. A method to determine this heat is Isothermal Titration Calorimetry (ITC) which measures the released or absorbed heat upon mixing of two solutions. Recently, ITC has become a very popular tool to study association reactions in biochemical processes, such as protein/lipid interactions, enzyme kinetics or antibody studies. Advantages of ITC are its high sensitivity (it detects heat in the μcal range), the relatively fast data aquisition ($\sim$2 hours/ experiment), the small working volume needed for one measurement and the modest experimental constraints for obtaining data. The most important feature of ITC is that the measured reaction heat can be used to determine the complete thermodynamic properties of a physical or chemical process, i.e. the enthalpy ΔH, the free energy ΔG, the entropy ΔS, the equilibrium constant K and the reaction stoichiometry, n (see chapter 2.2).

A schematic picture of the instrument setup is shown in Figure 3.1. The main parts of the machine are the injection syringe containing one reaction partner, the sample cell containing the other reaction partner and the reference cell, filled with the
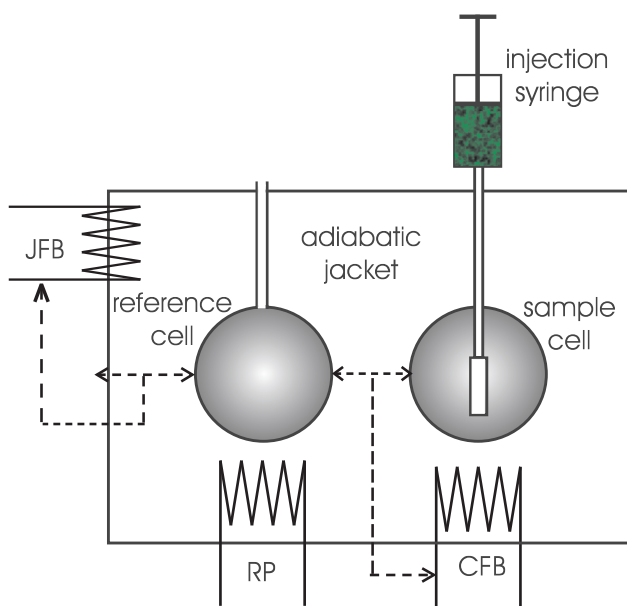
Figure 3.1: Diagram of ITC cells and syringe. The reference and the working cell are enclosed in an adiabatic jacket. The titrant is injected via a syringe with a rotating flat tip.The temperature control is achieved by three electrical feedback systems, jacket feed back (JFB), reference power (RP) and control feed back (CFB) (reproduced from [30]).

buffer or solvent used to prepare the sample solution. The two spherical cells of the same volume are enclosed in an adiabatic jacket and connected to the outside through narrow access tubes. The reference and the sample cell are connected to two resistive heaters, the reference power (RP) and the control feed back (CFB), respectively. A thermoelectric device measures the temperature difference (ΔT) between the two cells. The adiabatic jacket containing the sample and the reference is heated by a third heating system, the jacket feed back (JFB), keeping the temperature of the adiabatic jacket at the same temperature as the reference cell. This prohibits a heat exchange between the cells and the environment.

The mixing of the solution in the syringe and the titrated solution in the sample cell occurs by injecting small aliquots of titrant (typically 5 - 20 μl) into the sample solution. The addition of the titrant is performed automatically from the precision syringe driven by a computer-controlled stepper motor. The rotation of the syringe assures a complete mixing of the two reactants.
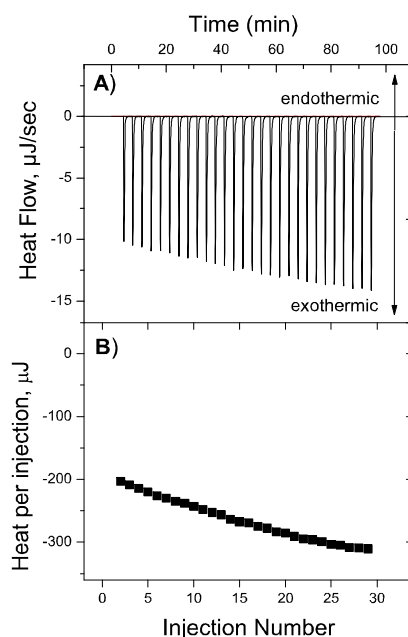
Figure 3.2: Dilution measurement. A) Raw ITC data from injecting water (10 μl aliquots) into 0.55 N NaPAA1 with subtracted baseline. B) Heat per injection obtained from integrating the heat flow over time.

The injection of the titrant causes a chemical reaction in the sample cell, which generates or absorbs heat. This heat is determined by measuring the power which is required to keep the reference and sample cell at the same temperature ($\Delta T = 0$). The reference cell is heated continuously with a very low power (RP) of e.g. 20 μW and the experiment can be considered as "isothermal" because the increase in temperature is also low (30-60 mK h^{-1}). To keep the temperature difference at zero, heat is either added to the sample or to the reference cell, as appropriate, using the CFB system. An exothermic reaction yields a negative change in the power signal since the heat evolved chemically provides heat that the resistive heater no longer requires to supply. Similarly, endothermic reactions cause a positive signal.

The power signal is measured in J s^{-1} as a function of time. Integrating the power required to maintain $\Delta T = 0$ over time yields the heats of reaction of each injection. In the analysis, a baseline is subtracted from the data before integration. It corresponds to the signal between two consecutive injections when no change in the

heat flow is detected. Since the filling and mounting of the syringe may cause slight inaccuracy of the volume of the first injection, a first injection with a small volume (2μl) is made and the corresponding heat is not included in the evaluation.

Figure 3.2 illustrates a typical ITC experiment. The upper panel shows the heat flow (μJ s^{-1}) caused by the injection of 10 μl aliquots of water into a solution of 0.55 N NaPAA1 in the working cell. Each peak corresponds to the heat consumed during one injection. Integrating the heat flow peaks yields the heat of each injection, Δh_i, in μJ (lower panel).

In this work, ITC was used for measurements of the heat of dilution of inorganic salts and polymers (chapter 4) and the enthalpy of ion binding to polymers and lipid membranes (chapter 5 and 6). The instrument used here is a VP-ITC Microcalorimeter from MicroCal (Northhampton, MA). The volume of the reference and the sample cell is 1.4424 ml and the total volume of the syringe is 0.282 ml. The reference cell is filled with water. All experiments are performed at 25°C at a stirring rate of 310 rpm. Unless otherwise stated, the total number of injections for each experiment is 29 starting with the first injection of 2 μl which is ignored and proceeding with 28 injections of 10 μl. The injection time for all injections is 4 s. The data analysis was performed using the Origin software provided by MicroCal [31], [30].

For calculations of specific heats normalized over the moles of injected solute or sample in the working cell, it is important to note that only the *working* volume of the ITC cell, V_0, is sensed calorimetrically. This is realized in practice by displacing a volume of the sample solution after each injection into the narrow communication tube connecting the sample cell to the outside. In other words, each injection i of volume V_i acts to drive a volume V_i of liquid out of the working volume up into an inactive tube. Thus, the total number of moles of sample molecules initially in V_0 at the beginning of the experiment is distributed into a larger volume, $V_0 + V_{i,tot}$ where $V_{i,tot}$, is the sum of the individual injection volumes. This must be taken into account when calculating concentrations of injected solute and sample.

3.3.2 Ion Selective Electrodes

When an ionic solution is added to a polymer or vesicle suspension, only some of the added ions bind while the rest remains free in the bulk solution. The extent

of ion binding is determined by the respective binding constant. Consequently, the knowledge about the amount of bound analyte can be used to determine binding constants of the reaction. Different methods to study counterion-polyion interactions exist, such as ion selective electrodes [32], conductivity [33], [34] or voltametry [35], [36]. In this work, the amount of free calcium and potassium was measured with a Ca^{2+} and K^+ Ion Selective Electrode, respectively.

An Ion Selective Electrode (ISE) is a chemical sensor that selectively detects a specific ion in the presence of other ions or compounds in a solution. The main advantages of ISEs compared to other analytical techniques is their robustness, the simple handling and the possible application over a wide concentration range. To measure ion binding equilibria, as performed in this work, ISEs are particularly useful, since they measure the activity of the ion under study without any separation operation. In contrast, e.g. ion chromatography requires a separation of the different ions in solution which can lead to changes in the equilibrium resulting in systematic errors. Compared to conductivity measurements, the data analysis using ion selective electrodes is more straight forward. One big draw back of the electrodes is the possible interference with other compounds absorbing on the membrane of the sensor.

A schematic picture of an electrochemical cell consisting of the ion selective electrode and a reference electrode is shown in Figure 3.3. The two electrodes are immersed in the electrolyte solution and each of them is connected to one clamp of a voltmeter. As the figure illustrates, every electrochemical voltage metering detects the sum of two potentials: the galvani potentials at the ISE and the reference electrode. This is true, if the metal/metal thermal potentials at the voltmeter/electrode interfaces can be neglected compared to the galvani potentials, which is generally the case.

The key component of a potentiometric ISE is the ion-selective membrane which is electrochemically active towards a certain ion. The potential difference at the electrode/electrolyte interface is a function of the activity of a specific ion and is a result of the physicochemical processes at the interface. At the membrane/solution boundary, the anisotropy of dispersion forces leads to a partial charge separation resulting in an electrostatic potential between the membrane and the solution. The
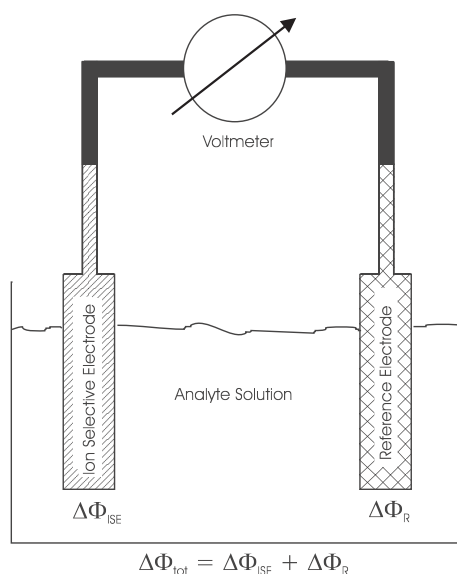
Figure 3.3: Schematic picture of an electrochemical cell. The voltmeter measures the sum of the galvani potentials at the ion selective electrode and the reference electrode.

charge distribution at the interface follows the models of an electrical double layer as described in chapter 2.4.1. However, the ions which are enriched in the electrical double layer do not have to stop in front of the membrane. In fact, most of the ion selective membranes are permeable to specific ions, so that these can pass through the membrane and the other way around, if they gain energy by doing so. The direction and extent of this phase change of charge carriers is governed by the chemical potential equilibrium, i.e. the minimization of energy.

The electrical and chemical equilibrium processes together determine the equilibrium galvani potential, $\Delta\Phi_{eq}$, given by the Nernst equation:

$$\Delta\Phi_{eq} = \Delta\Phi_0 + k\lg a \tag{3.1}$$

where $\Delta\Phi_0$ denotes the standard equilibrium galvani potential (which is a function of the reference electrode and internal electrolyte solutions), k the Nernst factor (59.16 mV at 25°C for a monovalent ion) and a the activity of the ion in the sample solution.

How can the above mentioned potential difference between the electrode and the

electrolyte be measured? The only way to do so is to connect the ISE to one clamp of the voltmeter and a reference electrode, immersed in the same electrolyte solution, to the other clamp. In this way, the potential inside the electrolyte solution is discharged to the second clamp of the voltmeter. However, at the phase boundary between the reference electrode and the electrolyte, the analogous physicochemical processes as for the ISE take place, and an additional galvani potential, $\Delta\Phi_{Ref}$, is measured by the voltmeter. A separation of the total measured potential into an ion selective and a reference potential is not possible. Thus, the goal of the measurement with an electrochemical cell is to measure only the changes of the galvani potential at the ISE and to keep the galvani potential at the reference electrode as constant as possible. This is realized in practice by immersing the reference electrode cartridge into a special vascular electrode filled with a reference electrolyte, which is separated from the solution under study with a diaphragm. In order to minimize the mixing of the reference electrolyte with the solution, which would render the electrolyte ineffective, the mixing is decelerated by keeping the electrolyte/solution contact zone small. For details in the construction of ISEs and reference electrodes as well as the choice of the reference electrolyte the reader is referred to the literature [32].

In practice, there are two methods to determine the activity of a target ion in a solution. One method, named the standard addition method, involves addition of a known quantity of analyte to the solution. If the slope of the electrode is known, the amount of free analyte in the solution can then be calculated from the change in the electrode potential. However, this method can only be applied for complexation reactions (an ion L binding to the complexing agent M to form a complex LM) when the complexing agent is in excess, i.e. 20-100 times larger than the concentration of added ion.

The second way to measure the activity of the ion under study, which was used in this work, is by a calibration curve. The potential measured for a series of calibration solutions in the range of concentration of interest and plotted as a function of the logarithm of the respective activity can be used to determine the unknown activity of the analyte in a solution. The concentration of the ion can only be determined from the calibration curve, if the activity of the solution in the calibration solution and the analyte solution is the same, which is the case if the ionic strength of the solutions
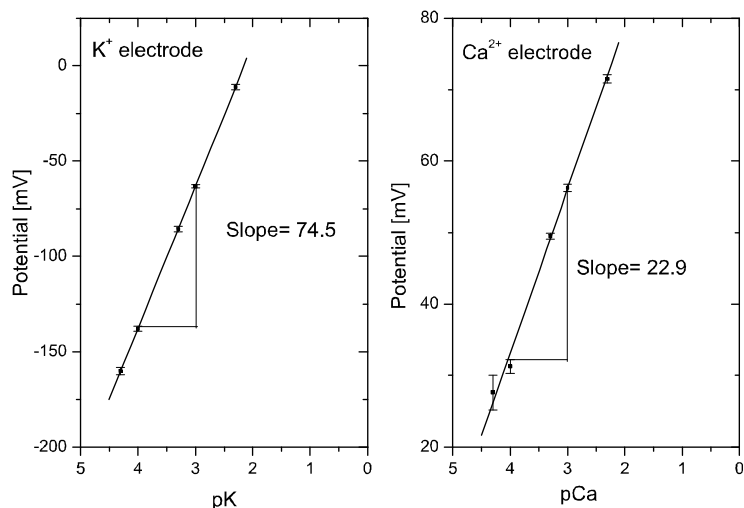
Figure 3.4: Calibration curves of a K^+ and Ca^{2+} Ion Selective Electrodes. The error was determined using five consecutive measurements of the calibration solutions.

are equal. Usually, this is achieved by adding an appropriate ionic strength adjuster (ISA) to both, the analyte and the calibration solution. The ISA solution has a high ionic strength so that the differences in the ion strength of the two solutions are negligible. In this work, the addition of an ISA solution was avoided due to its possible competition in the binding reaction. However, the calibration was performed with and without the ISA solution showing that the difference in the measured potential lay within the error of the calibration curve.

The theoretical value of the linear response slope of the calibration curve is, according to the Nernst equation (equation 3.1), 59.16 mV/decade (at $25°C$) for monovalent and 29.58/decade for divalent ions. Examples of two calibration curves are presented in Figure 3.4.

An important characteristic of the electrode is its response towards other ions, since a membrane is not only sensitive to a single type of ion but is also slightly permeable to other ions. In order to minimize the effect of interfering ions, the molar ratios of the interfering ion to the ion under study must lie below the values given by the electrode manufacturers. In this work, this condition was always observed.

There are different types of ion-selective membranes: solid membrane (e.g. glass

membrane or crystal membrane), liquid membrane (based on e.g. classical ion-exchanger, neutral or charged carrier) or a membrane in a special electrode (gas-sensing or enzyme electrode). According to the nature of the binding sites, the membranes can be classified as membranes containing fixed sites and membranes containing mobile ion-exchangers or ionophores. The binding sites are incorporated in the membrane matrix, which determines the internal polarity, lipophilicity, transport and other mechanical properties of the membrane.

In this work, Ca^{2+} and K^+ electrodes with liquid ion selective membranes were used. Liquid (organic) phases with ion-exchange properties are generally stabilized against the external solution within a polymer or ceramic membrane. The main components of a liquid membrane are the ionophores, that are charged or uncharged ion carriers able to complex ions reversibly and to transfer them through the organic membrane. These ionophores are mobile in the free and the complexed forms. The mobile binding sites are dissolved in a suitable solvent and usually trapped in a matrix of organic polymer. The analyte mobility and the ion-exchange equilibrium together determine the selectivity of a membrane towards a certain ion. Examples for Ca^{2+} and K^+ selective ionophores are shown in Figure B.2.

Ca^{2+} Ion Selective Electrode (ISE)

The Ca^{2+} Ion Selective Electrode used in this work was purchased from Mettler Toledo, Switzerland. Its ion selective membrane is a liquid membrane made from a poly(vinylchloride) polymer-matrix. The precision of the instrument is better than $\pm\,4\%$ of the measured Ca^{2+} concentration, and the limit of detection is 10^{-6} mol l^{-1}. The calibration of the electrode was carried out with $CaCl_2$ solutions with concentrations in the range of 1×10^{-6} M to 5×10^{-3} M. The calibration curve of measured voltage versus the logarithm of $CaCl_2$ concentration was consequently used to determine the concentration of free calcium ions in the polymer solutions. The reference electrode used together with the Ca^{2+} ISE was an Inlab 301 from Mettler Toledo, Switzerland, equipped with a ceramic membrane and a 3 M KCl solution as reference electrolyte.

K$^+$ Ion Selective Electrode (ISE)

The K$^+$ Ion Selective Electrode used here was purchased from Mettler Toledo, Switzerland, was equipped with an ion-selective poly(vinylchloride) polymer-matrix. The limit of detection is 10^{-6} mol l^{-1} and the precision of the instrument is $< \pm 2\%$ of the measured K$^+$ concentration if the molar ratio of Na$^+$/K$^+$ is < 2000. An Inlab 302 from Mettler Toledo, Switzerland, was used as reference electrode. It contains a removable polytetrafluorethylene (PTFE) sleeve as diaphragm and a bridge electrolyte chamber filled with a 3 M KCl solution. An 0.1 M tetraethylammoniumchloride (TEACl) solution was used as reference electrolyte. KCl solutions with concentrations in the range of 2×10^{-5} M to 5×10^{-3} M were used for the calibration of the electrode. The concentration of free potassium ions in the polymer solutions was determined from the calibration curve of measured voltage versus the logarithm of the KCl concentration.

3.3.3 Differential Scanning Calorimetry (DSC)

The DSC instrument measures the heat capacity of a solution as a function of temperature and can be used to study thermal transitions, to determine melting temperatures as well as thermodynamic parameters associated with these changes. In this work, DSC experiments were performed to investigate thermal phase transitions of the vesicles in the absence and presence of calcium.

High sensitivity calorimeters are usually equipped with twin cells, the reference and the sample cell, and operate in a differential mode. The sample cell is filled with the studied solution and an equal volume of solvent or buffer is placed in the reference cell. Both cells are heated or cooled quasi-adiabatically at a constant scan rate. Since the heat capacities of the solution in the sample cell and the solvent in the reference cell differ, a certain amount of electrical power is required to balance the temperature difference between the two cells. The power difference (J s^{-1}), after normalization by the scanning rate (K s^{-1}) is a direct measure of the heat capacity difference (J K^{-1}) between the solution and the solvent. To obtain the partial specific heat of the solution, the partial specific heat of the solvent has to be subtracted [31].

The instrument used in this work is a VP-DSC Microcalorimeter from MicroCal

(Northhampton, MA). The lipid concentration of solutions used for the DSC measurements was 1 mg/ml and the samples were examined at a scanning rate of 30 K h^{-1} by applying two heating and two cooling cycles between 2°C and 22°C. Baseline subtractions were performed using the MicroCal DSC data analysis software. The influence of calcium on the phase separation of PS/PC (2:8) LUVs was studied by adding calcium to the vesicle solution yielding the desired molar ratios of Ca^{2+} to lipid.

3.3.4 Electrophoresis

When Ca^{2+} binds to the surface of a vesicle the net surface charge changes. The measurement of the vesicles surface charge as a function of Ca^{2+} concentration can therefore provide useful information about the extent of Ca^{2+} binding. However, the surface charge of a colloidal particle cannot be measured directly. Instead, the charge at the shear plane, which is an imaginary surface separating the thin layer of liquid bound to the solid surface from the rest of the liquid, is measured. The electrical potential at this shear plane is called the zeta potential, ζ [37].

In this work, the zeta potential of the vesicles as a function of added Ca^{2+} concentration was measured by electrophoresis. Electrophoresis is the movement of charged colloidal particles in an electrical field. The instrument used here is a Melvern Zetasizer 3000 HS (Malvern Instruments Ltd, Malvern UK). It measures the migration rate of dispersed particles under the influence of an electric field using Laser Doppler Velocimetry. The observed velocity divided by the strength of the applied electrical field is a direct measure of the electrophoretic mobility, μ, of the particles examined. The zeta potential can then be calculated from the mobility, μ, using the Smoluchowski [38] relation ($\zeta = \mu\eta/\varepsilon$, where η and ε are the viscosity and permittivity of the solution, respectively).

3.3.5 Dynamic Light Scattering (DLS)

To investigate if calcium induces fusion or aggregation in the vesicle solutions under study, the vesicle size distribution as a function of added calcium was determined with Dynamic Light Scattering. DLS is the most straight forward way to determine

the hydrodynamic radius and polydispersity of colloidal particles. In a DLS machine, a beam of monochromatic light passes through the sample under study. When the beam passes through the colloidal dispersion, the particles or droplets scatter some of the light. As a result of Brownian motion, neighboring particles within the illuminated zone will cause constructive and destructive interference of the scattered light. This interference gives rise to the intensity fluctuations of the scattered light which contains information about the particle motion. The time-dependent fluctuations in the scattered intensity are measured by a suitable detector such as a photomultiplier. Analysis of the time dependence of the intensity fluctuation yields the diffusion coefficient of the particles. The diffusion coefficient can then be used to calculate the hydrodynamic radius of the particles via the Stokes Einstein equation.

In this work, DLS was used to determine the size distributions of the vesicles and PNIPAM particles in the absence and presence of added salt. The DLS machine employed here is an ALV-NIBS High Performance Particle Sizer (ALV-Laser Vertriebsgesellschaft m.b.H., Langen, Germany). The instrument uses a 2 mW HeNe Laser at a wavelength of 632.8 nm and detects the scattered light at an angle of 173°. All measurements were performed at 25°C. The autocorrelation function is measured using exponential spacing of the correlation time. Data analysis was performed with software provided by ALV. The intensity weighted size distribution was obtained by fitting data with a discrete Laplace inversion routine.

3.3.6 Spectrophotometry

Above certain concentration ratios calcium causes precipitation of the polymers. To determine the corresponding precipitation limits of the different polymers, turbidity measurements where performed with a UV-Visible Spectrophotometer Helios Gamma from Thermo Spectronic, UK. The instrument measures the absorbance of a sample as a function of the wavelength with respect to a reference. The absorption is measured by passing a beam of light through a sample and measuring the intensity of transmitted light reaching a detector. The pH of PAA, Sokalan and PAsp solutions of concentrations 0.08 N, 0.105 N and 0.037 N, respectively, was adjusted to 7 using NaOH. Small aliquots of an 0.014 N $CaCl_2$ solution were injected into the polymer solutions until the measured absorbance increased significantly at the onset of pre-

cipitation. To avoid contributions to the signal from precipitate formation, all the titration measurements were performed at concentration ratios below the measured precipitation limits.

When Ca^{2+} binds to the vesicle surface, this may cause aggregation or fusion of the vesicles which can be detected from the change in the solution turbidity. To investigate vesicle aggregation, 10 μl aliquots of an 0.014 N $CaCl_2$ solution were injected into 1.4424 ml of an 0.008 N DOPS/DOPC (2:8) solution extruded in 0.01 N NaCl and the absorbance was measured as a function of added Ca^{2+}. In order to determine the enthalpy associated with aggregation, the absorbance of 1.4424 ml of 0.01 N NaCl containing the same aliquots of $CaCl_2$ was measured and subtracted from the total absorbance.

3.3.7   Phase Contrast Microscopy

Phase Contrast Microscopy was used to visualize the effects of Ca^{2+} binding on lipid membrane fluctuations. The phase contrast microscope is widely used for examining transparent and colorless objects which would be very difficult to see in ordinary bright field microscopy. Phase Contrast Microscopy enhances the contrasts of the object by using the fact that light passing through a transparent part of the specimen travels slower and, due to this, encounters a phase shift compared to the uninfluenced light. This change in phase cannot be seen with the human eye. However, the microscope increases the phase difference to half a wavelength by a transparent phase-plate. The obtained difference in brightness makes the transparent object shine out in contrast to its surroundings.

To visualize the effects of Ca^{2+} binding to vesicles on their fluctuation, vesicles in a solution of 0.01N NaCl and glucose (preparation see chapter 3.2.2) were observed in the optical chamber of the microscope. A solution of 0.014 N $CaCl_2$, 0.01 N NaCl and glucose was slowly flushed into the chamber by gentle pumping and the changes in fluctuations were monitored with a camera. To avoid any osmotic effects, the osmolarity of the latter solution was carefully matched with the one of the vesicle suspension.

Chapter 4

The Heat of Dilution of Inorganic Salts and Polyelectrolytes

The importance of the interactions of inorganic salts and polyelectrolytes is immense. The number of applications is boundless in a wide range of fields. The interactions of ions with water are crucial for the specificity of ion binding and ion complexation in cells is crucial for the activities of biomolecules such as enzymes and drugs [1], [2]. They also regulate the structures of micelles and the Hofmeister effect, which drives partitioning, permeation and folding and binding processes [7], [8]. Despite the significance of ions/polymers, the understanding of their behavior is still limited. The ions are often treated as coulumbic point charges and water as an unstructured medium, loosing the richness and complexity of system responses.

To get a better understanding of the interactions of ions with their local environment, and to evaluate the role of different (poly)ions on the structure of water, we study the heat of dilution[1] of various inorganic and polyelectrolyte salt solutions. We use the heat of dilution as a scale of water structure making and breaking by the ions[2]. As a tool for this research, we use Isothermal Titration Calorimetry (ITC), which has become a very popular technique for studying heats of reactions. Calorimetric investigations belong to the most precise among the thermodynamic methods

---

[1]The heat of dilution is referred to as the heat generated or released when solvent is added to a solution

[2]The term "water structure" is generally defined by means of the average number of hydrogen bonds in which a water molecule participates [39]. The degree of water structuring is mainly determined by two quantities: the increase or decrease in the viscosity of water due to added salt and entropies of ion solvation [40].

yielding information on ion-ion and ion-solvent interactions.

There is an abundance of studies on the heat of dilution of various simple electrolyte solutions over a wide range of temperature, pressure and molality. Some of these experiments were performed using a flow calorimeter [41], [42], where the heat of laminar friction when solution flows through the cell has to be taken into account. Other investigations [43] use a batch calorimeter to study heats of dilution by mixing two solutions. Here, we use a high sensitivity titration calorimeter. The main advantages of this instrument compared to flow and batch calorimeters are its high sensitivity, the lack of interfering heat effects such as laminar friction and the small quantity of sample per step of dilution (typically 10 μl) allowing very high resolutions.

In many of the previous works the heat of dilution was determined by titrating a salt solution of a certain concentration into the solvent yielding a final salt concentration [44], [45]. In contrast to these experiments, we designed an experiment that determines the heat of dilution of a salt solution by titrating the solvent into a solution of a certain salt concentration yielding a very high resolution with respect to the covered concentration range, as explained in chapter 4.1. Using this procedure, we first measured the heat of dilution of various inorganic salts which is discussed in chapter 4.2 together with the simplistic model we developed allowing a quantitative comparison of the different ions. In chapter 4.3, we then go on to apply this knowledge to polyelectrolytes and compare their interactions with water to their low molecular weight salts.

4.1 Design of the Experiment

One experiment consists of a sequence of titrations, where 10 μl aliquots of water are added to a salt solution in the cell, yielding at a given initial concentration of the salt solution, C_i, a final concentration of the diluted salt solution, C_f. Due to the small volume of the syringe (288 μl), compared to the volume of the working cell (1442 μl) only a narrow interval of concentrations can be covered by one titration measurement. In order to span a larger concentration range we performed a series of dilution measurements with different initial concentrations of the electrolyte in the working cell. Of course, for covering a larger concentration interval we could have performed the inverted measurement, i.e. injecting the electrolyte solution into water.
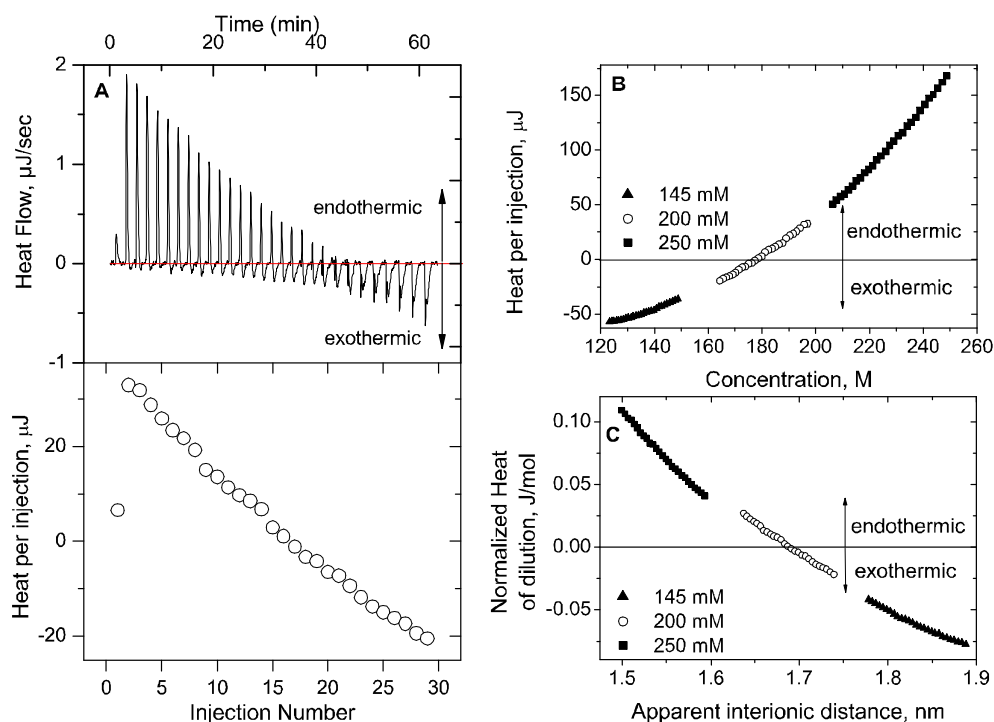
Figure 4.1: Dilution measurements. A) Raw ITC data from injecting water (10 μl aliquots) into 0.2 N NaCl with subtracted baseline (upper panel). Heat per injection obtained from integrating the heat flow over time (lower panel). B) Heat per injection as a function of Na$^+$ concentration for three separate dilution measurements at different initial concentration of NaCl in the working cell. The open circles correspond to the data in A). C) Normalized Heat for three dilution measurements as a function of apparent interionic distance. The heat is normalized by the moles Na$^+$ present in the system.

However, plotting the resulting molar heat of several measurements on a master curve would not be possible due to inadequacy of the starting and final solution volumes of two consecutive measurements.

Figure 4.1 represents an example of a dilution measurement. Figure 4.1 A shows the raw data of one dilution experiment of NaCl with initial concentration of 0.2 N. The upper panel shows the heat flow (mJ s^{-1}) caused by the consecutive injection of 10 μl aliquots of water into the solution of NaCl. Integrating the heat flow peaks yields the heat of each injection (lower panel). Figure 4.1 B shows three separate dilution experiments of NaCl solutions of 0.25 N, 0.2 N and 0.145 N. The upward and downward arrows indicate the direction of the peaks for an endothermic and an

exothermic signal, respectively. Note that in the course of a dilution measurement the salt concentration in the working cell decreases, therefore the slope of the heat dependence in Figure 4.1 B is inversed compared to the one in the lower panel of Figure 4.1 A. Figure 4.1 C shows the normalized heat of the three dilution measurements as a function of interionic distance of the ions. The heat is normalized by the number of Na$^+$ ions and is plotted as a function of some apparent interionic distance. The latter is defined assuming that the ions are point charges:

$$d = \frac{1}{\sqrt[3]{C_i N_A n}} \tag{4.1}$$

where C_i is the concentration of the solution in mol l^{-1}, N_A is Avogadro's number and n is the total number of ions that form when the salt is dissolved, i.e. $n = 2$ for monovalent 1:1 and $n = 3$ for divalent 2:1 salts. For lucidity, in the following figures of dilution series we will indicate only 3 to 6 evenly spaced data points from each separate titration measurement to avoid overcrowding.

4.2   Heat of Dilution of Inorganic Salts

A large set of salts was studied. To compare them, we use sodium chloride as a reference salt. In a first step, we studied the influence of different cations on the structure of water by measuring chloride salts with various cations. Then, the influence of the anions was investigated by varying the anion and keeping sodium as the cation. The concentration ranges of the solutions used in the dilution experiments are given in Table A.1.

The heats of dilution of different (Cl$^-$, Br$^-$, I$^-$, SO$_4^{2-}$, CH$_3$COO$^-$) sodium salts are presented in Figure 4.2 A). All of the anions show an endothermic heat of dilution at high concentrations changing to exothermic heats at lower concentrations. Acetate is the only exception showing an exothermic behavior over the whole concentration range.

One can compare the effect of different ions according to their heat of dilution at a fixed concentration or according to the concentration at which they produce the same heat effect. Hofmeister effects are generally ordered by the former way. Ordering the anions towards increasing heat of dilution at the concentration where
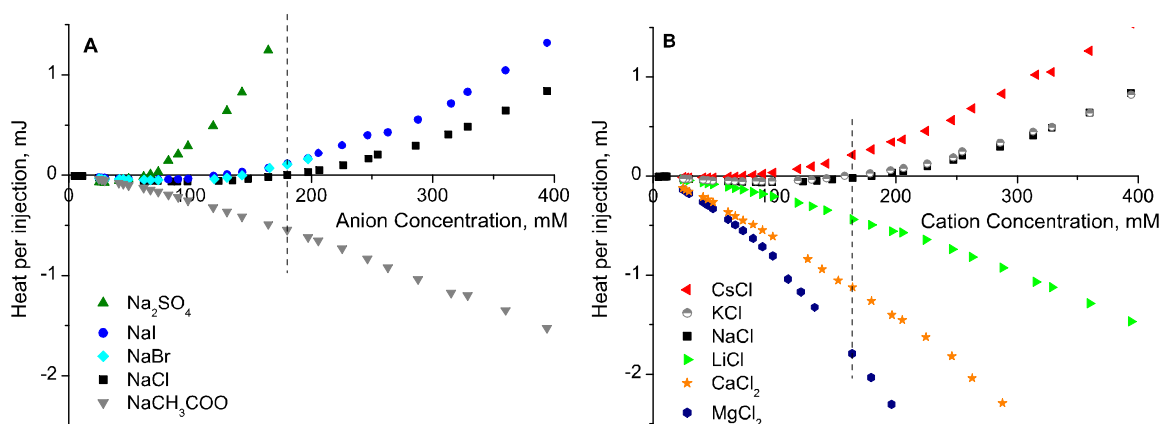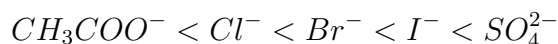
Figure 4.2: Heat per injection as a function of anion/cation concentration. A) Sodium salts B) Chloride salts. The dashed lines indicate the concentration at which the heat of dilution of the reference salt NaCl is zero.

NaCl is "neutral", i.e. where its heat of dilution is zero (as indicated by the dashed lines in Figure 4.2 A), we find the following series:

$$CH_3COO^- < Cl^- < Br^- < I^- < SO_4^{2-}$$

This order is in agreement with the general Hofmeister series, despite the position of SO_4^{2-}, which is located left of Acetate in the general lyotropic series (see Table 2.1). We interpret the heat of dilution as a manifestation of the Hofmeister series with kosmotropes having a negative heat of dilution (releasing heat upon dilution) and chaotropes having a positive heat of dilution (taking up heat upon dilution). This is meaningful, since the formal break up/melting of the water structure is accompanied by a loss of "melting enthalpy". The observation is in agreement with neutral polar organic solutes of moderately concentrated solutions (0.1 M - 1 M) where the heat of dilution is diagnostic for the lyotropic effects, with chaotropes taking up heat upon dilution and kosmotropes giving off heat upon dilution [7]. The only exception in the above mentioned order is sulphate, which is a kosmotrope in the general ranking of the lyotropic effects and shows a chaotropic behavior in this ranking.

The heats of dilution of the various alkali (Li^+, Na^+, K^+, Cs^+) and earth alkali (Ca^{2+}, Mg^{2+}) chloride salts are plotted in in Figure 4.2 B. Comparing the different

chloride salts we find that the large ions (Cs^+ and K^+) and Na^+ have an endothermic heat of dilution at high concentrations and switch to an exothermic heat of dilution at lower concentrations. The small cations, on the other hand, (Li^+, Ca^{2+}, Mg^{2+}) show an exothermic behavior over the whole concentration range. Clearly, the divalent ions have a stronger effect on the heat of dilution than monovalent ones.

Ordering the cations towards increasing heat of dilution at the concentration where the heat of dilution of NaCl is zero, we find the following ranking:

$$Mg^{2+} < Ca^{2+} < Li^+ < Na^+ < K^+ < Cs^+$$

Comparing this series with the general lyotropic series, we find that contrary to the anions, chaotropic cations release heat upon dilution whereas kosmotropes take up heat upon dilution. We observe that the measured heats of dilution are correlated to the heat of solution of the respective salts (see Table A.2), i.e for negative heats of solution we observe exothermic dilution and similarly, for positive heats of solution, we measure endothermic dilution. In both cases, the magnitude of the heat of solution is indicative for the magnitude of the heat of dilution. We can also correlate the heat of dilution with the hydration number of the cations (given in Table 4.1), where the larger the hydration number[3] of the cation the more exothermic its heat of dilution.

We observe that there is an asymmetry between the effects of chaotropic and kosmotropic anions and cations. The reason for this behavior is not clear. A possible explanation could lie within the differing donor/acceptor behavior of cations and anions towards protons of the hydrogen-bond water network. Cations, acting as proton donors, possibly influence their local environment on a short range scale whereas anions, acing as proton acceptors, show long-range interactions on the structure of water. A difference in the behavior of cations and anions on the structure of water is also found to be relevant for ion binding onto neutral polymer gels, as discussed in chapter 6.2.

For anions and cations, we observe that salts showing an exothermic heat of dilution over the whole concentration range have hydration numbers larger than four

---

[3]These hydration numbers are electrostatically based [46]. The only quantities required for their calculation are the charge and ionic radius of the ions.

Name of ion	Ionic radius, Å	Hydration number
Li^+	0.71	5.2
Na^+	0.97	3.5
K^+	1.41	2.6
Cs^+	1.73	2.1
Ca^{2+}	1.03	7.2
Mg^{2+}	0.70	10.0
Cl^-	1.80	2.0
Br^-	1.98	1.8
I^-	2.25	1.6
SO_4^{2-}	2.30	3.1
CH_3COO^-	1.62	2.2

Table 4.1: Ionic radius and hydration number of selected ions. Data reported from [46].

(the only exception is the acetate ion) whereas the other salts have hydration numbers smaller than four. Knowing that the average number of hydrogen bonds in liquid water is four [10], we conclude that ions increasing the number of hydrogen bonds compared to pure water enhance water structure leading to exothermic heats of dilution while the other ions are disordering, causing endothermic heat of dilution at large concentrations. Comparing the heats of dilution of the anions with the cations, we find that divalent ions have a stronger effect on the heat of dilution than monovalent ones.

It is also interesting to consider the behavior of the measured heat of dilution in the two limits of concentrations, i.e close to the solubility limit and at infinite dilution. Let us consider the extreme limit of very high salt concentrations, approaching the solubility limit. In this case, undissolved crystal aggregates could exist in the solution so that the measured heat would be the sum of the heat of dissociation of aggregates and the heat of dilution of the concentrated solution. Thus, towards the limit of solubility, the measured heat signal approaches the heat of dissolution. Towards the other extreme, at very small concentrations, the heat of dilution of all salts approaches the value of 0.01mJ (corresponding to a normalized heat of dilution of 1 J/mol, see Figure 4.3 and 4.4). This consistent behavior could be indicative for an artifact in the measurement or a continuous experimental error. To investigate these possibilities, we measured the heat of reaction of titrating water into pure water. We find, that the
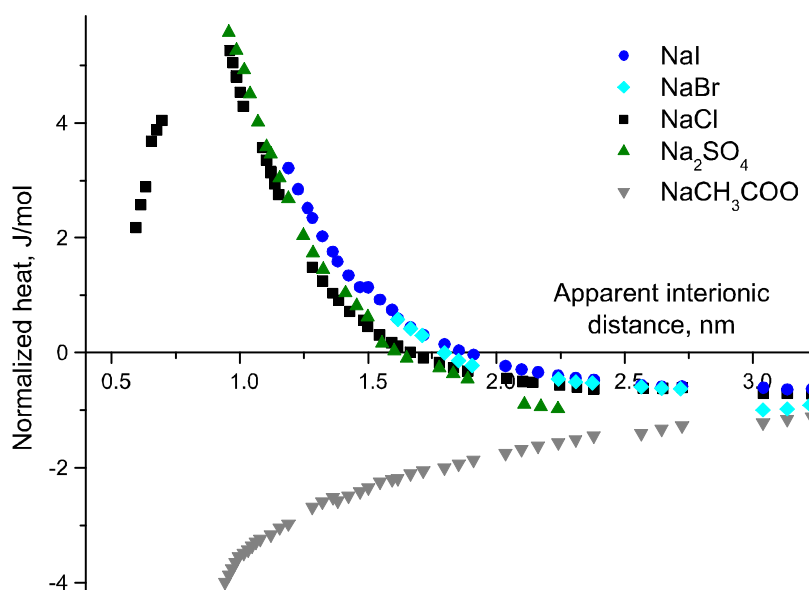
Figure 4.3: Normalized heat of various sodium salts as a function of apparent interionic distance. The heat is normalized over the moles of Na^+ present in the system.

titration of water into water gives rise to an exothermic heat flow of -1μcal (for a $10\mu l$ injection), which is ten times smaller than the measured limit value of the heat of dilution of the salts at very small concentrations. Still, the reason for the consistent limit value of 0.01 mJ for all of the salts is not clear, but in the present context, it shall not be further discussed. We assume that the measured heat of a water into water injection is caused by the mechanical work of the injection which dissipates in the form of heat.

To get a better understanding of the interactions of the ions with their environment and to interpret our data on a molecular scale, it is useful to normalize the heats of dilution over the moles of unaltered counterions, Na^+ or Cl^- present in the system. Plotting the normalized heats as a function of the apparent interionic distance (equation 4.1), as explained in Figure 4.1 C, provides useful information on the long-range and short-range interionic interactions.

The normalized heats of the sodium and chloride salts are shown in Figure 4.3 and 4.4, respectively. Obviously, the measured effects are in the order of 1 J/mol, i.e. indeed very tiny and only revealed by the very high sensitivity of the setup.
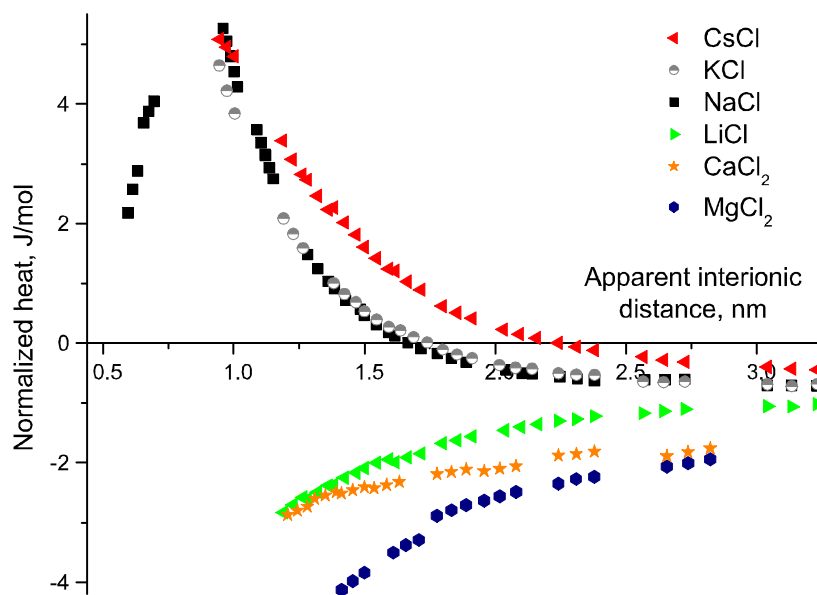
Figure 4.4: Normalized heat of various chloride salts as a function of apparent interionic distance. The heat is normalized over the moles of Cl⁻ present in the system.

Interestingly, the effects are also much smaller than the thermal energy of the system, which is 3000 kJ/mol at 25°C. The released heat cannot be explained with change in the pH of the system[4] but rather speaks for a local rearrangement of water molecules around the ions.

For all of the measured salts, we detect changes in the heat of dilution even beyond apparent interionic distances of 3 nm, where two ions are separated by ∼10 layers of water molecules (assuming a mean van der Waals diameter of water of 2.82 Å[47]). This value should be compared with the corresponding Debye length (see equation 2.5), e.g. 0.56 nm in 0.1 M Na₂SO₄. We have to conclude that both, anions and cations, have a long range influence on the structure of water far beyond the first hydration shell. In contrast to this, the widely used solvation-shell model [13] assumes that only the water molecules in the first hydration shell rearrange around the ion whereas subsequent solvent layers are only slightly perturbed in structure by

---

[4]The released heat associated with the change in the pH is negligible compared to the measured signal. It can be calculated from the dissociation enthalpy of water 492 kJ/mol. For the ions presented here, the heat associated with a change in pH is of the order of a few mJ whereas the heat of dilution is of the order of a few kJ.

the central ion and in most cases, these additional layers are treated as continuous dielectric medium.

We assume that the heat of dilution measured by ITC is the sum of two heat effects, resulting from an endothermic and an exothermic process. Since the positive heat of dilution is dominant for small interionic distances we suppose that the measured heat effects are mainly associated with the separation of contact ion pairs (X^+Y^-) upon dilution. The result are loose ion pairs $(X^+||Y^-)$ where the ions are separated by one or more layers of water. Of course, these processes depend on the overall salt concentration, i.e. on the presence of coions in the vicinity of the association pairs. In fact, the notation of the ion pais, (X^+Y^-) and $(X^+||Y^-)$, is only symbolic and can reflect more complex interactions. Here, we intend to give only a possible illustration.

The presented model is supported by the fact that evidence for ion- pairs in salt solutions has been found in a number of salt solutions. For instance, dynamic light scattering experiments revealed that in aqueous solutions simple electrolytes, such as NaCl, aggregate even at moderate concentrations ($\sim$0.1 M) [48]. From molecular dynamics simulations it was found that in a 1 M NaCl solution at 25°C, about 25% of the ions are included in neutral clusters formed by a minimum of four ions [49] and the small and large ionic clusters are stabilized by hydration molecules [50]. Another example is CsCl, which was found to be ion-paired to an appreciable extent [51].

Since the contact ion pairs are held together by strong electrostatic attraction of the oppositely charged ions, this process requires a large amount of energy, resulting in an endothermic heat of dilution. The corresponding equilibrium can be described with an equilibrium constant K_1 and a heat of reaction ΔH_1:

$$X^+Y^- \overset{K_1}{\rightleftarrows} X^+||Y^- + \Delta H_1 \tag{R1}$$

The exothermic heat of dilution, which is dominant at large interionic distances, is interpreted as the heat arising from a complete separation of the loose ion pairs, yielding freely hydrated ions. This process can be described by the equilibrium between the loose ion pairs and the hydrated ions with an equilibrium constant K_2 and a heat of reaction ΔH_2:

$$X^+||Y^- \overset{K_2}{\rightleftarrows} X_{aq}^+ + Y_{aq}^- + \Delta H_2 \tag{R2}$$
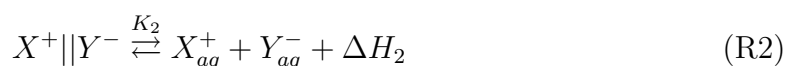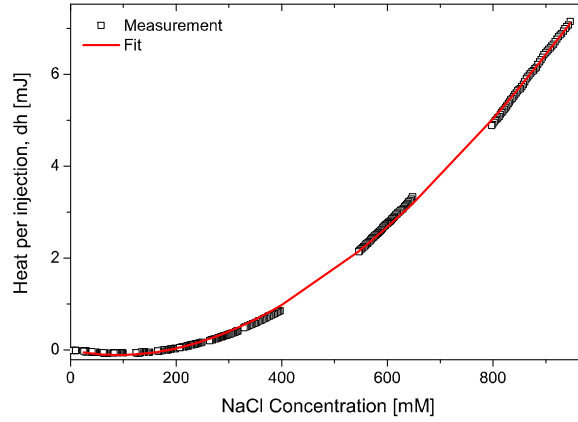
Figure 4.5: Experimental heat per injection and curve fit of sodium chloride. The fis was performed using equation 4.4.

The mass balance of the system is then given by

$$C_{tot} = [X^+Y^-] + [X^+||Y^-] + [X^+_{aq}] \tag{4.2}$$

where C_{tot} denotes the total salt concentration in the cell, and the brackets denote the concentrations of the respective species. The total energy change dh following an injection into the cell volume V is given by:

$$dh = d[X^+||Y^-]V\Delta H_1 + d[X^+Y^-]V\Delta H_2 \tag{4.3}$$

i.e. dh is given by the sum of the heat associated with the separation of contact ion pairs and the heat released due to the hydration of the individual ions.

Combining equations 4.2 and 4.3 with the laws of mass action for reactions R1 and R2, we find a fitting equation with the measured enthalpy change as independent variable, the total salt concentration in the cell as dependent variable and the four fitting parameters K_1, ΔH_1, K_2 and ΔH_2:

$$dh = -C_{tot}dV\left[\frac{4\Delta H_1}{a}\left(1 - \frac{1}{\sqrt{1 + C_{tot}a/K_2}}\right) + \frac{\Delta H_2}{\sqrt{1 + C_{tot}a/K_2}}\right]$$

where $a = 4(1 + K_1)/K_1$. Obviously, ΔH_1 and a as well as a and K_2 are coupled,

	|| SO_4^{2-}	Cl^-	I^-
A	Cs^+	/	-109	/
	Na^+	-554	-376	?
	Li^+	/	57	/
	Mg^{2+}	/	?	/
B	Cs^+	/	2.42	/
	Na^+	2.09	0.42	?
	Li^+	/	2.58	/
	Mg^{2+}	/	?	/
ΔH_2	Cs^+	/	44	/
	Na^+	144	56	38
	Li^+	/	29	/
	Mg^{2+}	/	109	/
$\Delta H_1/K_2$	Cs^+	/	-265	/
	Na^+	-1156	-155	-149
	Li^+	/	148	/
	Mg^{2+}	/	445	/

Table 4.2: Results of the Curve Fits for different salts. The slash indicate absence of performed measurement for the corresponding salt (see text for details).

so that we can not determine these parameters independently. However, $A = \Delta H_1/a$ and $B = a/K_2$ can be determined from a fit. Thus, the final fitting equation contains the three fitting parameters A, B and ΔH_2 :

$$dh = -C_{tot}dV \left[A \left(1 - \frac{1}{\sqrt{1 + C_{tot}B}} \right) + \frac{\Delta H_2}{\sqrt{1 + C_{tot}B}} \right] \tag{4.4}$$

Clearly, curve fits with more than two fitting parameters hold the risk of unsound results. Thus, multiple datasets were simultaneously fit to the same model to gain reliable values for the fitting parameters. Note that the number of fitting parameters per curve decrease with the number of measurements fitted simultaneously. In this way, the determination of fitting parameters becomes more robust. The obtained curves properly fit the measurements, as shown exemplified for NaCl in Figure 5.4. The results for the values for A, B and ΔH_2 of various anions and cations are given in Table 4.2. For the two salts NaI and MgCl$_2$ the curve fits do not yield unique values for the parameters $\Delta H_1/a$ and a/K_2, i.e. these parameters are coupled, indicated in the table by the question marks at the respective positions. However, the product

of these two fitting parameters, $\Delta H_1/K_2$, remains constant and is therefore listed in the last row of the table. Comparison of the results to the Hofmeister series is not streight forward, since the different measurements of the series give a rank ordering with slight alterations. Here, the anions and cations are ordered according to the general Hofmeister series with respect to $\Delta H_1/K_2$.

For the anions, the parameter ΔH_2 decreases with increasing chaotropy whereas the effect is inverse for the cations and Li^+ breaks out of the series. On the other hand, the values for $\Delta H_1/K_2$ are consistent with the lyotropic series, rising with increasing chaotropy. We therefore choose to interpret the measured heats of dilution as manifestation of Hofmeister interactions.

4.3 Heat of Dilution of Polyelectrolytes

Here, we monitor the interactions of poly(sodium acrylate) (NaPAA) and poly(sodium styrene sulphonate) (NaPSS) (see Figure B.1 for the molecular structures) with water by ITC and compare them to the corresponding low molecular weight salts, containing the functional groups of the polymers, sodium acetate and sodium sulfate. In attempt to characterize the role of the backbone of the polymer and its hydrophobicity on its interaction with water we performed dilution measurements with the polymers and with their corresponding low molecular weight salts. NaPAA1, NaPAA2, NaPAA3 and NaAc were titrated with water at different starting concentrations of the chemicals in the cell. Several sets of ITC experiments are presented on Figure 4.6. The released heat is normalized by the moles Na^+ in each system.

The dilution of NaAc is exothermic over the whole examined range of concentrations. The magnitude of the signal increases with concentration. The released heat cannot be explained with change in the pH of the system[5] but rather suggests a local exothermic binding and rearrangement of water molecules around the acetate anion. NaPAA, on the contrary, is only weakly exothermic and shows nearly ideal behavior over the whole examined concentration range up to 1 N solutions. Within the whole

---

[5]In the measuring concentration interval the pOH of the NaAc solution varies from 4.6 at 1 N to 5.4 at 0.03 N. The released heat associated with this change in the pOH is negligible compared to the measured signal. It can be calculated from the dissociation enthalpy of water 492 kJ/mol. For the discussed concentration interval we obtain a value of the order of –14 mJ which is negligible compared to the measured 0.9 kJ.
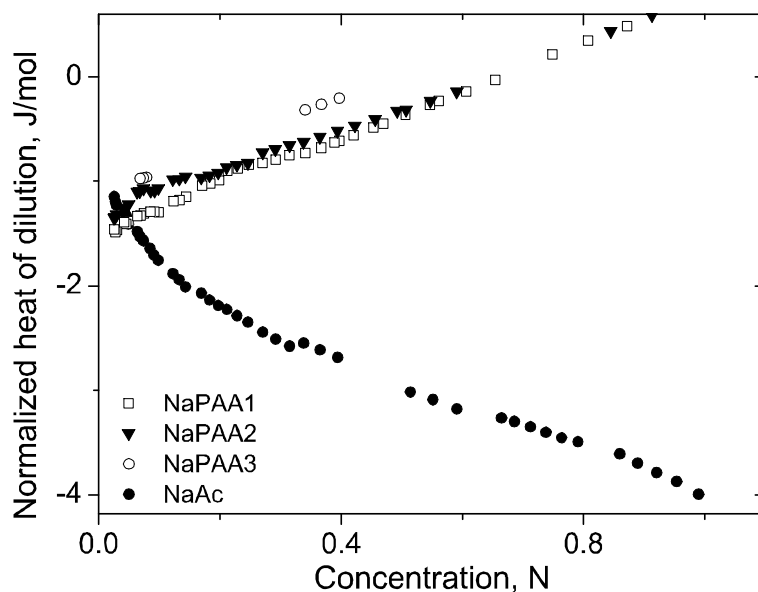
Figure 4.6: Experimental heats of dilution for NaAc, NaPAA1, NaPAA2 and NaPAA3. The heat is normalized by the moles Na^+ present in the system.

concentration range the heat of dilution of the three NaPAA samples with different molecular weights is within 2 J/mol, indicating that the heat of dilution depends only weakly on molecular weight, at least in the examined range. It is worth mentioning that NaPAA shows no solution limit or mixing gap with water, i.e. the free energy of mixing is negative in the whole composition range. It is interesting to note that in the low concentration limit both the low molecular salt and the polymers yield similar heats of dilution. One may speculate that in this regime the two compounds are indistinguishable from the point of view of the water molecules, i.e. the presence of the hydrophobic backbone of the polymer has no influence in this range and is not seen by the majority of rather distant water molecules. However, this proximity in the dilution heats could also be due to compensating contributions.

In a similar way we compare the dilution of NaPSS and its low molecular equivalent Na_2SO_4 (see Figure 4.7). At small concentrations of Na_2SO_4 the signal is slightly exothermic, but turns strongly endothermic at higher concentrations. This is consistent with the thermal effects occurring throughout the crystallization of Na_2SO_4 from water solutions. The enthalpy turn from exo- to endothermic behavior corresponds
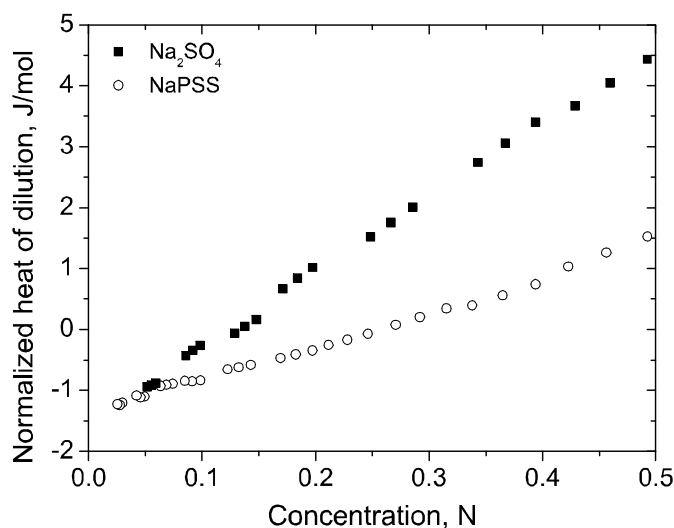
Figure 4.7: Experimental heats of dilution for NaPSS and Na_2SO_4. The heat is normalized by the moles of Na^+ present in the system.

to a favourable effect of the SO_4^{2-} on the long range structure of water, whereas the short range contributions (observed predominantly at higher concentrations) are strictly heat-consuming.

The curve of NaPSS starts exothermic, but turns only to slight endothermic behavior, and is overall closer to the ideal athermal behavior. This, at first glance, is somewhat counterintuitive. NaPSS is definitely more hydrophobic than Na_2SO_4 but gives a less endothermic signal. This implies that appropriate fit of the molecules to the water structure is more important than the usually overestimated backbone "hydrophobicity". The data are also in agreement with dilution data of sodiumdodecylsulfate in water at 25°C [52] where close to athermal dilution was demonstrated as well, and is interpreted to be coherent with the general knowledge coined as "the hydrophobic effect"[53], [40].

Comparison of the data of NaPAA and NaPSS (Figure 4.6 and Figure 4.7) shows that the dilution of PSS is slightly more endothermic. However, both polymers show similar, nearly ideal behavior, making both systems the ideal model systems they are known for. It is worth noting that the described effects are in this case of the order of 0.001 kJ/mol, i.e. indeed very tiny and only revealed by the very high sensitivity of the setup. Again, the similarity is somewhat surprising as both polyelectrolytes differ

significantly in their chemical composition and in the polarizability of their charges.

Because we are interested in the thermodynamics of the specific interaction of those polyelectrolytes with Ca^{2+}, we also have to analyze the heat of dilution of CaPAA. This was studied only in the concentration range of 0.06 N up to 0.64 N which is the limit set by the solubility of the polymer. It is very interesting to note that just like NaPAA, CaPAA also shows practically athermal behavior. Dilution measurements with CaPAA (data not shown) revealed that the heat of dilution in the examined concentration range is small and almost constant, equal to $\sim$-0.6 J/mol. This value is close to the signal obtained from diluting NaPAA which suggests that when part of the Na^+ counterions are replaced by Ca^{2+} the dilution of the polymer is effectively unchanged. This is consistent with the general observation that water is more influenced by the anions than by the cations [7], but it does not mean that the close-distance hydration of both species is similar.

Chapter 5

Binding of Ca^{2+} to 1D Polymers and 2D Lipid Bilayer Membranes

The binding of metal ions to polyelectrolytes and low molecular weight compounds has been widely studied [54], [55]. Prevalent theories for the effects of salts on the stability and conformational transitions of polyelectrolytes are Manning's counterion condensation theory [56] and the cylindrical Poisson-Boltzmann model. According to these models, the only property of an ion that is significant is its charge. This means that all 1:1 salts should according to the theory give the same result. However, polyelectrolytes and vesicles show remarkable ion specificity whether containing charged or uncharged groups. Ion specific, or Hofmeister, effects are important in a number of biophysical processes including the conformational transition of macromolecules [57] and the driving force behind them could be the influence of the various ions on the structure of the solvent (see chapter 2.3.2).

Studies on the binding of calcium to poly(acrylic acid) reveal that the process is driven by a gain in entropy by the release of hydration water [58], [59]. Also, studies on the binding of alkaline earth cations to low molecular weight compounds [60] and the binding of Ca^{2+} and La^{3+} to lipid vesicles [61] show that binding of the ions must be entropy driven. However, the molecular origin of this entropy gain remain to be determined.

To learn about the competition of electrostatic and entropic forces, we compare the binding of Ca$^{2+}-$ ions to a one-dimensional polymer chain to the binding to lipid vesicles which the ions perceive as two-dimensional surfaces. As vesicles we

use negatively charged phosphatidylserine-phosphatidylcholine membranes where the functional carboxylate groups mimic the functional group of the poly(acrylic acid) (PAA) which we use as a polymer. To gain insight into the forces responsible for the process, the thermodynamics of the process, i.e. the energetic and entropic contributions, have to be included. Another property which we are interested in, is the structure of the solvent. To obtain all of this information, single isotherms do not give enough information and should be expanded by calorimetry [62]. Thus, the tool for this research is a combination of a Ca^{2+} ion selective electrode and Isothermal Titration Calorimetry (ITC).

In chapters 5.1 and 5.2 we discuss the driving forces of calcium binding to the polymer chain and to the negatively charged lipid membrane, respectively. In chapter 5.3, we then compare the mechanisms of ion binding to the one-dimensional system with the binding to the two-dimensional surface.

5.1 Binding of Ca^{2+} to Polymers

Many feed waters contain large amounts of calcium bicarbonate. If the temperature is increased or the pressure is decreased, the soluble calcium bicarbonate salt is converted into the hardly soluble calcium carbonate. Thus, whenever feed water is heated, e.g. in heating elements or washing machines, this leads to the formation of incrustation (called *scaling or limescale*), caused by the deposition and crystal growth of inorganic salts, such as CaCO$_3$. All devices that heat water are affected by limescale deposits and the life time of the heating elements in these devices is shortened. Also, clothes washed in hard water can suffer damage to fibers, shortening their life span, or are at least unpleasant to wear. Incrustation can be controlled by the use of dissolved polymers, so called *scale inhibitors*, which consist of polymers with a negatively charged chain. Hereby, the crystal growth is prohibited through the binding of Ca^{2+}-ions onto the polymer so that they are no longer available for the growth of calcite crystals [63].

In nature, scaling also plays an important role. Shellfish, for instance depend on the lime dissolved in liquid water because they require it to build up their shells. However, here, the lime does not form the typical rhombohedral calcite crystals but the well known large diversity of forms. To accomplish the rough crystal formation

of the inanimate nature, these species use peptides, e.g. poly(aspartic acid), which effects the mineralization process of the shell in a way that the rounded shapes of biominerals are formed.

In chapter 5.1.1, we provide an insight into the forces responsible for binding of calcium to a model for the standard scale inhibitor, poly(acrylic acid). We then go on to expand these findings to other scale inhibitors, a technical one, Sokalan, and poly(aspartic acid), a model for those peptides that nature uses[1], in chapter 5.1.2.

5.1.1 The Standard Scale Inhibitor: Poly(acrylic acid) (PAA)

Here, we examine the calorimetric effects of the specific counterion binding of $Ca^{2+}-$ ions onto the standard scale inhibitor poly(acrylic acid) sodium salt (NaPAA). Three polymers (NaPAA1, NaPAA2, NaPAA3) were available for these studies with increasing chain length. We use NaPAA3 for these experiments because it has the highest molecular weight among the three NaPAA samples (see chapter 3.1.1) which allowed us to measure the amount of bound calcium with the Ca^{2+} electrode. In contrast, NaPAA1 and NaPAA2 are not useable for the Ca^{2+} electrode due to their small size, generating unexpected secondary electrode signals which can be stronger than the signal generated by Ca^{2+} (see Figure 5.2). Furthermore, since the molecular weight of NaPAA3 is similar to Sokalan we are able to compare those two polymers free of molecular weight effects.

When a $CaCl_2$ solution is added to the NaPAA3 solution, Na^+ ions are monotonically released and Ca^{2+} ions complex the acrylate groups yielding a neutralization of the polymer. Precipitation occurs above a critical ratio, r, which is defined [64] as the minimum molar ratio of added Ca^{2+} to carboxylate binding sites at which precipitation occurs:

$$r = \frac{[Ca^{2+}]}{[COO^-]}$$

where the brackets denote molar concentrations of the respective species. In order to prevent precipitation in the sample cell of the ITC, the initial concentration of the polymer solution was chosen so that the binding of Ca^{2+} to the carboxyl groups of the polymer does not lead to a complete neutralization and resulting precipitation. In

---

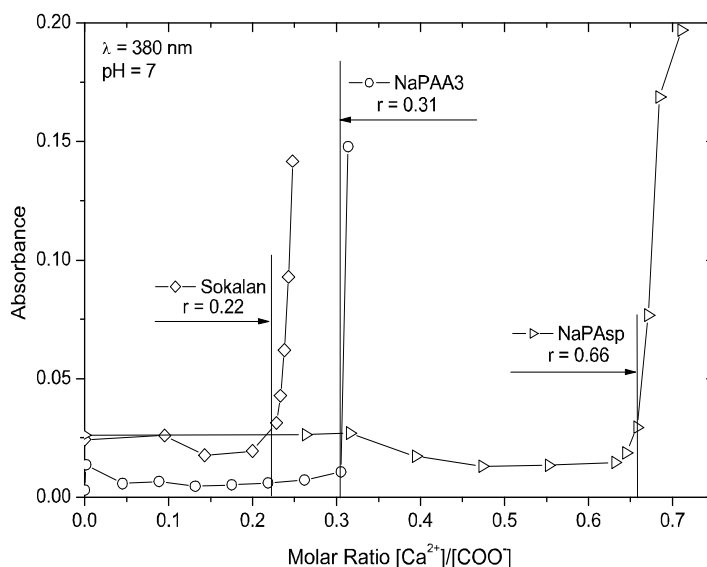[1]In nature, a combination of glutamic and aspartic acid is used.

Figure 5.1: Turbidity measurements. 0.2 N solution of CaCl$_2$ is titrated into 0.08 N NaPAA3, 0.037 N NaPAsp and 0.105 N Sokalan (pH 7). The absorbance at 380 nm is plotted as a function of molar ratio of added Ca^{2+} to carboxylate groups.

this work, r was determined by following the absorbance of the solution. In Figure 5.1 the absorbance of an 0.08 N NaPAA3 solution is plotted as a function of molar ratio of added Ca^{2+} to carboxyl groups for titration with an 0.2 N CaCl$_2$ solution. At the onset of precipitation, the absorbance increases significantly. The critical ratio r was measured to be 0.31 and the initial NaPAA3 concentration was consequently set to 0.08 N. Figure 5.1 also includes the turbidity measurements of Sokalan and NaPAsp, where r is found to be 0.22 and 0.66, respectively. Considering that each Ca^{2+} binds two carboxylic groups, we observe that the technical scale inhibitor Sokalan precipitates below the stoichiometric equivalence of 0.5, showing a very ion sensitive solubility. The natural scale modifier NaPAsp precipitates at calcium loads beyond stoichiometric equivalence implying lower ion sensitive solubility and operation even under extreme conditions.

As we have seen in chapter 4.3, the heats of dilution for both, NaPAA and Ca-PAA, are close to zero. Thus, the binding heat of Ca^{2+} onto NaPAA can simply be determined by titrating a dilute CaCl$_2$ solution into NaPAA. Any measured heat can then be ascribed to the sum of the heat of dilution of CaCl$_2$ and the desired binding

of Ca^{2+} onto the polymer. These experiments essentially follow earlier experiments on Ca^{2+} binding onto NaPAA [64], [58], [65].

The measured molar enthalpy change following the stepwise addition of 8 μl aliquots of an 0.2 N CaCl$_2$ solution into an 0.08 N solution of NaPAA3 is shown in Figure 5.2 A. The total enthalpy measured in the ITC experiment is the sum of the enthalpy associated with the interaction of Ca^{2+} with the polymer chain and the heat of dilution of the salt and polymer solutions. In order to determine the enthalpy associated with the counterion binding, the dilution enthalpy of an 0.2 N CaCl$_2$ solution into pure deionised water was measured and subtracted from the total enthalpy. The measurements illustrate that the dilution enthalpy of the CaCl$_2$ solution is negative, but also much smaller in magnitude than the complexation enthalpy. The heat of dilution of the NaPAA3 solution in this concentration region is almost constant ($\sim$-0.1 mJ) and can be neglected compared to the heat of the titration of CaCl$_2$ into NaPAA3 which varies from 5.2 mJ to 17 mJ.

The interaction of Ca^{2+} ions with the NaPAA3 solution is, contrary to expectations based on Coulombic pair potentials, a strongly endothermic process, as previously observed by Pochard et al. [58]. As there is no doubt that Ca^{2+} binds deliberately onto NaPAA and that the change in the free energy of binding is negative, the driving force of the reaction is an increase in the entropy, which is believed to be primarily due to the liberation of water molecules. The total amount of released water molecules is given by the dehydration of Ca^{2+} and COO$^-$ minus the rehydration of Na$^+$ and the bidentate Ca$^{2+}-$(COO)$_2$ complex.

When CaCl$_2$ is added to a polymer solution, some (or all) of the Ca^{2+} ions might bind to the polymer while others (or none) might remain free in the bulk solution. Therefore, the decrease of the reaction enthalpy with increasing concentration of added calcium could be caused by two effects: Either the reaction heat drops because the amount of Ca^{2+} bound to the polymer decreases or because the molar binding enthalpy falls. Both effects could also occur simultaneously. The answer to this question was studied by using a calcium ion selective electrode to determine the binding isotherm.

In Figure 5.2 B, the concentration of free and bound calcium for two different Na-PAA solutions (0.06 N NaPAA2 and 0.08 N NaPAA3) following the stepwise addition
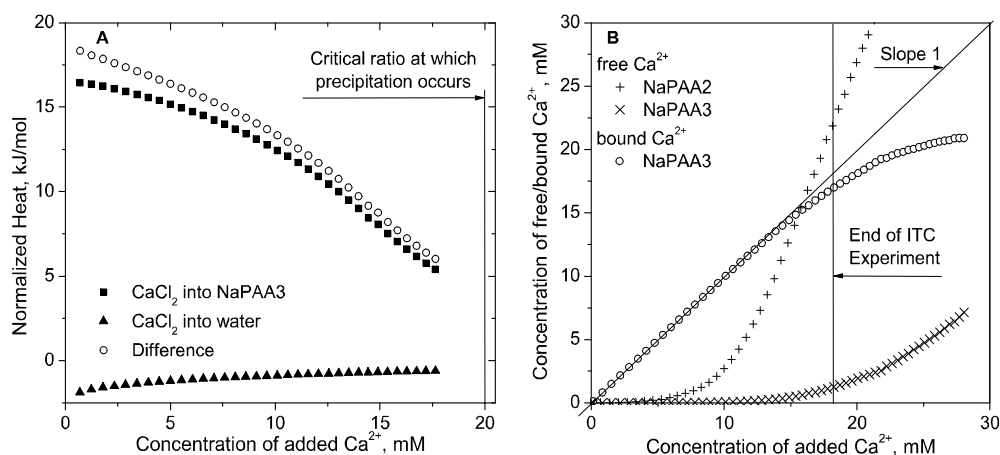
Figure 5.2: Binding isotherms A: ITC experiments: Titration of 0.08 N NaPAA3 solution at pH 7 and water with 0.2 N CaCl$_2$. The difference of the two signals is the heat associated with the interaction of Ca^{2+} with the polymer chain (the heat of dilution of NaPAA3 is negligible). The heat is normalized by the moles of injected Ca^{2+}. B: Calcium electrode isotherms. 0.2 N CaCl$_2$ solution is titrated into 0.06 N NaPAA2 and 0.08 N NaPAA3 at pH 7. Free (measured) and bound calcium is plotted as a function of added Ca^{2+}. The line indicated with "Slope 1" represents the case of 100% binding. The unrealistic excess of the apparent concentration of free calcium for the measurements with NaPAA2 is presumably due to additional signal of the polymers passing through the calcium electrode membrane (see text for details).

of an 0.2 N CaCl$_2$ solution is plotted as a function of the concentration of added Ca^{2+}. The amount of bound divalent ion was determined by measuring the concentration of free calcium in the polymer solution after each injection with the Ca^{2+} electrode and subtracting this value from the concentration of added calcium. The line indicated with "Slope 1" represents the case of 100% binding of the added Ca^{2+}. In the case of NaPAA2, the apparent concentration of free Ca^{2+} "exceeds" the concentration of added Ca^{2+} above ˜15 mM. This unrealistic artifact can be explained by a continuous decrease in the radius of gyration of the polymers upon the formation of CaPAA2 which has been reported by Huber [66]. The latter eventually become small enough to pass through the ion selective porous membrane and contribute to the measured electrochemical potential difference. We just present this very special artifact to alert other groups that low molecular weight fractions in the polymers may seriously comprise the outcome of binding measurements. Hence, the binding isotherm could not

be measured for NaPAA2 and NaPAA1, which gives similar results.

The binding isotherm of NaPAA3 presented in Figure 5.2 B shows that almost all of the added Ca^{2+} ions bind to the polymer while only a few remain free in the bulk solution. Just before the precipitation limit (r = 0.31), the amount of free calcium increases. Knowing the amount of bound Ca^{2+} the the molar enthalpy of binding , i.e the heat per bound Ca^{2+}, $dH_{B,i}$, can be calculated from:

$$dH_{B,i} = \frac{dh_i}{n_{B,i}}$$

where dh_i is the measured heat per injection (in J) and $n_{B,i}$ is the moles of bound Ca^{2+} per injection. The latter is given by:

$$n_{B,i} = [Ca_{B,i}^{2+}]V_i - [Ca_{B,i-1}^{2+}]V_{i-1}$$

where $[Ca_{B,i}^{2+}]$ and $[Ca_{B,i-1}^{2+}]$ are the concentrations of bound ion after injection i and $i-1$, respectively, and V_i and V_{i-1} are the total cell volumes after injection i and $i-1$, respectively.

We find that the molar enthalpy of binding of Ca^{2+} to PAA is continuously linearly decreasing with the calcium loading (up to 40 %), as presented in Figure 5.3. This is contrary to other observations reported in the literature [58] (this study was performed for lower overall calcium concentrations).

The binding isotherm from the Ca^{2+} ISE was fitted following the model for the formation of a ternary complex as described in chapter 2.4.2. However, here we assume that the ternary complex consists of the divalent Ca^{2+} ion and two dependent (instead of independent) COO$^-$ binding sites, i.e. one $(COO^-)_2$ complex. This 1:1 equilibrium is then described by

$$Ca^{2+} + (COO^-)_2 \overset{K}{\rightleftarrows} Ca[COO]_2$$
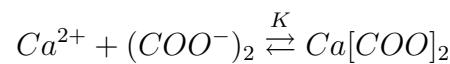
and the binding constant K can be calculated from
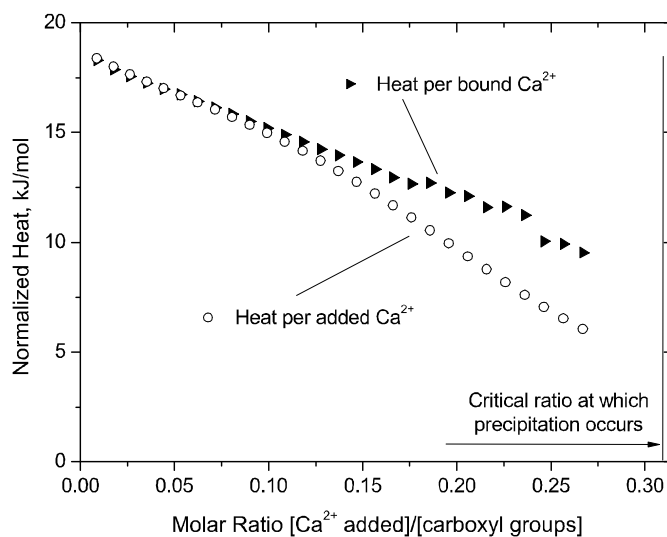
$$K = \frac{[Ca_B^{2+}]}{[Ca_F^{2+}][(COO^-)_2^F]} \tag{5.1}$$

Figure 5.3: Normalized heat. (o) Heat normalized over the moles of added Ca^{2+} as obtained from the ITC experiments. (►) Heat normalized over the moles of bound Ca^{2+} as determined with Ca^{2+} Ion Selective Electrode. The binding enthalpy is linearly decreasing with Ca- loading.

where $[Ca_B^{2+}]$ and $[Ca_F^{2+}]$ are the concentrations of bound and free Ca^{2+}, respectively, and $[(COO^-)_2^F]$ denotes the concentration of free carboxylate complex. The concentration of free binding site complexes is related to the concentration of bound ion, $[Ca_B^{2+}]$, and total amount of carboxyl COO$^-$ groups, $[COO^-]$, by

$$[(COO^-)_2^F] = 0.5[COO^-] - [Ca_B^{2+}]$$

The binding constant can be used to determine the Gibbs free energy change, ΔG. However, to calculate ΔG, the equilibrium constant must be dimensionless. In this work, this is done by expressing the binding constant as

$$K_A = KC_T$$

where C_T corresponds to the total concentration of the solution (=55.56 mol l^{-1}). It should be noted that in this model, we assume that the concentration of Ca^{2+} is the same in the bulk solution and close to the polymer rod. We therefore do not account for possibly elevated Ca^{2+} concentrations in the vicinity of the polymer.
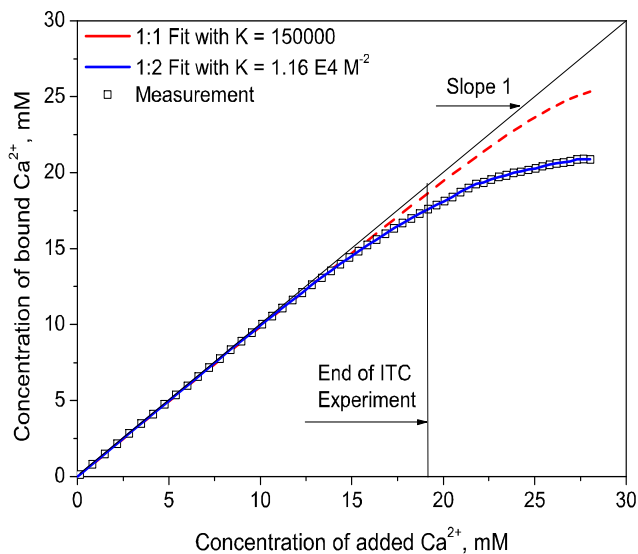
Figure 5.4: Binding isotherm from Ca^{2+} ISE. Measurement (■) and fits according to 1:1 and 2:1 binding model.

Fitting the binding isotherm with this model yields an equilibrium constant of ca. K_A = 150000, with deviations from the ideal binding when approaching the precipitation limit, as shown in Figure 5.4. Above this limit, CaPAA precipitates and forms a hydrophobic, not water swollen phase. The decreasing ability of the polymer to bind calcium is therefore presumably due to the approaching phase transition and the coupled conformational changes and progressing collapse of the CaPAA, burying the remaining binding sites for Ca^{2+} in the interior of the hydrophobic coils. The calcium induced shrinking of polyacrylate chains and the coupled transformation of a gaussian coil into some globular structure with increasing Ca-loading was nicely quantified by Huber et al. [66], [67], [68], supporting this interpretation.

On the base of this equilibrium constant, a free energy of binding of $\Delta G_{Ca-bind} = -29.6\ kJ/mol$ is calculated using equation 2.2. As we have seen from the Ca^{2+} ISE, for low Ca^{2+} concentrations, practically all of the added Ca^{2+} ions bind. We can therefore use the molar binding enthalpy of the first injection ($\Delta H_{Ca-bind} = 17$ kJ/mol) to calculate the binding entropy from equation 2.1. We obtain a binding entropy $\Delta S_{Ca-bind}$ of $19kT/mol$, where k is the Boltzmann constant and T is the temperature. Assuming that the entropy gain comes from the release of molecules, i.e. a gain in translational energy, this corresponds to the liberation of ~10 water molecules and

two sodium ions per bound Ca^{2+}. However, a gain in translational energy might not be the only reason for the entropy gain. In fact, entropic contributions might also arise from conformational changes of the polymer chain. This possibility can be investigated in future by adding only very small concentrations of Ca^{2+} to the polymer chain so that conformational changes can be ruled out.

We have also fitted the experimental data with a 1:2 binding model, according to equation 2.10, assuming that a ternary complex is formed where one Ca^{2+} ion binds to two independent binding sites. As shown in Figure 5.4 this model describes the curve over the whole concentration interval. At higher Ca^{2+} concentrations, it describes the binding curve better than the 1:1 model, since it accounts for crosslinking of individual polymer chains and eventual precipitation of the polymer coil. Nevertheless, for the calculation of the binding constant, we used the 1:1 model, which fits the curve well for lower Ca^{2+} concentrations, since we assume that at low concentrations, the ion rather binds to two dependent than to two independent binding sites.

The fact that the endothermic character of binding enthalpy is decreasing while the binding on the contrary is, at most, slightly weakened indicates that also the binding entropy changes with concentration in an appropriate fashion. This effect is well known for many thermodynamic phenomena in water and was coined as "enthalpy-entropy compensation"[53], [40]. It strongly supports our view that the endothermic character of binding is coming from the water structure and not from the ion binding process itself. Similar measurements were also performed at elevated temperatures (45°C), but did reveal a very similar behavior. This is why we omitted the presentation of those data in the present context.

5.1.2   Comparing the Quality of Different Scale Inhibitors

It is also interesting to compare the calorimetric binding curve of the NaPAA3 with two other technical scale inhibitors, NaPAsp and Sokalan, as presented in Figure 5.5. The molecular structure of these polymers is given in Figure B.1. Similarly to Na-PAA3, the heats of dilution of these polymers are negligible. The initial concentrations of the polymer solutions were again chosen so that the complexation of Ca^{2+} with the carboxyl groups of the polymers does not lead to precipitation in the working cell before the end of the ITC experiment. As presented in Figure 5.1, r was
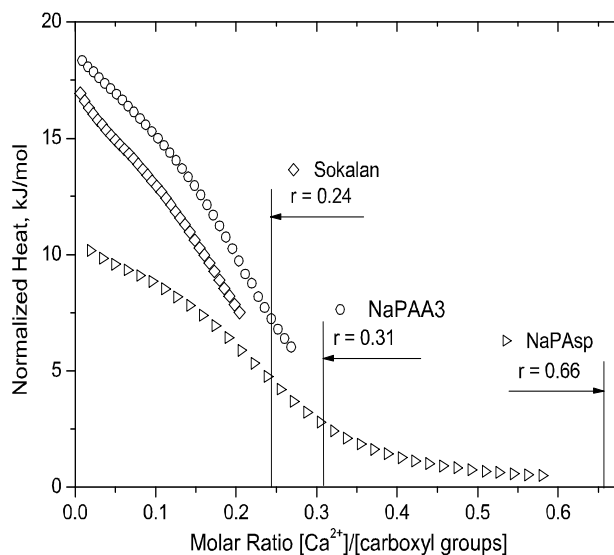
Figure 5.5: Binding titration of NaPAA3, Sokalan and NaPAsp. The heat is normalized by moles Ca^{2+} injected into the system. Straight lines indicate the critical ratio r, at which precipitation occurs.

measured to be 0.22 for Sokalan and 0.66 for NaPAsp. Correspondingly the working concentrations of the polymers were selected to be 0.105 N and 0.037 N, respectively.

We observe that the NaPAsp (a natural scale modifier) precipitates at much higher calcium loads. The value of $r = 0.66$ is beyond stoichiometric equivalence (considering that each Ca^{2+} binds two carboxylic groups) and implies lower ion sensitive solubility. Obviously the nature of Ca^{2+} binding to NaPAsp is more elaborated involving collapse and stability. For this polymer, the binding is also less endothermic than for the other two examples, but it saturates at about the same levels of binding.

For Sokalan, the Ca^{2+} electrode was used to determine the amount of bound calcium in the course of the titration experiment, revealing similar curves as for NaPAA3. This is shown in Figure 5.6, where the concentration of free and bound Ca^{2+} for the three different polymer solutions (0.08 N NaPAA3, 0.037 N NaPAsp and 0.105N Sokalan (pH 7)) following the stepwise addition of 0.2 N CaCl$_2$ solution is plotted as a function of the concentration of added Ca^{2+}. As mentioned before, the line indicated with "Slope 1" represents the case of 100% binding of the added Ca^{2+}.
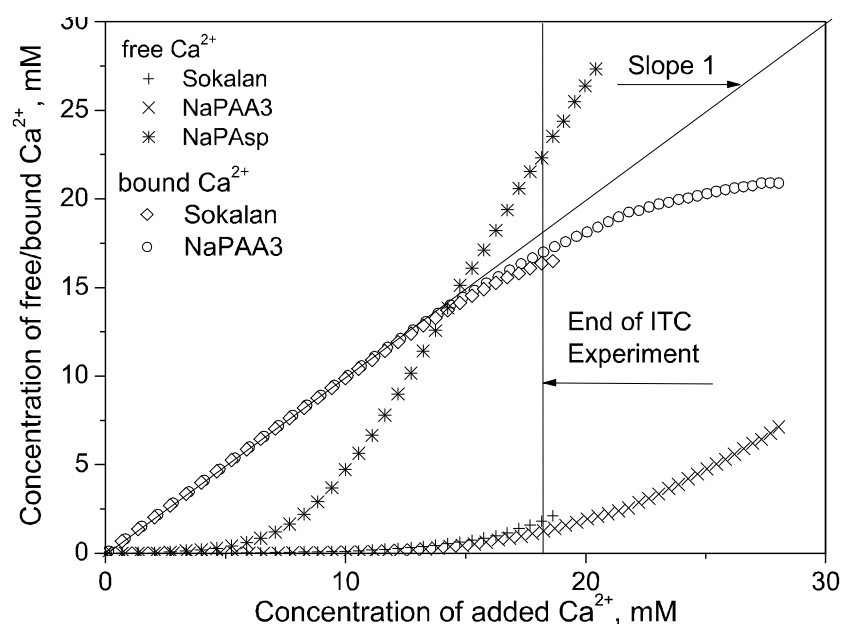
Figure 5.6: Calcium electrode isotherms. 0.2 N solution of CaCl$_2$ is titrated into 0.08 N NaPAA3, 0.037 N NaPAsp and 0.105 N Sokalan (pH 7). Free (measured) and bound calcium (see legend) is plotted as a function of added Ca^{2+}. The line indicated with "Slope 1" represents the case of 100% binding. The unrealistic excess of the apparent concentration of free calcium for the measurements with NaPAsp is presumably due to additional signal of the polymers passing through the calcium electrode membrane (see text for details).

Similarly to the case of NaPAA2, the Ca^{2+} electrode cannot be used for NaPAsp due to its small size.

In the context of the present experiments, we can only speculate about the nature of the unexpected endothermic binding character and its dependence on the chemical constitution of the polymer backbone. Obviously, both PAA and Sokalan fit well to the water structure, whereas the complexes with Ca^{2+} do not and require major, enthalpically unfavourable rearrangements of the water which leads to dehydration and finally precipitation of a hydrophobic complex. This is much less the case for polyaspartate where the amide bonds in the backbone ensure higher hydrophilicity which keeps the Ca-complex in solution. The lowered heat flow value suggests that the amide structure must also influence the hydrophobicity of the neighboring carboxylic acid sites, potentially via some type of amphiphilicity allowing lower polarity gradients or "molecular surface tensions". We have to conclude that nature has developed more

elaborated principles for Ca^{2+} binding and stabilization than technology.

This scenario implies seriously altered target structures for the development of optimized scale inhibitors: it is in the end not the charge or charge density which is decisive, but the induction of a transition from a very hydrated to a rather unhydrated polymer state by ion binding. It is the very special charm of this model that one can now easily prescibe additional features like ion selectivity of binding, which is found in a number of cases, but cannot be explained by electrostatic models.

5.2   Binding of Ca^{2+} to Lipid Membranes

Having studied the binding of Ca^{2+} to charged polymer chains, we want to confer our knowledge from the one-dimensional to a two-dimensional geometry by studying the interaction of Ca^{2+} with a charged lipid bilayer.

Calcium plays an important role in many biological processes such as endocytosis, protein signalling or fusion. In these processes, the ion interacts with the membrane of the cell triggering the respective event. Biological membranes are complex systems, containing a diverse set of molecules such as lipids, sterols and proteins. In most membranes the lipids are the two-dimensional matrix holding the rest of the molecules and among the different lipids found in biological membranes, phospholipids play an important role. The phospholipids can be either charged or neutral but zwitterionic. Most biomembranes contain roughly 10 % charged lipids [69], such as phosphatidylserine, whereas the remaining lipid fraction is zwitterionic or uncharged, consisting in particular of phosphatidylcholines or phosphatidylethanolamines.

It is well known that divalent ions interact strongly with charged lipids, but also moderately with uncharged lipids [70]. When a metal ion approaches a lipid membrane surface, it experiences several forces. The assembly of charged phospholipids into a continuous membrane gives rise to a surface potential leading to long-range electrostatic, coulombic forces. This electrostatic attraction increases the interfacial ion concentration compared to that in the bulk solution (as discussed in chapter 2.4.1). Besides being attracted to the surface, the ions can form coordination complexes with one or more of the lipid phosphate groups. In the case of phosphatidylserine, the carboxylate group offers an additional binding site for the ion. Since the phospholipid polar headgroups in aqueous solutions are typically hydrated [71], the

ion-phospholipid interactions leading to the formation of coordination complexes are mediated by dehydration forces.

The complex formation between metal ions and phospholipids is a dynamic process with lifetimes in the range of 10^{-5} s [72], [73], [74] and it is difficult to distinguish between physical adsorption and chemical binding. Hence, in this work, the term "binding" stands for both, the electrostatic attraction to the membrane and the chemical binding to individual binding sites.

The present study attempts to gain a deeper insight into the interaction of Ca^{2+} with negatively charged phospholipid membranes. The process is studied as a function of surface charge using large unilamellar vesicles (LUVs) with an average diameter of 60 nm. As a negatively charged lipid we use phosphatidylserine (DOPS), which is the major anionic phospholipid in most mammalian cell membranes. Also, as mentioned before, the carboxylate groups of DOPS mimic the binding site of the poly(acrylic acid) so that we can compare the one-dimensional to the two-dimensional binding. As a neutral lipid we use phosphatidylcholine (DOPC).

In chapter 5.2.1 we characterize the vesicle system under study and present the general considerations leading to the design of the experiment. We then discuss the high sensitivity titration calorimetry experiments used to determine enthalpies of Ca^{2+} binding to lipid vesicles of varying surface charge in chapter 5.2.2. To obtain a deeper insight into the origins of the calorimetric effects, we investigate aggregation and fusion of the vesicles as well as phase separation of the lipids in the presence and absence of Ca^{2+}, as presented in chapters 5.2.3 and 5.2.4, respectively. Finally, in chapter 5.2.5 we discuss the measurements of the amount of bound ion using a Ca^{2+} ion selective electrode together with the problems and limitations we observed with this method.

5.2.1 The System

When an aqueous solution of lipid vesicles is titrated into a concentrated salt solution, the vesicles burst due to the binding of the divalent ion and the osmotic gradient across the vesicle membrane. To avoid this rupture of the vesicles, we performed the inverse experiment, i.e we titrated a CaCl$_2$ solution into the vesicle solution yielding a high resolution with respect to the ion to lipid ratio. Any osmotic effects were avoided

by extruding the vesicles in an NaCl solution and titrating them with an isoosmolar CaCl$_2$ solution. This also reduces the complexity of the binding process.

However, the presence of NaCl screens the surface charge which leads to a decrease in the binding of Ca^{2+}: An increase in the NaCl concentration by a factor of 10 reduces the concentration of bound Ca^{2+} by a factor of 100 [75]. To determine the optimum concentration of NaCl in terms of maximum binding and ITC heat signal, a set of ITC experiments were performed where vesicle solutions extruded in different NaCl solutions were titrated with equiosmolar CaCl$_2$ solutions. The optimum NaCl concentration was found to be 0.01 N and correspondingly, the concentration of the injected CaCl$_2$ solution was set to 0.014 N. To obtain a high resolution in the molar ratio of Ca^{2+} to lipid in the course of the ITC experiment, the concentration of the lipids was set to 0.008 N. This leads to a maximum ratio of Ca^{2+} to the PS (for one used PS concentration) on the outside of the vesicles at the end of the ITC experiment of 0.34.

To investigate the influence of surface charge, DOPS/DOPC lipid mixtures with PS mole fractions, γ_{PS}, of 0 (i.e pure DOPC), 0.11, 0.2 and 0.25 were studied. This PS range spans the levels of charge found in most biological membranes.

Under certain conditions the two species of PS/PC lipid systems do not mix well [76]. Phase separation in lipid membranes is exhibited by splitting of the heat capacity peak. To investigate whether DOPS and DOPC phase separate under the present conditions, we performed DSC experiments measuring the phase transition of the extruded vesicles at a PS mole fraction γ_{PS} of 0.2, as presented in chapter 5.2.4.

5.2.2 Isothermal Titration Calorimetry Experiments

The isotherm of calcium binding to negatively charged DOPS/DOPC vesicles was measured with Isothermal titration calorimetry (ITC). All of the ITC experiments presented here were performed by titrating 10 μl aliquots of an 0.014 N CaCl$_2$ solution into 0.008 N LUVs in 0.01 N NaCl. The first injection of 2 μl is ignored.

The measured enthalpy change following the stepwise addition of a CaCl$_2$ solution into DOPS/DOPC ($\gamma_{PS} = 0.2$) is shown in Figure 5.7. In order to determine the enthalpy associated with the calcium binding, the dilution enthalpy of the 0.014 N CaCl$_2$ solution into an 0.01 M NaCl solution was measured and subtracted from the
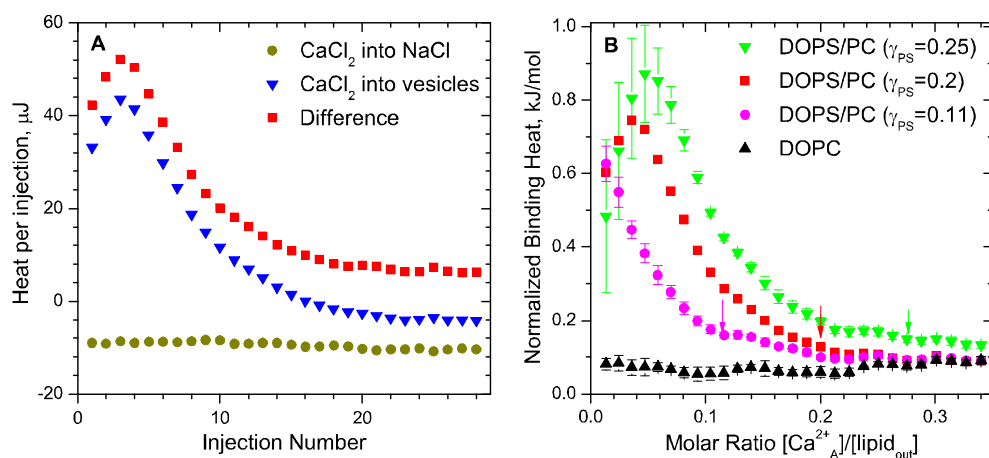
Figure 5.7: Binding Isotherms. A: Titration of 0.008 N DOPS/DOPC ($\gamma_{PS} = 0.2$) LUV and 0.01 M NaCl solution with 10 μl aliquots of 0.014 N CaCl$_2$. The difference of the two signals is the heat associated with the interaction of Ca^{2+} with the lipid bilayer (the heat of dilution of the vesicles is negligible). B: Molar binding heat of DOPS/DOPC vesicles with PS fractions of 0, 0.11, 0.2 and 0.25. The heat is normalized over the moles of added Ca^{2+}. Arrows indicate the point where the ratio of added Ca^{2+} to PS in the external leaflet of the vesicle membrane exceeds one.

total enthalpy. The difference will be subsequently denoted as *binding heat*. The dilution enthalpy of the vesicle solution can be neglected. Besides dilution, there are additional heat effects which can contribute to the total measured heat of reaction, such as enthalpy changes due to variations in the headgroup hydration and headgroup interactions or by rearrangements of the fatty acyl chains [60]. DSC measurements can yield information about the occurrence of these effects as presented in chapter 5.2.4.

It is well known that the affinity of anionic PS bilayers for Ca^{2+} is suppressed as the membrane surface charge density is decreased upon incorporation of the zwitterionic lipid PC [77]. To investigate the influence of surface charge density on the binding enthalpy we also performed the titration of 0.014 N CaCl$_2$ into pure DOPC and into DOPS/DOPC vesicles solutions with PS mole fractions of 0.11 and 0.25. The measured binding heats normalized over the moles of added Ca^{2+} as a function of molar ratio of added Ca^{2+}, [Ca$_A^{2+}$], to total lipid concentration on the outside of the vesicles, [lipid$_{out}$], are shown in Figure 5.7 B together with the results for normalized

binding heat for $\gamma_{PS} = 0.2$. The error bars were determined by averaging over three experiments. The black arrows indicate the point where the ratio of added Ca^{2+} to PS at the outside of the vesicles exceeds one.

In the case of pure DOPC, the binding enthalpy remains constant within the error of the measurement. Obviously, binding of Ca^{2+} to PC is not saturated at the end of the ITC experiment, where the ratio of [Ca$_A^{2+}$] to [lipid$_{out}$] is 0.34. This confirms the general observation that divalent cations adsorb to the zwitterionic phosphatidylcholine (PC) with ion to lipid stoichiometries of 1:1 to 1:3 [70].

An increase in surface charge fraction leads to an increase in the binding enthalpy. With increasing concentration of added calcium, the binding enthalpies of all of the charged vesicles approach the value of pure DOPC. Thus, we assume that in the case of the charged vesicles, the Ca^{2+} ions present initially in the solution mainly interact with the negatively charged PS carboxylate groups and phosphate moieties. When these groups are fully occupied, the ions continue to bind to the neutral PC headgroups. This interpretation is supported by the fact that the ions bind to the vesicles beyond Ca^{2+} to PS ratios of 1:1 (ion-to-lipid stoichiometries of divalent ions binding to PS membranes are reported to be 1:1 and 1:2 [70]). Thus, beyond the point of stoichiometric equivalence, the ions bind to the vesicles. A preferential interaction of cations with negatively charged components in a mixture has already been previously proposed [78], [79].

The measured binding enthalpies again demonstrate that the binding of Ca^{2+} onto mixed DOPS/DOPC lipid membranes is an endothermic process. Thus, the binding of Ca^{2+} to the lipid bilayer must be entropy driven. This is in good agreement with the studies on the binding of alkaline earth cations to low molecular weight compounds [60] and the binding of Ca^{2+} and La^{3+} to lipid vesicles [61] which are also entropy driven. The molecular origins of this entropy gain is a release of water molecules from the surface hydration layer of the lipid membrane and the dehydration of the Ca^{2+} ion upon binding.

At PS mole fractions of 0.2 and 0.25, a maximum appears in the binding enthalpy which is shifted to higher concentrations of added Ca^{2+} with increasing PS mole fraction. This maximum in the binding enthalpy is indicative for a secondary process, such as fusion, aggregation or phase separation. These processes were investigated

using Spectrophotometry and Differential Scanning Calorimetry (see chapters 5.2.3 and 5.2.4). The decrease of the reaction enthalpy with increasing concentration of added calcium could be caused by a decrease of bound Ca^{2+} and/or by a decrease in the heat per bound Ca^{2+}. To answer this question a calcium ISE was used to determine the amount of bound Ca^{2+} (see chapter 5.2.5).

5.2.3 Fusion and Aggregation Effects

The cohesion or aggregation of phospholipid membranes may affect ion binding. For instance, the affinity of Ca^{2+} for pure PS vesicles increases significantly if vesicle aggregation is induced by the addition of a 0.6-0.8 mM CaCl$_2$ solution [77]. In contrast, the binding of Ca^{2+} to PC bilayers is reduced upon decreasing the intermembrane separation [80]. In an ITC experiment, fusion or permanent aggregation would disturb the measurement, since it would lead to a precipitation of the dispersion and a thermodynamic equilibrium could not be reached despite continuous stirring of the solution in the cell [81]. Information about these effects is therefore essential for the interpretation of our ITC experiments.

Fusion and aggregation is sensitive to a number of parameters such as temperature, osmotic gradients and vesicle size [82] and several groups have shown that these effects can be induced by the addition of Ca^{2+} [82], [81], [83], [84]. In this work, the influence of calcium on fusion and aggregation of the vesicle systems under study was determined with Dynamic Light Scattering (DLS) and Spectrophotometry.

The DLS experiments were performed to measure the mean radius of the vesicle solutions before and after the ITC experiments. The unweighted size distribution of pure DOPC and DOPS/DOPC (at PS mole fractions of 0.11, 0.2 and 0.25) before and after the ITC experiments are shown in Figure 5.8. As the figure illustrates, the maximum in the size distribution does not change for any of the systems. The slight change in the peak width is in the order of the error of the measurement and can therefore not be attributed to fusion. Thus, from DLS experiments, no obvious fusion or aggregation can be detected.

However, as mentioned before, the maximum in the binding enthalpy for $\gamma_{PS} \geq 0.2$ is indicative for some secondary process such as aggregation. Spectrophotometry is a
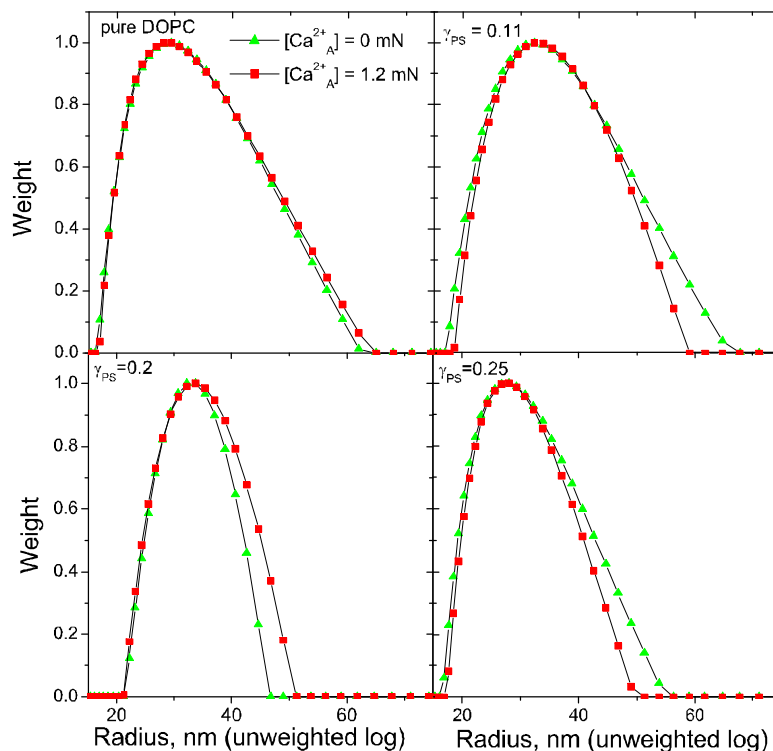
Figure 5.8: Unweighted size distribution of DOPS/DOPC vesicles in 0.01 M NaCl with PS mole fractions γ_{PS} of 0, 0.11, 0.2 and 0.25. The green curves are the DLS measurements performed before the ITC experiment ($[\text{Ca}_A^{2+}] = 0$ mN) and the red curves after the ITC experiment ($[\text{Ca}_A^{2+}] = 1.2$ mN).

technique which is very sensitive towards aggregation effects in colloidal dispersions. Thus, we measured the absorbance of a PS/PC vesicle solution as a function of added Ca^{2+}. The measured change in the absorbance at 350nm, A_{Ca}, following the stepwise addition of an 0.014 N CaCl$_2$ solution into an 0.008 N DOPS/DOPC ($\gamma_{PS} = 0.2$) solution is shown in Figure 5.9. The absorbance due to dilution of the vesicle solution, A_{dil}, was determined in a separate experiment by addition of the same aliquots of an 0.01 N NaCl solution to the vesicle solution. The change in the absorbance associated with the calcium binding, A_{Bind}, was then calculated from the relation $A_{Bind} = A_{Ca} - A_{dil}$. The resulting difference in absorbance, which will be further denoted as "binding absorbance", is plotted on the right ordinate of Figure 5.9.
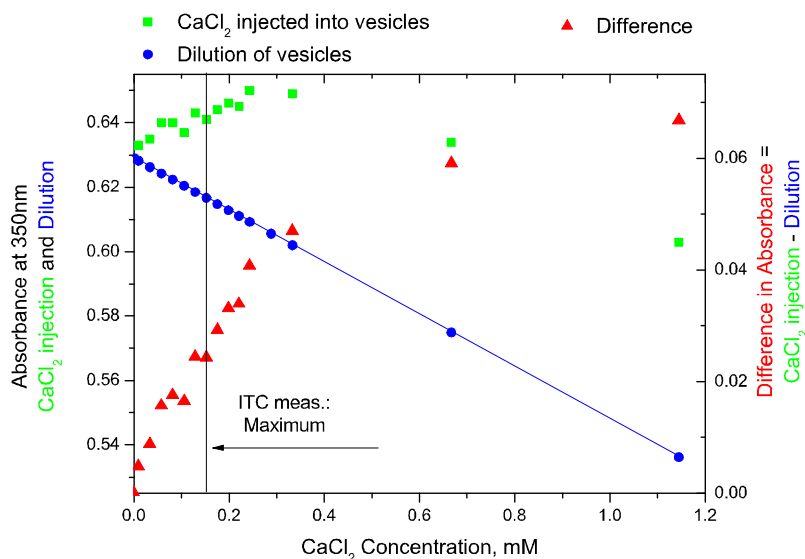
Figure 5.9: Turbidity measurements. Measured absorbance (at 350 nm) of 0.008 N DOPS/DOPC ($\gamma_{PS} = 0.2$) LUVs upon titration with small aliquots of 0.014 N CaCl$_2$ and same amount of 0.01 N NaCl. The difference of the two signals is the absorbance associated with the interaction of Ca^{2+} with the lipid bilayer.

As the measurement demonstrates, the binding absorbance increases upon the addition of CaCl$_2$. This increase in the binding absorbance is indicative for vesicle aggregation. We assume that after binding of Ca^{2+} on the outside of the vesicles, the membranes get in close contact with each other so that they become susceptible to aggregation. However, the aggregation process does not lead to a precipitation of the solution, since with increasing Ca^{2+} concentrations, the binding absorbance approaches a constant value indicating a standstill of the aggregation process. In contrast, further aggregation would eventually lead to precipitation, which would become obvious from a decrease in the measured binding absorbance. Thus, the constant binding absorbance suggests that the resulting solution of small aggregates of vesicles is diluted upon further addition of CaCl$_2$. We conclude that the addition of Ca^{2+} leads to the formation of small aggregates of vesicles which remain stable in the solution. With increasing calcium concentration, the formation of aggregates is eliminated.

Aggregation and fusion of mixed PS/PC membranes has been extensively studied. In a previous work, Düzgünes et al. [82] have studied the parameters that lead

to fusion and aggregation of PS/PC membranes in the presence of calcium. They argue that aggregation is enabled by the formation of coordination complexes between neighboring PS molecules. As measured by DSC and discussed in the next section, the PS/PC ($\gamma_{PS} = 0.2$) LUVs solution studied here does contain PS enriched domains. These could indeed enable the formation of transient aggregates.

5.2.4   Phase Transitions in the Presence of Ca^{2+}

The binding of Ca^{2+} can induce phase separation and influence phase transitions in the lipid systems, which could lead to additional heat signals in the ITC measurements. Additionally, changes in phase transitions can give a hint on hydration/dehydration effects of the lipids upon ion binding. To investigate the influence of calcium on the phase transition in the present system we studied the thermal phase transition of PS/PC vesicles as a function of added Ca^{2+} using Differential Scanning Calorimetry (DSC). As mentioned before, we used SOPS and SOPC instead of DOPS and DOPC due to the temperature restrictions of the machine applied in these experiments.

The thermal phase transition of DOPC and DOPS from the ordered gel phase to the disordered liquid- crystalline phase are reported in the literature to occur at –17°C [85] and –11°C [86], respectively. Thus, the phase transition of a homogeneous lipid mixture will presumably lie in between these values. However, the DSC machine used in this work is restricted to temperatures above 2°C. Hence, SOPC and SOPS with gel to liquid crystal phase transitions above this temperature (5.5°C, data not shown, and 17°C [87], respectively) were used for the DSC experiments instead of DOPC/DOPS. The only difference between SOPC/PS and DOPC/PS is that the latter have two unsaturated chains whereas the former have only one unsaturated chain while the headgroups essential for Ca^{2+} binding are identical.

The specific heat capacity of the a SOPS/SOPC ($\gamma_{PS} = 0.2$) LUVs solution with increasing amounts of added CaCl$_2$ is shown in Figure 5.10. When no Ca^{2+} is present, the lipid mixture shows two endothermic phase transitions centered at 7.5°C and 12.5°C. This is indicative for the existence of two phases, i.e. the formation of lipid rafts. In particular, the two peaks at 7.5°C and 12.5°C can be assigned to PC and PS enriched domains, respectively. Thus, at a PS mole fraction of 0.2, some phase
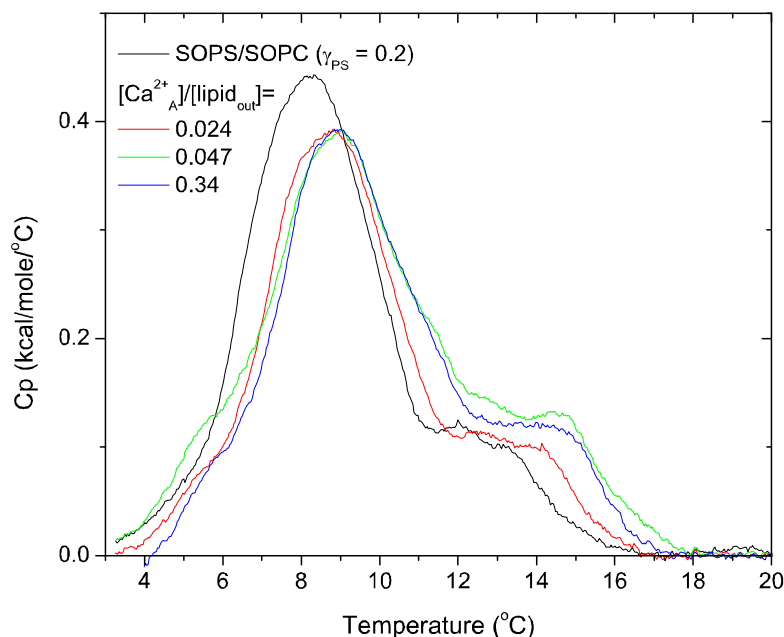
Figure 5.10: DSC heating curves of SOPC/SOPC ($\gamma_{PS} = 0.2$) LUVs in 0.01 N NaCl with increasing amounts of added CaCl$_2$ (molar ratio of added Ca^{2+} to total lipid concentration as indicated).

separation occurs. The reason for this phase separation could be attractive dispersion interactions at close approach [88]. Since an increase in the incorporation of PS in the membrane would lead to a further phase separation, we conclude that for a PS fraction of 0.25 the lipid mixtures phase separate as well. As for a γ_{PS} of 0.11, we speculate that there will be little phase separation in the system.

Increasing the ion to lipid ratio leads to a shift of the two phase transition peaks to higher temperatures. The measured phase transitions were observed in three consecutive heating and cooling scans. This indicates that the formation of the phases is stable. These results are in agreement with previous measurements where the endothermic transition of PS is shifted to higher temperatures due to Ca^{2+} [89], [90].

Because the phase transition temperatures of both domains are increased, we conclude that Ca^{2+} does not only bind to the charged PS but also to the zwitterionic PC headgroups. However, since the temperature shift of the PS enriched domain is larger than the one of the PC enriched domain, the interaction of the ion with PS is stronger than with PC. The shift in the phase transition temperature indicates that binding of

Ca^{2+} induces structural changes of the lamellar phase and of the hydrocarbon chain packing, which is well known for the binding of divalent cations to negatively charged membranes. Since the observed phase transitions are shifted to higher temperatures, the gel packing of the chains in the presence of Ca^{2+} is energetically more stable. This speaks for a tight binding of Ca^{2+} to the lipids encompassed by the dehydration of the lipid membrane interface and the divalent ion.

5.2.5 Determination of Ca^{2+} Binding Using Ca^{2+} Ion Selective Electrode

The amount of bound Ca^{2+} upon the titration of the vesicles can further elucidate the interaction of the divalent ion with the lipid membranes and provide useful information for the determination of the binding enthalpy and binding constants. In this study, we use a Ca^{2+} Ion Selective Electrode to determine the amount of bound ion for a pure DOPC LUVs solution and a DOPS/DOPC LUVs solution with PS fraction of 0.2.

Ca^{2+} Binding to Pure DOPC

The binding of Ca^{2+} to pure PC membranes has been extensively investigated. The ion-to-lipid stoichiometries of divalent cations binding to PC bilayers were concluded from NMR measurements to vary from 1:1 to 1:3. Studies on Ca^{2+} adsorption to PC membranes from Altenbach and Seelig [72] and Seelig [91] reveal that the interaction is best described by the formation of a ternary complex of Ca^{2+} to phospholipids, i.e an ion-to-lipid stoichiometry of 1:2, and a binding constant of 20 M^{-1}. At low calcium concentrations however, the binding is found to be nonspecific, i.e. given by a 1:1 partitioning.

In this work, the amount of bound Ca^{2+} was determined from a calibration curve preceding the measurement. The amount of bound Ca^{2+} as a function of molar ratio of [Ca$_A^{2+}$] to [lipid$_{out}$] for the titration of a 0.0016 N DOPC LUV with an 0.014 N CaCl$_2$ solution is plotted in Figure 5.11 A. The amount of bound Ca^{2+} was determined by subtracting the amount of free Ca^{2+} from the concentration of added calcium. The line indicated with "Slope 1" represents the case of 100% binding of the added Ca^{2+}.

The experiment shows that Ca^{2+} indeed binds to the zwitterionic PC headgroups.
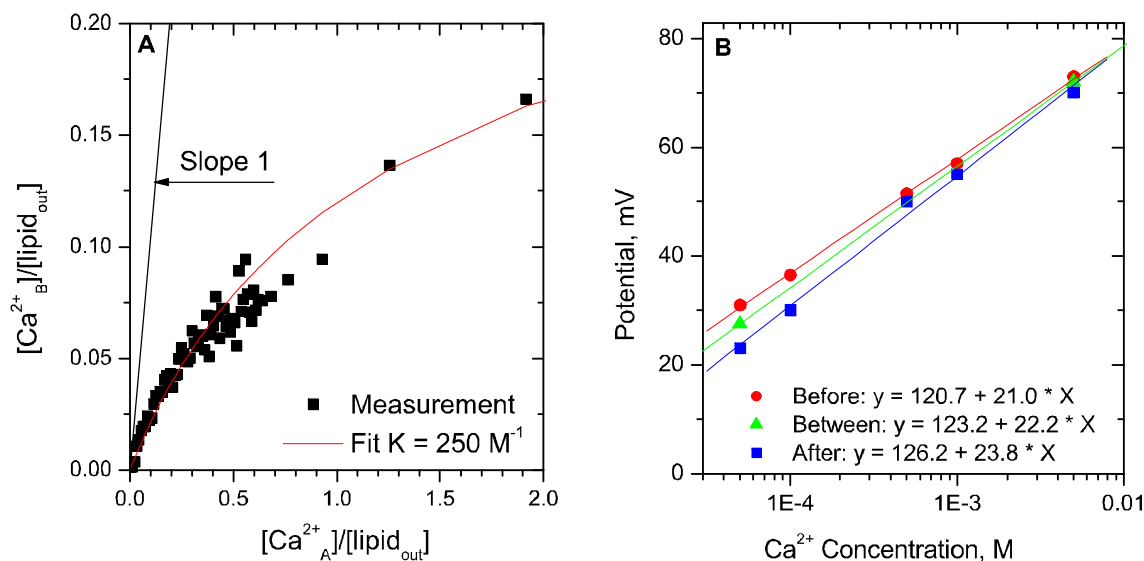
Figure 5.11: A: Binding isotherm of the titration of an 0.0016 N DOPC LUVs solution in 0.01 N NaCl with 0.014 N CaCl$_2$. The line indicated with "Slope 1" represents the case of 100% binding. The concentration of bound ion [Ca$_B^{2+}$] was determined using a calibration curve before the measurement. The measurement was fitted with a 1:2 binding model from Seelig [91]. B: Calibration of the Ca^{2+} ISE preceding, following and in the course of the titration of the DOPC LUVs. The slope and intersection of the calibration curve changes indicating that the vesicles interact with the ion selective membrane.

For very small calcium concentrations, almost all of the added ions bind to the vesicles while only a few remain free in the bulk solution and binding of Ca^{2+} is not saturated at [Ca$_A^{2+}$] to [lipid$_{out}$] ratios of 2. These results affirm the interpretation of the ITC experiments that Ca^{2+} binding is not saturated at the end of the ITC experiment. Fitting this curve with the 1:2 binding model from Seelig [91], we obtain a binding constant of 250 M^{-1}. This value is an order of magnitude larger than the value of 20 M^{-1}, now established in the literature. A first trial to explain this discrepancy could be the interaction of the vesicle solution with the ion selective membrane leading to errors in the measured concentration of free Ca^{2+}.

To study a possible interaction of the vesicles with the electrode membrane, we performed a calibration of the ISE preceding, following and during of the measurement. Repetitive experiments revealed that the respective calibration curves differ in their slope and intersection, as shown in Figure 5.11 B. This is indicative of an inter-

action of the vesicles with the hydrophobic membrane causing an additional change in the electrochemical potential difference. We can only speculate that the change in the slope is caused by the adsorption of lipid onto the ion selective membrane of the electrode. The resulting layer of lipid could lead to two effects: Either the attraction of Ca^{2+} ions to the electrode is enhanced compared to the bulk solution because of the affinity of Ca^{2+} to PC, which would result in an apparent increase of the measured potential. Or, the lipid layer on the electrode surface prohibits the transport of ions across the electrode membrane. This would lead to an apparent decrease in the measured electrochemical potential difference. Thus, the two proposed processes effect the calibration curve in the opposite direction. The behavior of the calibration curve upon the addition of calcium therefore changes as a result of the sum of the two effects. Clearly, this causes an error in the measured concentration of free Ca^{2+} but due to the two described opposing mechanisms, we cannot assess whether the measured free Ca^{2+} concentration is an under- or overestimation of the "real" ion concentration. Nevertheless, we can estimate the error of the measurement from an averaged fit of the three calibration curves. However, calibrating the electrode in the course of the measurements bears the problem of memory effects of the electrode, which are unveiled by a slow adjustment of the measured potential after exchanging the calibration solution with the vesicle solution. Therefore, we do not present the data from this measurements in the present context.

To our knowledge, the described effect of the vesicles on the calibration of an ion selective electrode has not yet been reported in the literature. We therefore present these observations to alert other groups to take care that neutral phospholipid membranes may seriously comprise the outcome of binding measurements using hydrophobic ion selective electrodes.

A fit of a binding isotherm determined with a calibration following the measurement yields a binding constant of 130 M^{-1}(data not shown). This value is closer to the binding constant reported in the literature. However, direct comparison with the literature is not straightforward, since there is a number of parameters, which can influence the binding of Ca^{2+} to the membrane, such as the concentration of NaCl present in the system or the curvature of the vesicles.

Ca^{2+} Binding to PS/PC Membranes

In the case of charged membranes, ion selective electrodes can monitor the ion concentration in the bulk solution, but when studying charged surfaces and interfaces one should be aware that they do not allow to distinguish between Ca^{2+} residing within the double layer near the membrane surface and Ca^{2+} actually bound to the headgroups of the phospholipid membrane. Consequently, the fraction of counterions immobilized in the diffusive part of the double layer could be erroneously ascribed to the bound fraction of ions. It is therefore essential to differentiate between *intrinsic* and *apparent* binding constants. While the former is given by the *surface* concentration of the binding ions, the latter is a function of the *bulk* ion concentration. Without additional information on the surface potential, ion selective membranes can therefore only be used to determine apparent binding affinities [92], [93]. The interpretation of the results is further complicated by the presence of Na$^+$, which is also known to bind to PS, although with a lower affinity [93], [94].

As for the binding of calcium to DOPC, the amount of bound Ca^{2+} to DOPS/DOPC ($\gamma_{PS} = 0.2$) LUVs was determined from a calibration curve preceding and following the measurement. Again, the interaction of the vesicles with the ion selective membrane counterfeit the calibration curves. The amount of bound ion was calculated using the calibration curve before and after the titration. Figure 5.12 B shows the titration curve of an 0.0027 N DOPS/DOPC ($\gamma_{PS} = 0.2$) LUVs solution with small aliquots of an 0.014 N CaCl$_2$ solution. The line indicated with "Slope 1" represents the case of 100% binding of the added Ca^{2+}. The two titration curves strongly deviate. Although we can not make any quantitative conclusion on the distribution of the titration curve, we can derive qualitative information from the measured isotherm. For small concentrations of added Ca^{2+}, we assume that the true binding curve will follow the curve using the calibration before the measurement whereas for increasing concentrations, the curve will approach the isotherm determined after the titration. The point where the molar ratio of added Ca^{2+} to PS at the outside of the vesicles, [PS$_{out}$], equals 1 is indicated in the graph with black arrows.

For small Ca^{2+} concentrations, almost all of the added ions bind to the vesicles while only a few remain free in the bulk solution. Obviously, Ca^{2+} binds to the vesicles up to ratios far beyond the expected stoichiometric equivalence of 1 (considering that
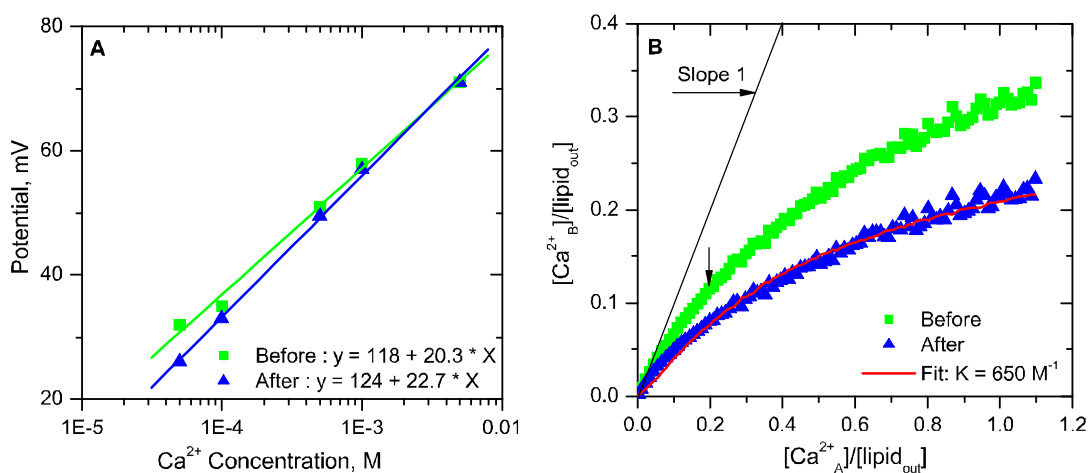
Figure 5.12: A: Calibration of the Ca^{2+} ISE before and after the titration of the PS/PC mixture. The slope and intersection of the calibration curve changes indicating that the vesicles interact with the ion selective membrane. B: Binding isotherm of the titration of a DOPS/DOPC ($\gamma_{PS} = 0.2$) LUVs solution in 0.01 N NaCl with CaCl$_2$. The concentration of bound ion [Ca$_B^{2+}$] was determined using the calibration before and after the measurement. The line indicated with "Slope 1" represents the case of 100% binding. The black arrow indicates the point where the molar ratio of added Ca^{2+} to PS at the outside of the exceeds one.

each Ca^{2+} binds to one PS headgroup). The facts that Ca^{2+} binding to the vesicles is observed beyond the point of PS headgroup saturation and that the binding heat approaches the value of Ca^{2+} binding to pure PC (as measured by ITC) strongly maintains the theory that Ca^{2+} first primarily binds to the PS headgroups and when these are fully neutralized it binds to the PC headgroups.

Fitting the binding isotherm after the ITC experiment with the 1:2 binding model from Seelig (as discussed in the section on Ca^{2+} binding to pure DOPC), we find a binding constant of 650 M^{-1}.

Comparing the binding of Ca^{2+} to pure DOPC to Ca^{2+} binding to DOPS/DOPC vesicles containing 20% charged lipids ($\gamma_{PS} = 0.2$) allows to estimate the role of electrostatic effects on ion binding. The presence of charges on the vesicle surface leads to an accumulation of ions in the diffusive layer and to a binding of the ions in the Stern layer. Comparing the binding constants of Ca^{2+} binding to the charged vesicles to neutral DOPC (both calculated using the calibration curve after the measurement), we find that binding to the charged membrane is ~ 5 times larger. These binding

constants were determined using the same 1:2 binding model. However, as previously mentioned, the ion selective membrane measures the ion concentration in the bulk solution. In the case of charged membranes, counterions immobilized in the diffusive part of the double layer are therefore erroneously ascribed to the bound fraction of ions. As a conclusion, the negatively charged PS/PC membranes attract the Ca^{2+} ions thereby enhancing the local ion concentration on the membrane, lowering the detected amount of ions at the electrode. The binding constant calculated for the charged vesicles was determined without taking the local enhancement of Ca^{2+} ions on the vesicle surface into account. The larger binding constant in case of the charged vesicles compared to the neutral membrane could therefore be due to electrostatic effects.

To determine electrostatic effects on ion binding, electrophoresis measurement were performed. Binding of Ca^{2+} to the interface of the PS/PC membrane increases the vesicles surface potential. Knowledge about the vesicles surface charge as a function of added Ca^{2+} concentration can therefore provide additional information about the extent of Ca^{2+} binding. However, as discussed in chapter 3.3.4, the surface potential cannot be measured directly. Instead, the electrical potential at the shear plane, the zeta potential (ZP), which can be measured with electrophoresis, can be used as an approximate quantification of the surface potential of the vesicles in solution [20], [95].

Due to the zwitterionic character of the DOPC headgroups, the ZP of a pure DOPC LUVs solution is zero, as measured by electrophoresis. The incorporation of negatively charged PS into the membrane decreases the ZP leading to a negative surface potential. If Ca^{2+} is added to the negatively charged vesicle solution, the ions bind to the membrane and the negative charges of the PS headgroups are compensated by the bound divalent cations. As a consequence, increasing the divalent cation concentration may reverse the sign of the zeta potential for PS vesicles. Using electrophoresis we observed that the ZP changes from -42 mV for a 1 mN DOPS/DOPC LUVs solution to -35 mV at a Ca^{2+} concentrations of 0.17 mN (corresponding to a ratio $[\mathrm{Ca}_A^{2+}]/[\mathrm{lipid}_{out}]$ of 0.34). The total change in the zeta potential ΔZP is therefore 7 mV, indicating that Ca^{2+} binds to the negatively charged PS/PC membrane.

If we want to compare these findings to the binding of Ca^{2+} to pure DOPC, we

have to take into account that the ion surface concentration of the lipid membrane is increased by the incorporation of phosphatidylserine. The Ca^{2+} surface concentration can be estimated using the Boltzmann distribution (equation 2.6) where the surface potential is obtained from the Gouy-Chapmann theory (equation 2.7). For the PS/PC membranes with 20% surface charge in 0.01 N NaCl it was calculated to be ~30 times higher than the bulk Ca^{2+} concentration. Consequently, electrophoresis measurement for pure DOPC were performed at Ca^{2+} concentrations 30 times larger than for the PS/PC mixture. We find that the ZP changes from 3 in the case of pure DOPC to 12 for Ca^{2+} concentrations of 6.8 mN yielding a total change in the zeta potential of 9 mV, which is similar to that found for the mixed PS/PC ($\gamma_{PS} = 0.2$) membrane. We have to conclude, that the reason for an enhanced binding of Ca^{2+} to mixed PS/PC compared to pure PC membranes is an attraction of ions to the vicinity of the lipid bilayer due to the presence of charged phosphatidylserine.

5.2.6 Influence of Ca^{2+} Binding on Vesicle Surface Area

The methods presented so far have shown that binding of calcium to charged and uncharged lipid bilayer membranes is an endothermic process and therefore entropy driven. We assume that the gain in entropy comes from a release of water molecules from the hydration shell of the ion as well as a dehydration of the lipid membrane. This is supported by the observation that Ca^{2+} binds tightly to the membrane leading to a denser packing of the headgroups and the hydrocarbon chains. As a consequence, binding of the divalent cation to the vesicles should cause an increase in the bending elasticity of the membrane.

Here, we examined Ca^{2+} binding on the micron sclae, using phase contrast microscopy to monitor the changes in the surface area change of a vesicle upon the binding of Ca^{2+}. We observed a fluctuating, prolate, giant vesicle with a large surface area. Due to time constraints, we performed the measurements on a multilamellar instead of a unilamellar vesicle. However, the qualitative information we obtain is probably similar in both cases.

Shown in Figure 5.13 is a sequence of pictures of one DOPS/DOPC ($\gamma_{PS} = 0.2$) vesicle after injection of CaCl$_2$. Figure 5.13 A shows the fluctuating vesicle in a solution of 0.01 N NaCl and glucose. At this moment, the vesicle fluctuates strongly,
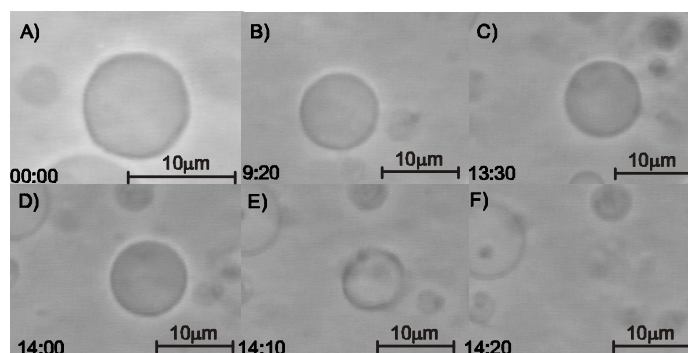
Figure 5.13: Sequence of pictures of a Giant DOPS/DOPC (γ_{PS}=0.2) vesicle in 0.01 N NaCl and glucose after injection of 0.014 N CaCl$_2$, 0.01 NaCl and glucose. Time is set to zero before injection and is shown on each figure (min:s). A: No CaCl$_2$ present, vesicle strongly fluctuates. B: CaCl$_2$ solution has reached the vesicle. C: Significant decrease of fluctuations. D: Fluctuations have ceased, vesicle spherical. E: Vesicle vanishes. F: Vesicle disappeared.

indicating a large excess surface area. An isotonic solution of 0.014 N CaCl$_2$, 0.01 N NaCl and glucose is then pumped into the chamber. After a few minutes (Figure 5.13 B), the CaCl$_2$ solution has reached the vesicle under study, but so far, no changes in its fluctuations are observed. After 13.5 minutes, we observe a significant decrease in the fluctuations of the vesicle (Figure 5.13 C) ceasing completely after 14 minutes (Figure 5.13 D). At this point the vesicles become completely spherical. Only a few seconds later, the vesicle bursts (Figure 5.13 E) and finally vanishes completely (Figure 5.13 F). We can exclude that the vesicle ruptures due to osmotic effects, since the osmolarity of the CaCl$_2$ solution was carefully matched with that of the vesicle suspension.

From these observations, we conclude that the binding of Ca^{2+} causes a decrease in the surface excess area of the vesicle. We attribute this to a tight binding of Ca^{2+} to the membrane encompassed by a dehydration of the ion as well as the lipid bilayer. A possible alternative interpretation for this behavior could be that the lipid bilayer "wraps" the ions effectively decreasing the vesicle surface area. As a result the membrane tension increases and the vesicle eventually ruptures and leaks.

5.3   1D to 2D - Comparison

The aim of this chapter was to compare the binding of Ca^{2+} to a one-dimensional polymer chain with the binding to a two-dimensional lipid bilayer membrane. As a polymer we used poly(acrylic acid) (PAA), where the carboxylate groups mimic the functional groups of the negatively charged phosphatidylserine-phosphatidylcholine membranes. Isothermal Titration Calorimetry (ITC) and Ion Selective Electrode (ISE) are used to measure the reaction enthalpy and binding isotherms.

Comparing the binding of Ca^{2+} to a one-dimensional polymer rod and to a two-dimensional membrane surface is not straight forward. In the case of the partially charged PS/PC lipid bilayer, the divalent ions can not only bind to the carboxylate groups of the PS headgroups but also to the phosphate groups of the zwitterionic PC headgroups offering an additional binding site compared to the polymer. Furthermore, in the case of the polymer, Ca^{2+} binding induces conformational changes. In contrast, the lipid membrane of LUVs is tensed so that conformational changes do not occur but aggregation of the vesicles might play a role in this case. Conformational and aggregation effects can lead to additional heat effects which can contribute to the total measured heat of reaction. Finally, as we have shown, the lipids of the PS/PC membrane might be phase separated leading to an inhomogeneous charge distribution. The binding process to these vesicles is therefore complex and the electrical double layer adsorption model is presumably too simple.

Despite the mentioned differences in the two systems, we combine the calorimetric and potentiometric experiments and compare the heat per bound ion. We find that both binding of Ca^{2+} to the polymer chain as well as to the lipid bilayer is an endothermic process, and therefore driven by a gain in entropy, i.e. by the liberation of water molecules from the hydration shells of substrate and adsorbate. The molar binding enthalpy can be up to 25 times larger for Ca^{2+} binding to the polymer than to the lipid membrane, as shown in Figure 5.14 A (this is true for the first injection, where in both cases almost all of the injected ions bind and therefore the heat per added Ca^{2+} equals the molar binding enthalpy). If binding is driven by a release of water molecules, a larger endothermic binding enthalpy is indicative of stronger hydration of the polymer chain as compared with the vesicle membrane.

Figure 5.14 B shows the molar ratio of bound Ca^{2+} to carboxylate group as a
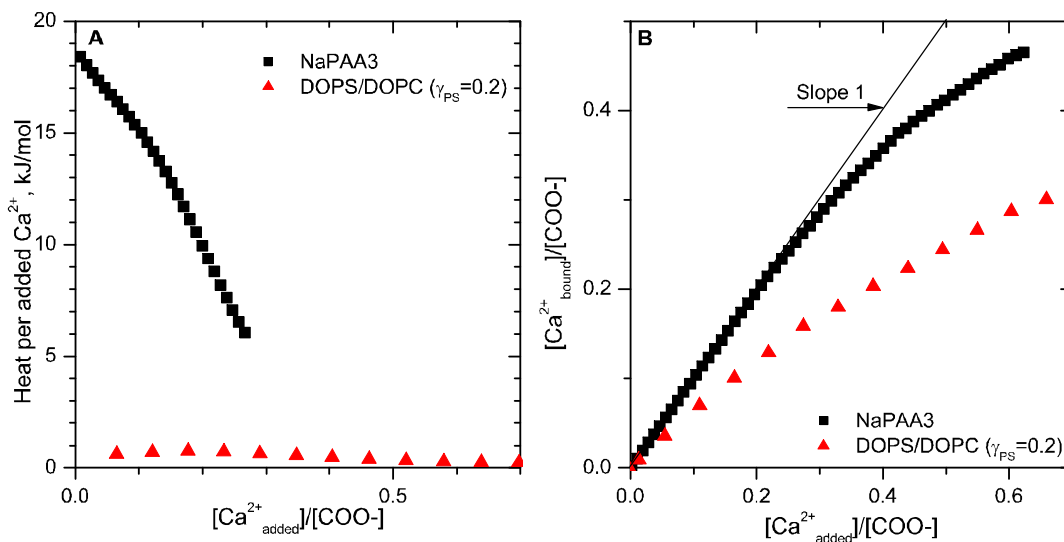
Figure 5.14: A: Binding isotherm of the titration of NaPAA3 and DOPS/DOPC ($\gamma_{PS} = 0.2$) LUVs with CaCl$_2$. The line indicated with "Slope 1" represents the case of 100% binding. B: Heat per added Ca^{2+} as a function of the molar ratio of Ca^{2+} to carboxylate groups for NaPAA3 (pH 7) and DOPS/DOPC ($\gamma_{PS} = 0.2$). The binding heat is ~25 times larger for the polymer than for the lipid membrane indicative for stronger hydration of the polymer compared to the lipid bilayer.

function of the molar ratio of added Ca^{2+} to carboxylate group for the one-dimensional and the two-dimensional binding. Clearly, the amount of ions bound to the polymer is higher than to the lipid membrane indicating that the binding of Ca^{2+} to the polymer is stronger than to the lipid membrane. Taking into account the observations on the giant vesicles, where we find that small amounts of Ca^{2+} already lead to a bursting of the vesicles, we conclude that weak binding of Ca^{2+} to cell membranes is a necessity for the survival of any organism, since stronger binding would presumably destroy any living cell.

We conclude that the driving force for Ca^{2+} binding in both systems is the dehydration of binding sites and the bound ion. We find that binding of Ca^{2+} to the polymer is stronger than to the lipid bilayer. Thus, if the driving force is a dehydration of substrate and adsorbate, the polymers' carboxylate groups must be more strongly hydrated than the binding sites of the lipid membrane. This can be easily visualized, since the one-dimensional polymer chain allows the carboxylate groups to

be surrounded from almost all directions. Whereas in the case of the two- dimensional lipid bilayer membrane, the binding sites are burried within the lipid membrane and therefore less exposed to hydration water.

Chapter 6

The K$^+$/Na$^+$ Specificity

The fact that living cells selectively retain potassium and exclude sodium has been known since the early days of molecular biology. In fact, the intracellular concentrations of potassium and sodium are 140 mM and 5 - 15 mM, respectively, whereas their extracellular concentrations are 5 mM and 145 mM, respectively [21]. This ion partitioning leads to electrical and chemical gradients across the cell membrane which are crucial for cell function.

Researchers have tried to understand the characteristic partitioning of sodium and potassium in cells and tissues for many years and there are two different theories on the cause of ion partitioning in living cells. Most physiologists believe that ions are pumped into and out of the cells via special proteins integrated into the membrane. These pumps are believed to use the cell energy for the ion transport. Crucial experiments and calculations have been performed that provide strong evidence for the existence of the pumps.

However, this picture is probably too simple, and particularly G. Pollack [96] summarized a number of circumstantial evidence that the potassium enrichment should be also due to physicochemical effects. For instance, one open question is whether pumps are thermodynamically feasible and the debate on whether the energy required for ion pumping can be provided by the cells net energy production is still going on [25], [97], [26]. The hypothesis challenging the conventional ion pump theory is that the ions are excluded from the cell due to their low solubilities in cellular water. It has been shown by nuclear magnetic resonance [22], [23], [24] that cell water is more structured than liquid water and less structured than ice. The supporters of this the-

ory believe that the special structure of cell water affects the solubility of various ions in the cell and accounts for selective ion exclusions. Many investigators, including advocates of pumps, agree that cell water is ordered differently than liquid water and that the picture of ion pumps is presumably too simple.

Motivated by this discussion, we analyze the preferential ion binding of K$^+$ versus Na$^+$ onto simple non-biological objects, namely the standard polyelectrolyte poly(acrylic acid) and microgels made of the electrically neutral poly(N-Isopropyl-acrylamide) (PNIPAAM). As these systems are clearly non-living and non-biological, it would be possible to reveal the existence of bare physicochemical effects for the buildup of concentration gradients.

In the experiments on binding of Ca^{2+} to negatively charged polyelectrolytes (see chapter 5.1), we proved by a combination of isothermal titration calorimetry (ITC) and an ion selective electrode (ISE), that the binding is not, as usually believed, driven by Coulombic interactions, but essentially due to entropic effects, provided by a favorable change of the hydration shells of both, polymers and ions [98]. As a general consequence of this work, it was evidenced above that ion binding onto polymers and gels does not rely on the presence of charges, but should be possible to larger extents also for polymers with a switchable hydration behavior.

Following these experiments we use ITC and a potassium ion selective electrode to study the K$^+$/Na$^+$ specificity. In chapter 6.1, we present the results for the binding of K$^+$ to NaPAA3 whereas chapter 6.2 contains the results on the binding of K$^+$ to PNIPAAM microgel particles.

6.1 Binding of K$^+$ to Poly(acrylic acid)

The measured molar enthalpy change following the stepwise addition of 10 μl aliquots of 0.1 N KCl into 0.08 N NaPAA3 (pH 7) is shown in Figure 6.1 A. The total enthalpy measured in the ITC experiment is the sum of the enthalpy associated with the interaction of potassium with the polymer chain and the heat of dilution of the salt and polymer solution. In order to determine the enthalpy associated with the binding of K$^+$, the heat of dilution of an 0.1 N KCl solution into pure deionized water as well as the heat of dilution of NaPAA3 with pure deionized water were measured and
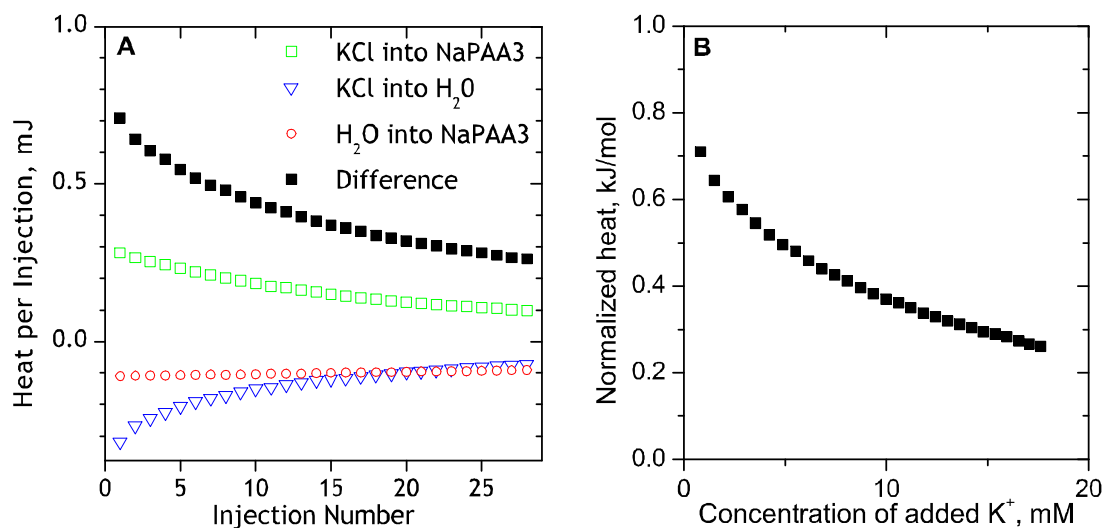
Figure 6.1: Binding Isotherms. A) Titration of 0.08 N NaPAA3 and water with 10 μl aliquots of 0.1 N KCl and titration of 0.08 N NaPAA3 with 10 μl aliquots of water. The heat associated with the binding of K$^+$ (denoted as "difference"), is given by the heat of injecting KCl into NaPAA3 minus the heat of dilution of KCl minus the heat of dilution of NaPAA3. B) Molar binding heat of potassium binding to NaPAA3. The heat is normalized over the moles of added K$^+$.

subtracted from the total measured heat. The measurements illustrate that the heat of dilution of KCl and the polymer is negative whereas the interaction of K$^+$ ions with the NaPAA3 solution is positive. The molar binding heat of shown in Figure 6.1 B, is the heat associated with the binding of K$^+$ normalized over the moles of added K$^+$. Obviously, K$^+$ binding to NaPAA is an endothermic process and must therefore be entropy driven.

When K$^+$ is added to the NaPAA solution, some of the K$^+$ ions bind to the polymer causing a release of Na$^+$ counterions while others remain free in the bulk solution. Knowledge about the amount of bound ion can enhance the understanding of the interaction of the ion with the polymer chain and provide useful information for determining binding constants. Here, we used a potassium ion selective electrode to determine the binding isotherm.

The amount of bound K$^+$ was determined from a calibration curve preceding and following the measurement. Repetitive experiments revealed that the respective
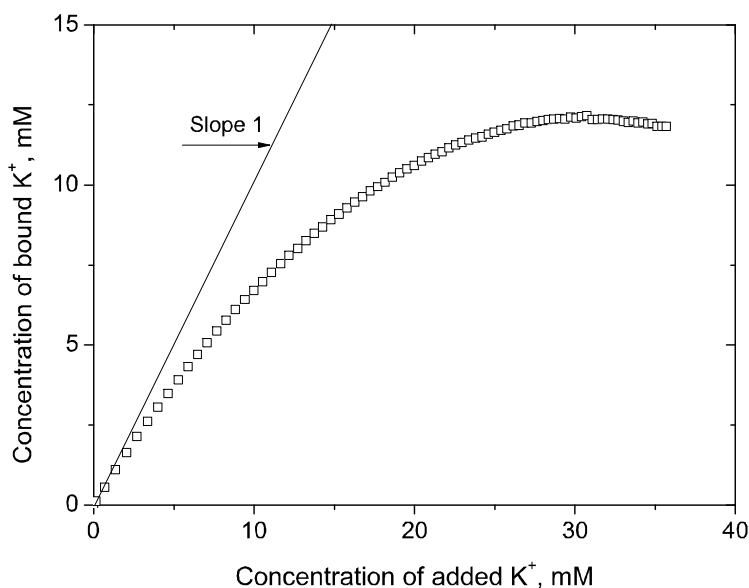
Figure 6.2: Binding isotherm of the titration of 0.08 N NaPAA3 with 0.1 N KCl. The concentration of bound ion was determined using the calibration preceding ($\triangle$) and following ($\square$) the measurement. The line indicated with "Slope 1" represents the case of 100% binding.

calibration curves slightly differ in their slope and intersection. This is indicative for an interaction of the polymer with the ion selective membrane causing an additional change in the electrochemical potential difference. We have already perceived this artifact with vesicles and ion selective membranes (see chapter 5.2.5) and present this observation to inform other groups that the interaction of solutes with ion selective electrodes may falsify binding measurements.

In Figure 6.2, the concentration of bound potassium (determined from the calibration curves preceding and following the measurement) for NaPAA3 following the stepwise addition of an 0.1 N KCl solution is plotted as a function of the concentration of added K^+. The amount of bound ion was determined by measuring the concentration of free potassium in the polymer solution after each injection with the K^+ electrode and subtracting this value from the concentration of added potassium. The line indicated with "Slope 1" represents the case of 100% binding of the added K^+.

The binding of potassium to NaPAA3 is an equilibrium process which can be

described by

$$K^+ + NaPAA3 \overset{C}{\rightleftharpoons} KPAA3 + Na^+$$
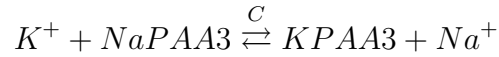
The equilibrium constant C is then given by

$$C = \frac{[K_B^+][Na_F^+]}{[K_F^+][Na_B^+]}$$

where $[K_F^+]$ and $[Na_F^+]$ are the concentration of free potassium and sodium, respectively, and $[K_B^+]$ and $[Na_B^+]$ denote the concentration of bound potassium and sodium, respectively. To calculate a binding constant for this process, we use the isotherm determined from the calibration following the measurement. Fitting the measured binding isotherm (data not shown), we find that $C = 0.2$, i.e. sodium binds stronger to the polymer than potassium. We conclude, that in the case of poly(acrylic acid), there is no specific ion binding of K^+ versus Na^+.

6.2 Binding of K^+ to Poly(N-Isopropylacrylamide)

Having studied the binding of K^+ to the charged chain of poly(acrylic acid), we want to confer our knowledge to the electrically neutral PNIPAAM and study the interaction of K^+ with the crosslinked polymer gel.

There is an abundance of experiments and applications for PNIPAAM summarized in a recommendable review from Schild [99] listing more than 300 references. Recently, the polymer has been mainly studied and applied due to its special thermal behavior in aqueous media. Namely, it is a member of a class of polymers termed thermo-responsive, which show inverse solubility upon heating. The temperature at which its macromolecular transition from hydrophilic to hydrophobic occurs is called the lower critical solution temperature (LCST). Experimentally, this lies between 30 and 35°C, the exact temperature being a function of the detailed microstructure of the macromolecule. The LCST of the PNIPAAM microgels used here is 32.5°C and the experiments are performed at 25°C, slightly below the collapse point of the microgel.

Polymer gels which are able to undergo changes in hydration by altered temperatures or other stimuli are well known and were pioneered by Tanaka [100], [101]. They are often also referred to as "intelligent gels" and are discussed as the operating

units of artificial soft machines [102]. In the present context, it is important to note that such gels also react towards salt, i.e. their phase transition depends on salinity [103]. Additionally, this shift depends on the type of salt and follows with respect to the anions the Hofmeister series [104], [105].

Curiously, in these examinations, it was always assumed that the ion concentration within and outside the gels is the same. Hence, a possible interaction of the polymer with the salt was ignored. However, our studies on the interactions of Ca^{2+} with polymers and lipid membranes clearly revealed that the ion does not only bind to the charged polymer and charged lipid vesicles but also to zwitterionic lipids. Thus, a lack of interactions of ions with an uncharged polymer gel seems unlikely, since any entropic interaction of polymer and salt would lower the activity of the salt thus allowing the polymer gel to take up salt throughout the dehydration collapse.

Since we were interested in the interaction of cations with the polymer gel, we used Isothermal Titration Calorimetry to measure the binding enthalpy of K^+ binding to PNIPAAM which yields information on the driving forces of ion/adsorbate interactions. Figure 6.3 A shows the molar binding enthalpy following the addition of 10 μl aliquots of 0.1 N KCl into an 0.44 N (0.5 wt%) microgel solution (pH 7). The heat associated with the interaction of K^+ with the polymer gel was determined by subtracting the heats of dilution of the polymer and the salt solution.

The binding enthalpy is endothermic and small compared to the enthalpy of binding to PAA. As binding of K^+ to the gel occurs deliberately, the driving force of the reaction is an increase in entropy, which is believed to be primarily due to the liberation of water molecules leading to a salting out of the polymer gel. An interaction of the salt with the polymer does obviously take place and the binding of the salt is driven by dehydration.

To further elucidate the interaction of potassium with the polymer gel, we determined the amount of bound K^+ upon the titration of the polymer gel with an ion selective electrode. The amount of bound potassium was determined from a calibration curve that was identical, both preceding and following the measurement. Thus, the polymer gel does not interact with the ion selective membrane, or if so, this is not detectable. Figure 6.3 B shows the titration curve of injecting 0.1 N KCl into 0.44 N PNIPAAM (pH 7). The molar ratio of bound ion, $[K^+_{Bound}]$, to monomer group, [NI-
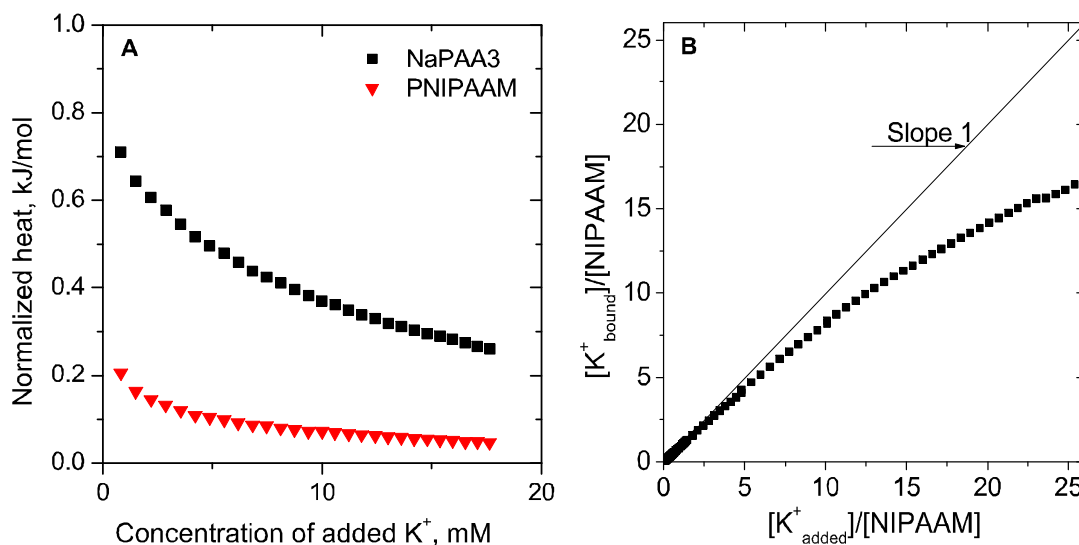
Figure 6.3: Binding Isotherms. A) Molar binding enthalpies of 0.08 N NaPAA3 and 0.44 N PNIPAAM titrated with 0.1 N KCl. The enthalpy associated with the binding of K$^+$ was determined from the heat of injecting KCl into the polymer minus the dilution enthalpy of KCl minus the heat of dilution of the polymer. This heat is then normalized by the moles of added K$^+$. B) Molar ratio of bound K$^+$ over monomer NIPAAM as a function of the molar ratio of added K$^+$ over the monomer NIPAAM. The line indicated with "Slope 1" represents the case of 100% binding.

PAAM], is plotted as a function of the molar ratio of added ion, [K$^+_{Added}$], to monomer group. The line indicated with "Slope 1" represents the case of 100% binding of the added K$^+$.

Unexpectedly, the microgel particles at lower salt concentrations adsorbs practically all of the added salt, i.e. they desalinate the solution very effectively. This continues up to very high salt concentrations until the ability for ion binding collapses. It is very surprising to see that the polymer gel binds the ion beyond molar ratios of 15. We have to conclude that the critical ion binding capacity is not defined by stoichiometry but by the structural collapse of the microgels as the particles start to phase separate from water.

So far, we have shown that the PNIPAAM microgel particles can carry large amounts of K$^+$ and combining ITC measurements with potentiometric measurements we have concluded that ion binding induces salting out of the polymer gel. However,
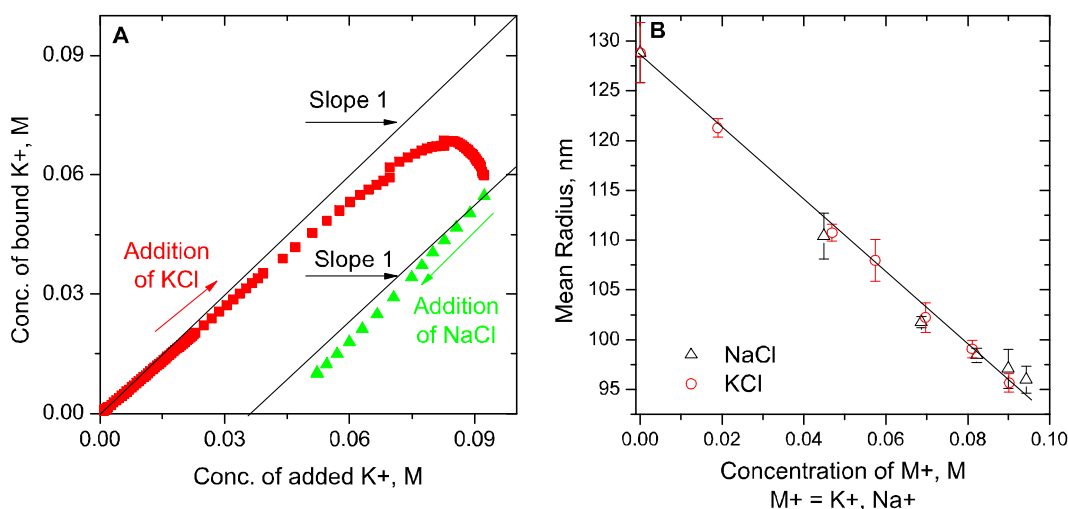
Figure 6.4: A) Binding isotherms of adding 0.1 N KCl to 0.44 N PNIPAAM and 0.1 N NaCl to the solution of K-PNIPAAM. B) Weight avaraged radius as a function of concentration of added KCl and NaCl to a solution of 0.44 N PNIPAAM. The black line is drawn as a guide to the eye.

we have not yet revealed, whether PNIPAAM salting out is cation specific. To answer this question, we used the PNIPAAM solution from the above mentioned ISE measurements, loaded with K$^+$ (which will be further denoted as K-PNIPAAM) and added small aliquots of 0.1 N NaCl to this K-PNIPAAM solution. A K$^+$ ion selective electrode was consequently used to determine the amount of released K$^+$ upon the addition of NaCl.

Figure 6.4 A shows the titration curve of 0.44 N PNIPAAM particles with 0.1 N KCl and the subsequent titration of K-PNIPAAM with 0.1 N NaCl. The lines indicated with "Slope 1" represent the case of 100% binding (in the case of adding KCl) and unbinding (in the case of adding NaCl). As already presented in Figure 6.3 B, potassium strongly binds to the gel and ion binding ability collapses only at extremely large K$^+$ concentrations. When NaCl is added to the K$^+$ saturated polymer gel, K$^+$ ions are released into the solution as revealed by the decrease in the amount of bound K$^+$. The molar ratio of released K$^+$ per added Na$^+$ was found to be 0.5.

We conclude that PNIPAAM microgel particles possess the capacity of loading large amounts of sodium and potassium. However, cation binding to PNIPAAM is not Na$^+$/K$^+$ specific.

These findings were verified using dynamic light scattering (DLS) to determine the particle size upon addition of the two salts, KCl and NaCl. The weight avaraged radius of the microgel particles as a function of added concentration of NaCl and KCl for the titration of 0.44 N PNIPAAM is shown in Figure 6.4 B. The error was determined by three consecutive measurements of the same solution.

For both salts, we observe a linear decrease of the particle size speaking for a salting out of the PNIPAAM upon addition of the cations. The decrease in the mean radius is identical for the two salts. The results strongly support the observation that both salts induce a dehydration and salting out of PNIPAAM microgel particles, which is not Na^+/K^+ specific.

However, here, we studied the interaction of two chloride salts with the polymer. Thus, a possible interpretation of the observation that PNIPAAM salting out is not cation specific, is that the polymer interacts with the anion and only weakly with the cation. This interaction leads to a dehydration of the anion and adsorbate. It has been previously observed that also nonionic species such as saccharides decrease the LCST of PNIPAAM [106]. This denotes that not only ions but also uncharged molecules can interact with the gel. The interaction with the microgel is therefore independent of charge.

Chapter 7

Summary and Outlook

The goal of this work was to study the binding of ions to polymers and lipid bilayer membranes in aqueous solutions. The influence of charge on the interaction of ions with polymers and membranes was investigated. Particular emphasis was given on the specific effects of ions on the structure of water.

In the first part of this work, the influence of various inorganic salts and polyelectrolytes on the structure of water was studied using Isothermal Titration Calorimetry (ITC). The heat of dilution of the salts was used as a scale of water structure making and breaking of the ions. NaCl was used as a reference salt and the effects of different cations (Li^+, Na^+, K^+, Cs^+, Ca^{2+}, Mg^{2+}) and anions (Cl^-, Br^-, I^-, SO_4^{2-}, CH_3COO^-) on the structure of water were studied by the heats of dilution of the chloride and sodium salts, respectively. The measured heat effects were found to be in the order of 1 J/mol and were related to a local rearrangement of water molecules around the ions. For the anions, the heat of dilution could be used as a manifestation of the general Hofmeister series, with kosmotropes having a negative heat of dilution and chaotropes having a positive heat of dilution. On the contrary, cations show the inverse behavior, i.e chaotropes release heat upon dilution whereas kosmotropes take up heat upon dilution. The molecular details for this asymmetry in anion and cation behavior remain to be determined. A simplistic model was developed allowing a quantitative comparison of the different ions. The total measured heat of dilution was attributed to the sum of two heat effects, resulting from an endothermic and an exothermic process. Endothermic heat effects were assumed to arise from the sepa-

ration of contact ion pairs and exothermic heat effects from a complete separation of the loose ion pairs, yielding freely hydrated ions.

Following this, the heat of dilution of two standard polyelectrolytes poly(sodium acrylate) (NaPAA) and poly(sodium styrene sulfonate) (NaPSS) was measured and compared to the corresponding low molecular weight salts, sodiumacetate (NaAc) and sodium sulfate. In agreement with the so-called hydrophobic effect, the higher hydrophobicity of the polystyrenesulfonate backbone remained unseen up to rather high polymer concentrations ($\sim$1 N). We related this observation to the specific structure of water screening the hydrophobic polystyrene-backbone. The dilution of NaPSS and NaPAA was found to be similar and practically athermal in both cases. NaAc was found to be exothermic over the whole examined range of concentrations, which was interpreted as a local exothermic binding and rearrangement of water molecules around the acetate anion.

Following this, the binding of Ca^{2+} to NaPAA was studied to learn about the competition between electrostatic and hydration forces. ITC and a Ca^{2+} Ion Selective Electrode were used to measure the reaction enthalpy and binding isotherm. Binding of Ca^{2+} ions to PAA, a spontaneous process, was found to be highly endothermic ($\sim$18 kJ/mol), i.e. the binding is solely driven by entropy. A relevance of long-range water structure effects onto the binding process could be excluded since the heat of dilution of all involved species was found to be about athermal. We concluded that, in contrast to the wide spread belief that Coulomb interactions provide the driving force for ion binding, liberation of water molecules from the hydration shells of the components is the driving energy source for the binding of multivalent ions onto polyelectrolytes. Comparing the binding of Ca^{2+} to three different industrial scale inhibitors, PAA, polyaspartic acid (PAsp) and Sokalan, we revealed that PAsp has the highest capacity of binding Ca^{2+}.

We then compared the binding of ions to the one-dimensional PAA polymer chain to the binding to lipid vesicles which the ions perceive as two-dimensional surfaces. As vesicles we used negatively charged phosphatidylserine-phosphatidylcholine membranes where the functional carboxylate groups mimic the functional group of the polymer. As for the polymer, Ca^{2+} binding was found to be endothermic and therefore driven by a gain in entropy. Thus, binding of Ca^{2+} was again found to be driven

by the liberation of water molecules from the hydration shells of ion and adsorbate. However, the heat of binding was found to be much smaller in magnitude ($\sim$1 kJ/mol) than for the binding to the polymer. ISE measurements revealed that binding of calcium to the polymer is stronger than to the lipid bilayer. We attributed the weaker binding of the ion to the lipid membrane to a weaker hydration of the two-dimensional surface compared to the one-dimensional polymer chain.

The experiments using ion selective electrodes showed that vesicles can interact with the ion selective membrane, leading to a change in the measured electrochemical potential difference. We therefore concluded that possible interaction of particles with ion selective membranes should always be verified since they can compromise the outcome of binding measurements. Alternative methods, such as conductivity could be used in future, to confirm the determined binding isotherms.

In the context of these experiments, it was shown that Ca^{2+} also binds to zwitterionic lipid vesicles. Here, binding was found to occur beyond ion to lipid stoichiometries of 1:1. Thus, it was shown that divalent ions do not only interact with charged polymers and lipids, but also with zwitterionic lipids. We concluded that interactions of ions with an uncharged polymers should also be possible.

Motivated by this observation, we studied the interaction of two salts, KCl and NaCl, to a neutral polymer gel, PNIPAAM, and to the ionic polymer PAA. Combining calorimetry and a potassium selective electrode we observed that the ions interact with both polymers, whether containing charges or not. In the case of the PNIPAAM particles, the interaction of the salt with the microgel was found to lead to a salting out of the polymer. We concluded that the interaction of ions with polymers does not depend on charge but is driven by dehydration of ions and the polymer gel. However, it was found that binding to these systems is not cation specific, since the two salts showed the same effects in decreasing the diameter of the particles. It was therefore concluded that the interaction of salts with the polymer gel is probably dominated by a dehydration of anions and that the cations play a minor role in salting out. Additionally, the binding isotherms showed that the gel has a huge capacity of ion binding. In fact, the critical ion binding capacity was found not to be defined by stoichiometry but by the structural collapse of the microgels. In future, these experiments should be verified using alternative methods, such as conductivity.

Bibliography

[1] F. Sussman and H. Weinstein. On the ion selectivity in Ca-binding proteins - the cyclo(-l-pro-gly-)3 peptide as a model. *Proc. Natl. Acad. Sci.*, 86:7880–7884, 1989.

[2] T.P. Lybrand, A. McCammon, and G. Wipff. Theoretical calculation of relative binding-affinity in host guest systems. *Proc. Natl. Acad. Sci.*, 83:833–835, 1986.

[3] S. Habuchi, H.B. Kim, and N. Kitamura. Water structures in ion-exchange resin particles: Solvation dynamics of nile blue a. *Anal. Chem.*, 73:366–372, 2001.

[4] M. Chavez-Paez, K. Van Workum, L. de Pablo, and L.L. de Pablo. Monte carlo simulations of wyoming sodium montmorillonite hydrates. *J. Chem. Phys.*, 114:1405–1413, 2001.

[5] V.L. Larwood, B.J. Howlin, and G.A. Webb. Solvation effects on the conformational behaviour of gellan and calcium ion binding to gellan double helices. *J. Mol. Model.*, 2:175–182, 1996.

[6] F. Hofmeister. Zur lehre von der wirkung der salze. II. *Arch. exp. Pathol. Pharmakol.*, 24:247–260, 1888.

[7] K.D. Collins and M.W. Washabaugh. The hofmeister effect and the behaviour of water at interfaces. *Q. Rev. Biophys.*, 18:323–422, 1985.

[8] M.G. Cacace, E.M. Landau, and J.J. Ramsden. The hofmeister series: salt and solvent effects on interfacial phenomena. *Q. Rev. Biophys.*, 30:241–277, 1997.

[9] P.A. Thiel. The interactions of water with solid surfaces: fundamental aspects. *Surf. Sci. Rep.*, 7:211, 1987.

[10] P.Raiteri, A. Laio, and M. Parrinello. Correlations among hydrogen bonds in liquid water. *Phys. Rev. Letters*, 93(8):087801–1–087801–4, 2004.

[11] S.J. Suresh and V.M. Naik. Hydrogen bond thermodynamic properties of water from dielectric constant data. *J. Chem. Phys.*, 113:9727–9732, 2000.

[12] R. Weber. *Photoelectron Spectroscopy of Liquid Water and Aqueous Solutions in Free Microjets Using Synchroton Radiation.* PhD thesis, Freie Universitt Berlin, 2003.

[13] J. Bockris and A.K.N. Reddy. *Modern Electrochemistry.* Plenum, New York, 1970.

[14] E.A. Vogler. Structure and reactivity of water at biomaterial surfaces. *Adv. Colloid Interfac.*, 74:69–117, 1998.

[15] R.L. Baldwin. How hofmeister ion interactins affect protein stability. *Biophys. J.*, 71:2056–2063, 1996.

[16] P.A. Grigorjec and S.M. Bezrukov. Hofmeister effect in ion-transport - reversible binding of halide anions to the roflamycoin channel. *Biophys. J.*, 67(6):2265–2271, 1994.

[17] K.H. Gustavson. *The Chemistry and Reactivity of Collagen.* Academic Press, New York, 1956.

[18] M. Yamasaki, H. Yano, and K. Aoki. Differential scanning calorimetric studies on bovine serum albumin: Ii. effects of neutral salts and urea. *Int. J. Biol. Macromol.*, 13:322–328, 1991.

[19] D.F. Evans and H. Wennerstrm. *The Colloidal Domain, Where Physics, Chemistry, Biology and Technology Meet.* VCH, New York, 1994.

[20] D. Huster, K. Arnold, and K. Gawrisch. Strength of Ca^{2+} binding to retinal lipid membranes: Consequences for lipid organization. *Biophys. J.*, 78:3011–3018, 2000.

[21] B. Alberts, D. Bray, J. Lewis, M. Raff, K. Roberts, and J.D. Watson. *Molecular Biology of the Cell.* Garland Publishing, Inc., New York, 3 edition, 1994.

[22] E. Odelblad, B. N. Bhar, and G. Lindstrom. Proton magnetic resonance of human red blood cells in heavy-water echange experiments. *Arch. Biochem. Biophys.*, 63:221–225, 1956.

[23] I.L. Cameron, K.R. Cook, D.Edwards, G.D. Fullerton, G. Schatten, H. Schatten, A.M. Zimmerman, and S. Zimmerman. Cell-cycle changes in water properties in sea-urchin eggs. *J. Cell. Physiol.*, 133(1):14–24, 1987.

[24] E.A. Lpez-Beltrn, M.K. Mat, and S. Cerdn. Dynamics and environment of mitochondrial water as detected by h nmr. *J. Biol. Chem.*, 271(18):10648–10653, 1996.

[25] G.N. Ling. *A Physical Theory of the Living State: the Assiciation-Induction Hypothesis.* Blaisdell Publ. Co., Waltham, MA, 1962.

[26] J.C. Freedman and C. Miller. Energy requirement of sodium-pump in muscle. *Fed. Proc.*, 33(5):1457–1457, 1974.

[27] R. Nayar, M.J. Hope, and P.R. Cullis. Generation of large unilamellar vesicles from long-chain saturated phosphatidylcholines by extrusion technique. *Biochim. Biophys. Acta*, 986:200–206, 1989.

[28] R.C. MacDonald, R.I. MacDonald, B.Ph.M. Menco, K. Takeshita, N.K. Subbarao, and L.-R. Hu. Small-volume extrusion apparatus for preparation of large, unilamellar vesicles. *Biochim. Biophys. Acta*, 1061:297–303, 1991.

[29] E. Evans and W. Rawicz. Entropy-driven tension and bending elasticity in condensed-fluid membranes. *Phys. Rev. Let.*, 64(17):2094–2097, 1990.

[30] H. Heerklotz and J. Seelig. Titration calorimetry of surfactant-membrane partioning and membrane solubilization. *Biochim. Biophys. Acta*, 1508:69–85, 2000.

[31] I. Jelesarov and H. R. Bosshard. Isothermal titration calorimetry and differential scanning calorimetry as complementary tools to investigate the energetics of biomolecular recognition. *J. Mol. Recognit.*, 12:3–18, 1999.

[32] K. Cammann and H. Galster. *Das Arbeiten mit ionenselektiven Elektroden.* Springer Verlag, Berlin Heidelberg New York, 3 edition, 1996.

[33] H. Eisenberg. Conductance of partially neutralized polymethacrylic and polyacrylic acids, using a polarization compensated twin cell. *J. Polym. Sci.*, 30(121):47–66, 1958.

[34] T. Kurucsev and B.J. Steel. Use of electrical transport measurements for determination of counterion association in salt-free polyelectrolyte solutions. *Rev. Pure Appl. Chem.*, 17:149, 1967.

[35] R.F.M.J. Cleven, H.G. de Jong, and H.P. van Leuwen. Pulse polyrography of metal polyelectrolyte complexes and operation of the mean diffusion-coefficient. *J. Electroanal. Chem.*, 202(17):57–68, 1986.

[36] H. van Leeuwen, R. Cleven, and J. Buffle. Voltametric techniques for complexation measurements in natural aquatic media - role of the size of macromolecular ligands and dissociation kinetics of complexes. *Pure Appl. Chem.*, 61(2):255–274, 1989.

[37] R.H. Mller. *Zetapotential und Partikelladung in der Laborpraxis.* Wissenschaftliche Verlagsgesellschaft mbH, Stuttgart, 1996.

[38] M. Smoluchowski. *Handbuch der Elektrizitt und des Magnetismus*, volume II. Barth-Verlag, Leipzig, 1921.

[39] Y. Marcus. Viscosity b-coefficients, structural entropies and heat capacities, and the effects of ions on the structure of water. *J. Solution Chem.*, 23(7):831–848, 1994.

[40] N.T. Southall, K.A. Dill, and A.D.J. Haymet. A view of the hydrophobic effect. *J. Phys. Chem.*, 106:521–533, 2002.

[41] R. Wachter and K. Riederer. Properties of dilute electrolyte solutions from calorimetric measurements. *Pure & Appl. Chem.*, 53:1301–1312, 1981.

[42] J. Barthel and J. Krner. Heat of dilution of electrolyte solutions. experimental method and data analysis. *J. Mol. Liq.*, 81:47–61, 1999.

[43] P.T. Thomson, D.E. Smit, and R.H. Wood. Enthalpy of dilution of aqueous Na_2SO_4 and Li_2SO_4. *J. Chem. Engin. Data*, 19(4):386–388, 1974.

[44] D.D. Ensor and H.L. Anderson. Heat of dilution of NaCl: Temperature dependence. *J. Chem. Engin. Data*, 18(2):205–212, 1973.

[45] H.P. Snipes, C. Manly, and D.D. Ensor. Heat of dilution of aqueous electrolytes: Temperature dependence. *J. Chem. Engin. Data*, 20(3):287–291, 1975.

[46] Y. Marcus. *Ion Properties*. Marcel Dekker, Inc., New York, 1997.

[47] F. Franks. *Water: A matrix of life*. Royal Society of Chemistry, Cambridge, 2 edition, 2000.

[48] Y. Georgalis, A.M. Kierzek, and W. Saenger. Cluster formation in aqueous electrolyte solutions observed by dynamic light scattering. *J. Phys. Chem. B*, 104:3405–3406, 2000.

[49] L. Degrve and F.L.B. da Silva. Large ionic cluster in concentrated aqueous nacl solution. *J. Chem. Phys*, 111(11):5150–5156, 1999.

[50] L. Degrve and F.L.B. da Silva. Detailed microscopic study of 1 m aqueous nacl solution by computer simulations. *J. Mol. Liq.*, 87:217–232, 2000.

[51] A.S. Levineand R.H. Wood. Heat of dilution of cesium chloride. *J. Chem. Engin. Data*, 15(1):33–34, 1970.

[52] S. Paula, W. Ss, J. Tuchtenhagen, and A. Blume. Thermodynamics of micelle formation as a function of temperature: A high sensitivity titration calorimetry study. *J. Phys. Chem.*, 99:11742 – 11751, 1995.

[53] C. Tanford. *The hydrophobic effect: Formation of Micelles in Biological Membranes.* Wiley, New York, 2 edition, 1980.

[54] G.S. Manning. Limiting laws and counterion condensation in polyelectrolyte solutions. 6. theory of the titration curve. *J. Phys. Chem.*, 85:870–877, 1981.

[55] F. Oosawa. *Polyelectrolytes.* Marcel Dekker, New York, 1971.

[56] G.S. Manning. The molecular theory of polyelectrolyte solutions with applications to the slectrostatic properties of polynucleotides. *Q. Rev. Biophys.*, 11:179–246, 1979.

[57] P.H. von Hippel and K.-Y. Wong. Neutral salts: the generality of their effects on the stability of macromoecular conformation. *Science*, 145:577–580, 1964.

[58] I. Pochard, P. Couchot, and A. Foissy. Conductometric and micorcalorimetric analysis of the alkaline-earth/alkali-metal ion exchange onto polyacrylic acid. *Colloid Polym. Sci.*, 277:818–826, 1999.

[59] M.R. Bhmer, Y. El Attar Sofi, and A. Foissy. Calorimetry of poly-(acrylic acid) adsorption on tio2. *J. Colloid Interf. Sci.*, 164:126–135, 1994.

[60] P. Garidel and A. Blume. Interaction of alkaline earth cations with the negatively charged phopholipid 1,2-dimyristoyl-sn-glycero-3-phosphoglycerol: A differential scanning and isothermal titration calorimetric study. *Langmuir*, 15:5526–5534, 1999.

[61] R. Lehmann and J. Seelig. Adsorption of Ca^{2+} and La^{3+} to bilayer membranes: measurment of the adsorption enthalpy and binding constant with titration calorimetry. *J. Phys. Chem. B*, 106:7908–7912, 2002.

[62] J. Lyklema. *Fundamentals of Interface and Colloid Science. Solid-Liquid Interfaces*, volume II. Academic Press, San Diego, 1995.

[63] J. Rieger. A new approach towards an untersanding of scaling in the presence of polycarboxylates. *Tenside Surfact. Det.*, 39:221–225, 2002.

[64] I. Pochard, P. Couchot, and A. Foissy. Potentiometric and conductometric analysis of the binding of barium ions with alkali polyacrylate. *Colloid Polym. Sci.*, 276:1088–1097, 1998.

[65] S. Lagerge, A. Kamyshny, S. Magdassi, and S. Partyka. Calorimetric methods applied to the investigation of divided systems in colloid science. *J. Therm. Anal. Calorim.*, 71:291–310, 2003.

[66] K. Huber. Calcium-induced shrinking of polyacrylate chains in aqueous solution. *J. Phys. Chem.*, 97:9825–9830, 1993.

[67] R. Schweins and K. Huber. Collapse of sodium polyacrylate chains in calcium salt solutions. *Eur. Phys. J. E*, 5:117–126, 2001.

[68] R. Schweins, P. Lindner, and K. Huber. Calcium induced shrinking of napa chains: A sans investigation of single chain behavior. *Macromolecules*, 36:9564–9573, 2003.

[69] R.A. Bckmann, A. Hac, T. Heimburg, and H. Grubmller. Effect of sodim chloride on a lipid bilayer. *Biophys. J.*, 85:1647–1655, 2003.

[70] G. Cevc. *Phospholipids Handbook*. Marcel Dekker, Inc., New York, 1993.

[71] R.P. Rand and V.A. Parsegian. Hydration forces between phopholipid bilayers. *Biochim. Biophys. Acta*, 988:351–378, 1989.

[72] C. Altenbach and J. Seelig. Ca^{2+} binding to phosphatidylcholine bilayers as studied by deuterium magnetic resonance. evidence for the formation of a Ca^{2+} complex with two phospholipid molecules. *Biochemistry*, 23:3913–3920, 1984.

[73] P.M. Macdonald and J. Seelig. Calcium binding to mixed phosphatidylglycerol-phosphatidylcholine bilayers as studied by deuterium nuclear magnetic resonance. *Biochemistry*, 26:1231–1240, 1987.

[74] P.M. Macdonald and J. Seelig. Calcium binding to mixed cardiolipin-phosphatidylcholine bilayers as studied by deuterium nuclear magnetic resonance. *Biochemistry*, 26:6292–6298, 1987.

[75] S. McLaughlin, N. Mulrine, T. Gresalfi, G. Vaio, and A. McLaughlin A. Adsorption of divalent cations to bilayer membranes containing ps. *J. Gen. Physiol.*, 77:445–473, 1981.

[76] J.Y. Huang, J.E. Swanson, A.R.G Dible, A.K. Hinderliter, and G.W. Feigenson. Nonideal mixing of ps and pc in the fluid lamellar phase. *Biophys. J.*, 2:413–42, 1993.

[77] R. Ekerdt and D. Papahadjopoulos. Intermembrane contact affects calcium binding to phopholipid vesicles. *Proc. Natl. Acad. Sci.*, 79:2273–2277, 1982.

[78] D. Papahadjopoulos. Surface properties of acidic phospholipids- interaction of monolayers and hydrated liquid crystals with uni- and bi-valent metal ions. *Biochim. Biophys. Acta*, 163:240, 1968.

[79] T. Seimiya and S. Ohki. Ionic structure of phospholipid membranes and ion binding of calcium ions. *Biochim. Biophys. Acta*, 298:546–561, 1973.

[80] D.H. Haynes. 1-anilino-8-naphtalenesulfonate: a fluorescent indicator of ion binding and electrostatic potential on the membrane surface. *J. Membrane Biol.*, 17:341–366, 1974.

[81] A. Blume and P. Garidel. *The Handbook of thermal analysis and calorimetry*, volume 4. Elsevier, Amsterdam, 1999.

[82] N. Duzgunes, S. Nir, J. Wilshut, J. Bentz, C. Newton, A. Portis, and D. Papahadjopoulos. Calcium- and magnesium induced fusion of mixed ps/pc vesicles: effect of ion binding. *J. Membr. Biol.*, 59(2):115–125, 1981.

[83] S. Ohki and H. Ohshima. Interaction and aggregation of lipid vesicles (dlvo theory versus modified dlvo theory). *Colloid. Surface. B*, 14:27–45, 1999.

[84] S. Ohki and K. Arnold. A mechanism for ion-induced lipid vesicle fusion. *Colloids and Surfaces B*, 18:83–97, 2000.

[85] R. Lewis, B. Sykes, and R. McElhaney. Thermotropic phase-behavior of model membrane composed of phosphatidylcholines containing cis-monounsaturated acyl chain homologs of oleic-acid - differential scanning calorimetric and p-31 nmr spectroscopic studies. *Biochemistry*, 27:880–887, 1988.

[86] J. Browning and J.Seelig. Bilayers of phosphatidylserine - deuterium and phosphorus nuclear magnetic-resonance study. *Biochemistry*, 19:1262–1270, 1980.

[87] D. Bach, E. Wachtel, N. Borochov, G. Senisterra, and R.M. Epand. *Chem. Phys. Lipids*, 63:105–113, 1992.

[88] B.W. Ninham. van der waals forces across triple-layer films. *J. Chem. Phys.*, 52:4578–4587, 1970.

[89] K. Jacobsen and D. Papahadjopoulos. Phase transitions and phase separations in phopholipd mambranes induced by changes in temperatur, ph, and concentration of bivalent cations. *Biochemistry*, 14(1):152–161, 1975.

[90] C. Newton, W. Pangborn, S. Nir, and D. Papahadjopoulos. Specificity of Ca^{2+} and mg^{2+} binding to phophatidylserine vesicles and resultant phase- changes of bilayer membrane structure. *Biochim. Biophys. Acta*, 506(2):281–287, 1978.

[91] J. Seelig. Interaction of phospholipids with Ca^{2+} ions - on the role of the phospholipid head groups. *Cell Biol. Int. Rep.*, 14:353–360, 1990.

[92] S.G.A. McLaughlin, N. Mulrine, T. Gresalfi, and G. Vaio. Adsorption of divalent cations to bilayer membranes containing ps. *J. Gen. Physiol.*, 77:445–473, 1981.

[93] S. Nir, C. Newton, and D. Papahadjopoulos. Binding of cations to phosphatidylserine vesicles. *Bioelectrochem. Bioenerg.*, 5:116–133, 1978.

[94] R. Kurland, C. Newton, S. Nir, and D. Papahadjopoulos. Specificity of Na^+ binding to phosphatidylserine vesicles from Na-23 NMR relaxation rate study. *Biochim. Biophys. Acta*, 551:137–147, 1979.

[95] A. Averbakh and V.I. Lobyshev. Adsorption of polyvalent cations to bilayer membranes from negatively charged lipid: estimating the lipid accessibility in the case of complete binding. *J. Biochem. Biophys. Methods*, 45:23–44, 2000.

[96] G.H. Pollack. *Cells, Gels and the Engines of Life. A New, Unifying Approach to Cell Function.* Ebner & Sons, Seattle, WA, 2001.

[97] R. Whittam. Active cation transport as a pace-maker of respiration. *Nature*, 19:603–604, 1961.

[98] C.G. Sinn, R. Dimova, and M. Antonietti. Isothermal titration calorimetry of the polyelectrolyte/water interaction and binding of Ca^{2+}: effects determining the quality of polymeric scale inhibitors. *Macromolecules*, 37(9):3444–3450, 2004.

[99] H.G. Schild. Poly(n-isopropylscrylamide): Experiment, theory and application. *Prog. Polym. Sci.*, 17:163–249, 1992.

[100] S. Hirotsy, Y. Hirokawa, and T. Tanaka. Volume-phase transitions of ionized n-isopropylacrylamide gels. *J. Chem. Phys.*, 87(2):1392–1395, 1987.

[101] M. Shibayama and T. Tanaka. Volume phase-transitions and related phenomena of polymer gels. *Adv. Polym. Sci.*, 109:1–62, 1993.

[102] Y. Ueoka, J. Gong, and Y. Osada. Chemomechanical polymer gel with fish-like motion. *J. Intel. Mat. Syst. Str.*, 8(5):465–471, 1998.

[103] T.G. Park and A.S. Hoffman. Sodium chloride- induced phase- transition in nonionic poly(n-isopropylacrylamide) gel. *Macromolecules*, 26(19):5045–5048, 1993.

[104] H.G. Schild and D.A. Tirrell. Microcalorimetric detection of lower critical solution temperature in aqueous polymer solutions. *J. Phys. Chem.*, 94:4352–4356, 1990.

[105] R. Freitag and F. Garret-Flaudy. Salt effects on the thermoprecipitation of poly-(n-isopropylacrylamide) oligomers from aqueous solution. *Langmuir*, 18:3434–2440, 2002.

[106] Y.H. Kim, I.C. Kwon, Y.H. Bae, and S.W Kim. Saccharide effect on the lower critical solution temperature of thermosensitive polymers. *Macromolecules*, 28(4):939–944, 1995.

[107] D.R. Lide. *CRC Handbook of Chemistry and Physics.* CRC Press, Boca Raton, 80 edition, 1999.

[108] N. Hubert, M Bouroukba, and L. Schuffenecker. Aqueous-solution of sodium-sulfate - determination of the dissolution enthalpy at 25, 27.5 and 45-degrees-c. *Thermochim. Acta*, 259(1):41–48, 1995.

[109] G.C. Sinke, E.H. Mossner, and J.L. Curnutt. Enthalpies of solution and solubilities of calcium chloride and its lower hydrates. *J. Chem. Thermodyn.*, 17(9), 1985.

[110] C. Shin and C.M. Criss. Standard enthalpies of formation of anhydrous and aqueous magnesium chloride at 298.15 K. *J. Chem. Thermodynamics*, 11:663–666, 1979.

Acknowledgements

First, to Prof. Markus Antonietti, for his constant support, patience and guidance throughout this work. For being a brilliant teacher and for giving me as an Engineer the chance to do a PhD in Physical Chemistry in his group. The excellent facilities and pleasant environment he provides creates a stimulating and inspiring working atmosphere, which was crucial for the outcome of this work.

I am happy to express my gratitude to my extraordinary supervisor, Dr. Rumiana Dimova, for her continual sustain and neverending encouragement, for challenging me in countless fruitful discussions, for her humor and exceptional friendship.

I am also very grateful to my group. Karin Riske and Jeremy Pencer for many useful suggestions and scientific discussions. Janina Beeg and Said Aranda for plums and oranges and for their friendship. Christopher Haluska for strength and success. Antje Reinicke not only for technical support and Thomas Francke for being a great striker. Vesco Nikolov for the excellent introduction into the world of giant vesicles and Pavel Kraikivski for geography lessons.

Doreen Eckhardt, Andreas Erbe, Matthijs Groenewolt and Christian Holtze suffered my amateur questions on chemistry most graciously. They were patient with me and generous with their time. My acknowledgments also to Ba Jianhua for being an incomparable office mate. To Özlem Sel for the synthesis of the microgel particles and for introducing me to the subject. And to Danielle Francke, Miles Page and Melanie Hertel for proofreading the thesis.

For their advice in scientific questions, I would like to acknowledge Hans Börner, Helmut Cölfen, Charl Faul, Bernd Smarsly and Klaus Tauer.

My special thanks to Hubert Motschmann for leading me through a difficult exam. And to Jan Kirkfeld and Thomas Gruhn for helping me out with Mathematica.

I would also like to thank Nadine Nassif, Nicole Gehrke, Rivelino Montenegro, Julien Polleux, Chrystelle Egger, Rémi Soula, Jan Hendrik Schattka, Magda Losik, Justyna Justynska, Samira Nozari, Ines Below, Torsten Brezesinski, Georg Garnweitner, Markus Niederberger, Hartmut Rettig, Helmut Schlaad, Reinhard Sigel, Antje Völkel and Rebecca Voß, who always helped me when I needed their assistance and provided a great working climate.

I acknowledge how much I owe to my parents, Erika and Ingolf Hertel for their infinite support, encouragement and confidence in me. To Ivonne, Melanie and Tobias for their open ear at any time and for their empathy. And finally, to my husband Christoph, for his endless love, refreshing humor and for the joy being next to him.

Appendix A

Tables

Polymer/Salt	Molecular weight [g/mol]	Degree of polymerization, DPn	Concentration range [N]
CaCl$_2$	111	-	0.03 − 0.32
CaPAA	5 × 103	55	0.06 − 0.64
CsCl	168	-	0.03 − 0.7
KCl	75	-	0.03 − 0.7
LiCl	42	-	0.03 − 0.5
MgCl$_2$	60	-	0.03 − 0.32
NaAc	82	-	0.03 − 1
NaBr	103	-	0.03 − 0.2
NaCl	58	-	0.03 − 4
NaI	150	-	0.03 − 0.7
NaPAA1	2.1 × 103	20	0.03 − 0.88
NaPAA2	5.1 × 103	55	0.03 − 1
NaPAA3	100 × 103	1410	0.08 − 0.4
NaPSS	8 × 103	40	0.03 − 0.5
Na$_2$SO$_4$	142	-	0.03 − 1
PAsp	20 × 103	145	0.037
Sokalan	70 × 103	740	0.105

Table A.1: Weight averaged molecular weight, degree of polymerization and concentration range of the polymer and salt solutions used in this work.

Salt	Heat of Solution [kJ/mol]
NaCl	3.88[a]
NaBr	-0.6[a]
NaI	7.53[a]
Na$_2$SO$_4$	-0.99[b]
CH$_3$COONa	-17.32[a]
LiCl	-37.03[a]
KCl	17.22[a]
CsCl	17.78[a]
CaCl$_2$	-82.8[c]
MgCl$_2$	-155.5[d]

Table A.2: Heat of Solution of various salts. The heat of solution is positive for exothermic and negative for endothermic solution processes. Data reported from: a [107]. b [108]. c [109]. d [110]
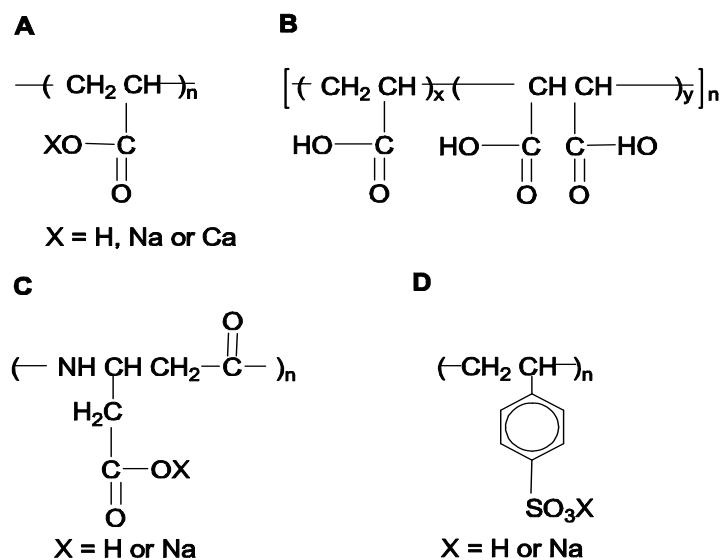
Appendix B

Chemical Structures

A

—(CH₂ CH)ₙ
│
XO—C
‖
O

X = H, Na or Ca

B

[(CH₂ CH)ₓ (—— CH CH ——)ᵧ]ₙ
│   │ │
HO—C   HO—C C—HO
‖   ‖ ‖
O   O O

C

                    O
                    ‖
(— NH CH CH₂—C—)ₙ
       │
      H₂C
       │
       C—OX
       ‖
       O

X = H or Na

D

(—CH₂ CH—)ₙ
        │

        SO₃X

X = H or Na

Figure B.1: Chemical structure of the used polymers. A: PAA, NaPAA1, Na-PAA2, CaPAA, NaPAA3 B: Sokolan; x/y =1 C: PAsp, NaPAsp D: PSS, NaPSS
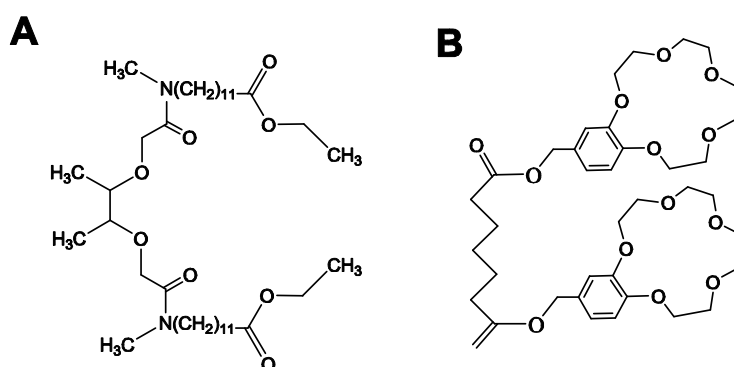
A

B

Figure B.2: Chemical structure of compounds with ion specific dissolving power. A: Ca^{2+} ionophore B: K$^+$ ionophore